Tomas Bata University in Zlín
Faculty of Technology

Doctoral Thesis Summary

Síťování, morfologie a vlastnosti polymerních směsí a kompozitů

Cross-linking, Morphology and properties in polymer blends and composites

Author: Ing Yasin Hamid

Degree programme: P2808 Chemistry and Materials Technology

Degree course: 2808v006 Technology of Macromolecular Compounds

Supervisor: Prof. Ing. Petr Svoboda

Zlín, March-2020

Published by Tomas Bata University in Zlín in the Edition Doctoral Thesis Summary.

The publication was issued in the year 2020

Keywords in Czech DMA, Electromechanic, Irradiation, Thermal conductivity, Carbon fiber, EVA, EBC

Keywords: DMA, Electromechanic, Irradiation, Thermal conductivity, Carbon fiber, EVA, EBC

Full text of the doctoral thesis is available in the Library of TBU in Zlín.

ISBN 978-80-……

Abstraktní:

Elektrické vodivé kompozity mají mnoho pokusů vyrobit originální materiál v technologii jako senzor. Bylo provedeno několik studií o reologické a lineární viskozitě s elektrickým odporem kompozitu. Účelem této studie bylo zkoumat vliv záření uhlíkových vláken (CF) a elektronového paprsku (EB) na mechanické vlastnosti za vysokých teplot, elektrické , mechanická a tepelná vodivost ethylenbutenového kopolymeru (EBC) a ethylenvinylacetátu (EVA). Polymerní kompozity byly připraveny smícháním na dvouválcovém mlýnu a Brabenderu. Po lisování byly vzorky EVA / CF ozářeny mezi 60 a 180 kGy a pro charakterizaci fyzikálních vlastností byla použita dynamická mechanická analýza (DMA). Byly hodnoceny účinky obsahu plniva a úrovně záření na mechanické vlastnosti EVA / CF. Bylo pozorováno, že se střihové napětí a modul zvyšují se zvyšováním hladiny plniva. Došlo však k dramatickému snížení poddajnosti. Bylo také ukázáno, že zavedení ozáření do EVA kompozitu zvyšuje smykové napětí a skutečnou část dynamického modulu smyku G 'v důsledku zvýšení molekulové hmotnosti a zesítění polymeru po ozáření.

Elektrické vodivé kompozity mají mnoho pokusů vyrobit originální materiál v technologii jako senzor. Bylo provedeno několik studií o reologické a lineární viskozitě s elektrickým odporem kompozitu. Žádná z nich však nebyla provedena na elektricky vodivých sazích (CB). V této studii byly zkoumány účinky různého obsahu sazí na ethylen-butenový kopolymer (EBC) na reologické a elektromechanické. Do EBC bylo zavedeno množství (0, 4,07, 6,31, 8,71 a 11,28) objemového podílu% CB. Dynamická mechanická analýza (DMA) a

Elektromechanická zkouška ukazují, že přidání CB do EBC by zvýšilo mechanickou viskozitu, moduly a elektrický odpor, zatímco by se výrazně prodloužilo prodloužení. Tyto práce demonstrují možnost výroby tenzometrických senzorů pomocí levné a víceúčelové techniky s potenciálními aplikacemi ve zdravotnických a elektromechanických senzorech.

Abstract:

Electric conductive composites have many attempts at producing original material in technology as a sensor. The fast development of smart sensors has contributed to smart elastic strain sensors. However, to date, the low stretch-ability and sensitivity of conventional metals or inorganic semiconductor-based strain sensors have restricted their application in this field to some extent [1-4]. Several studies have been done about rheological and linear viscosity with the electrical resistance of the composite. The purpose of this study was to investigate the effect of carbon fiber (CF) and electron-beam (EB) radiation on high-temperature mechanical properties, electrical, mechanical, and thermal conductivity of Ethylene Butene Copolymer (EBC) and Ethylene Vinyl Acetate (EVA). Polymer composites were prepared by mixing on a two-roll mill and Brabender. After compression molding, the EVA/CF samples were irradiated between 60 and 180 KGy, and dynamic mechanical analysis (DMA) was used to characterize physical properties. The effects of filler content and radiation level on the mechanical properties of EVA/CF were evaluated. The shear stress and modulus were observed to increase with increasing the filler level. However, there was a dramatic decrease in creep compliance. It was also shown that the introduction of irradiation on EVA composite increases the shear stress and the real part of the dynamic shear modulus G' due to the increase in molecular weight and cross-linking of the polymer after irradiation.

The effects of different carbon black content on Ethylene-butene copolymer (EBC) on rheological and electromechanical were investigated. The amount of (0, 4.07, 6.31, 8.71, and 11.28) volume fraction % of CB was introduced to EBC. The

Dynamic mechanical analysis (DMA) and Electromechanical test show that the addition of CB to the EBC would increase the mechanical viscosity, modules, and electric resistance while significantly decreasing in the elongation. These works demonstrate the possibility of producing strain sensors using a cheap and multipurpose technique, with potential health and electromechanical sensors.

Table of Contents

Introduction

Recently, there have been lots of polymer replacement interests instead of other materials like Metal, Wood, ceramics [5]. This because of the advantages that polymer offers over conventional materials like cost, easy to process, and productivity. [6]

To meet the high demands base on strength and stiffness for many applications, the polymeric materials must be reinforced like aerospace. Automotive, medical, chemical industry, electrical, construction, microelectronics, and sensors [7, 8]. Carbon fiber and glass fibers are more attractive in the academic and commercial fields due to their cost and functionality [7, 9-11].

There are two types of additives used in Polymer Composites. The reinforcing fibers in polymer composites are more responsible for their high stiffness and strength. That could satisfy with sufficient stress transfer to the matrix from fiber and vice versa, which can occur by suitable bonding between them [12]; Therefore, the properties and structure of the Fiber-Matrix play the primary role in both the physical and mechanical properties of Polymer Composites.

The most famous and ordinary fiber is carbon fiber, glass fiber, and amid family. The glass fiber has good tensile strength. However, it has low stiffness compared to other fibers. Nevertheless, due to limited recyclability and high-energy glass fibers requirements, they are still causing environmental problems. Because of trends

toward environmentally friendly, most of the research focuses on using environmentally friendly fibers as alternatives to glass fibers.

Carbon fiber is widely used in the industry nowadays. Carbon-filled polymer composites have been popular due to their extensive utilization in various electronic equipment like temperature, pressure, dielectric, strain, gas, and biosensor materials. Carbon fibers (CF) have become a critical reinforcing material in advanced composites because of their too high strength, stiffness, heat-resistance, and low weight. Fiber-reinforced polymer composites have a great interest due to their very high strength-to-weight and stiffness-to-weight ratios. These properties are significant in aerospace, engineering, marine industries, and automobile industries. The adhesion at the interface between matrix and fiber is an essential issue in controlling the composite properties. [13, 14]

An excellent interface between fiber and matrix can increase the stability and transfer the stress from matrix to fiber. However, chemical inertness and smooth surface of the fiber causes poor adhesion and lower enhancement in the properties of the composite. All these advantages can be combined and increase with a suitable matrix or achieve the excellent mechanical properties of composite parts built from both. [7, 14-17]

The relative properties of the most common fibers are given on the table 1.

Table 1.Mechanical properties of fibers [14]

Fiber	Density (g/cm^2)	Elongation (%)	Tensile strength (MPa)	Young's modulus (GPa)
Cotton	1.5-1.6	7.0-8.0	287-800	5.5-12.6
Jute	1.3	1.5-4.8	393-773	26.5
Flax	1.5	2.7-3.2	3451035	27.6
Hemp	1.5	1.6	690	70
Ramie	1.5	1.2-3.8	400-938	61.4-128
Sisal	1.5	2.0-2.5	511-635	9.4-22.0
Coir	1.2	30.0	175	4.0-6.0
wood	1.5	-	1000	40
Glass-E	2.5	2.5	2000-3500	70.0
Glass-S	2.5	2.8	4570	86.0
Aramid	1.4	3.3-3.7	3000-3150	63.0-67.0
Carbon	1.4	1.4-1.8	4000	230-240

Fillers are mainly used in composites in two forms. They are mainly used in particles and short fibers, usually added to the matrix to enhance and increase the

process's mechanical properties. Fillers' behavior in the composite mixture is affected by the particle size, distribution, surface at area shape, and surface chemistry. For example, Silicon carbide (SiC), which knows and ceramic material that compounds or silicon and carbon, could increase the abrasion resistance. Silicon carbon has unique physical properties, which enhance the chemical and mechanical properties. Meanwhile. It is resistant to high thermal, electron mobility, and excellent thermal conductivity.

Electrical properties can be affected by many fillers. For example, by adding conductive fillers, an electromagnetic shielding property can be built into plastics, which usually are poor electrical conductors. Carbon family fibers like carbon fiber, Carbon nanotube, Carbon black, and graphite are mostly used as a fiber to improve the electrical and thermal conductivity and mechanical and physical properties.

Electrically conductive composites have been adequately prepared by adding an electrically conductive filler to polymeric materials. Several researchers have investigated various inorganic fillers such as carbon black [18], carbon nanotubes (CNTs) [19], SiO_2 Nanoclay [20]. For example, conductive composites with carbon black (CB) are attractive due to their applications in the automotive, pressure sensor, and gas sensor.

Several categories could affect the fillers' function in composites, such as the size, roughness, and aspect ratio. If the filler's characterization is with a low aspect ratio, there will be less change in basic properties than unfilled polymers. However, it could improve thermal resistance, Strength, and solvent resistance. Nevertheless, the impact resistance and shrinkage will often be less than the unfilled polymer. On the

other hand, increasing the filler's aspect ratio up to 25, the filler can be characterized as a fiber. Fiber reinforcements will significantly affect the properties of the mixtures to which they are introduced. The fiber impact strength would increase, mainly if many fibers are oriented in the one direction in which a considerable difference is observed between the unfilled and filled polymer's modulus. Besides, increasing the aspect ratio could decrease the shrinkage in the order of the fiber.

Previously, Carbon fibers were made from natural cellulosic fibers such as linen or cotton for thousands of years. Nevertheless, it was Thomas Edison who, in 1978, produce carbon fiber from bamboos and cotton in his research for lamp filaments. In the meantime, the late 1950s, carbon fiber was interesting for scientists once carbon fiber was produced from synthetic rayon is in textile forms for high-temperature missile applications. [21]

Several studies have been done about the mechanical and electromechanical study of composites with conductive fillers [9, 22-26].The fast development of smart sensors has contributed to smart elastic strain sensors. However, to date, the low stretch-ability and sensitivity of conventional metals or inorganic semiconductor-based strain sensors have restricted their application in this field to some extent [1-4].Slobodian et al. [27] reported that the addition of multi-wall carbon nanotube (MWNT) up to 20 wt.% to poly (methyl methacrylate) (PMMA) could increase the conductivity up to 100 times. Spherical particles like Carbon Black in polymer/carbon black composites exhibit percolation threshold, frequently up to 15–

25 wt.%. However, lower values were also published. D'Aloia et al. [28] investigated that graphene's addition leads to an increase in the graphene-thermosets polymer's electromechanical and mechanical properties. As the graphene concentration increases, the graphene-polymer composite undergoes an insulator-to-metal transition due to the conductive filler presence inside the matrix. It is also reported that the addition of carbon nanotube to SEBS elastomer could increase electrical resistance. At the same time, the sample is stressed and decreasing when the sample recovers to initial deformation. Furthermore, it has been shown that the sample leads to stable after some aging cycles [29].Yang et al. [30] investigated the resistance response of CNT/ graphene RTV silicone rubber composites under static and dynamic cyclic loading. It is observed that CNT/graphene RTV silicone rubber composites exhibited a stable and reproducible resistance response under dynamic cyclic loading, indicating that they have potential applications in continuous monitoring. Mostly, strain sensors are based on piezoresistive materials, for example, those materials for which an applied strain, ε, results in a resistance change. Commonly, the gauge factor is measured at low strain, which is most metals is small in the range 2 for Nichrome V to 4.8 for Platinum[31]. However, composite strain sensors based on polymers filled with conductive fillers, like multiwalled carbon nanotubes[32] and carbon nanotube[33, 34], can gauge high gauge factors. Piezoresistive materials resistance increases with increasing tensile strain as they

have positive gauge factors because interparticle intersections dominate the piezoresistance in composites, leading absolutely to the Gauge factor higher than 0. A small number of materials with negative gauge factors[35]; polymer fibers coated with conducting polymers have demonstrated small negative gauge factors due to chain alignment effects.

Creep study of isotactic polypropylene (iPP)-based graphene nanocomposites used to evaluate the load transfer efficiency by Gaska[36] et al.. they have investigated that significant increase of Young's modulus with increasing filler content which indicates reasonably good dispersion and adhesion between isotactic polypropylene (iPP)-based graphene nanocomposites the and the filler content indicates reasonably good dispersion and adhesion between the iPP and the filler. Wang[37] et al. reported the same results for numerical analysis using the Finite Element Method used for unidirectional fibrous polymer matrix composites' computing material properties. Srivatsan and Sreekanth[38] investigated the experimental characterization of dynamic mechanical properties of carbon fiber-reinforced composite with sandwich configuration. The addition of carbon fiber up to 40% wt will increase the loss modulus and tan delta curve as the frequency increases. They also indicated that Carbon exhibiting high storage modulus due to its atomic structure directly indicates young's modulus. Sabet et al. [39] studied the impacts of graphene inclusion on the mechanical, electrical, and low-density

polyethylene. They reported that while the addition of 3 wt% of graphene had a significant impact on the performance and improvement of LDPE's electrical characteristics, which is because of the spreading of graphenes in LDPE, which makes to extend more conductive networks. The polymer composite's viscosity is rasing from 120.1 to 195.4 kPa because of the significant interaction between the filler and matrix that obstructed the movement of macromolecular polymeric links. Consequently, graphene has an excessive surface area and nanoscale fat surface that renders it generate resilient interfacial connections with LDPE and significantly affects an excellent consequence of LDPE's chain movement. It has been communicated that the mechanical properties and dynamic properties can be enhanced by entering the e-beam irradiation due to enhancing the filler to matrix interaction, shown in swelling resistance studies [40]. Introducing carbon fiber or nanotube to EVA can improve the modulus and the composite's tensile strength.

Polymer material radiation processing involves ionizing radiation of polymer treatment to enhance their chemical and mechanical properties. During the ionizing irradiation, polymers can cross-link, be grafted, or degrade. [41, 42] Mateev *et al*. investigated the effect of e-beam irradiation on the gel formation process of EVA/PE films in range 40-250kGy when the significant change in gel content occurred in range 40-170kGy [43]. This fact and our experience from our previous experiments [44] influenced our range of e-beam radiation, being this time 60, 120, and 180 KGy.

Electron beam (EB) irradiation on EVA/CF composite has been used in this study, and a variety of fiber concentrations has been investigated.

In this study, the electromechanical and rheological properties of electrically conductive carbon black (CB) on ethylene Butene copolymer have been investigated. The electrical conductivity of CB is studied both in terms of creep and filler content. The mechanical properties of EVA/CF composite under EB irradiation have been investigated in detail. Testing mechanical properties was done at room temperature (25 °C) and 150°C. We are presenting only high-temperature results since they better reflect the influence of e-beam cross-linking.

The amorphous polymer chains are held together by crystal lamellae and covenant bonds (from cross-linking). However, at 150°C, only the chemical cross-linking has the amorphous chain together.

1. History of Carbon Fiber

In the late 1960s, the high performance of carbon fiber was an exciting topic for the technical and commercial background of the polyacrylonitrile (PAN) process. It becomes more economical because of higher carbon yield, which is 50% compared to 30% for Rayan's fabrication process, and superior physical properties compare rayon-based fibers recognized as the most essential and promising precursor for manufacture and high-strength carbon fiber. [45]

Later, carbon fiber was prepared from the pitch of petroleum, asphalt, and coal tar. The process of carbon fiber from Pitch has lower quality compared to the PAN process. To improve the carbon fiber properties from Pitch, the starching treatment

should be done, which is an expensive process if it can give the carbon fiber excellent properties.

This expensive stretching treatment can be avoided using mesophase pitches, which are liquid crystalline in nature[21]. Unlike PAN, the high degree of molecular orientation of as-spun mesophase pitch fibers allows it to develop a genuinely graphitic crystalline structure during the carbonization/graphitization step[46]. Hence ultra-high-modulus carbon fibers are now produced from mesophase pitches.

2. Ethylene (Vinyl Acetate) (EVA)

Ethylene (vinyl acetate) is a copolymer with good clarity and gloss, low-temperature toughness, stress crack resistance, hot-melt adhesive waterproof properties, and resist UV radiation. EVA has a distinctive "vinegar" odor and is competitive with rubber and vinyl products in many electrical applications. EVA is prepared with solution polymerization, suspension polymerization, emulsion polymerization, and Bult polymerization. However, solution polymerization is preferred in this method; Methanol has mainly used a solvent with 2'-azobisisobutyronitrue, or organic peroxides 2, 2'-Azobis (4-methoxy-2, 4-dimethyl valeronitrile) is preferred as a catalyst. The polymerization in the range of 50-80. The ethene is pressured at 2-8 M Pa for 3-4 hours, and then the reaction is stopped with an inhibitor's addition to the reaction mixture. Unreacted ethylene gas evaporates and is removed from the solution. Eventually, methanol is recovered by precipitation with water-containing separating and purifying the solution. [47]

The properties of EVA are close to the elastomer material's flexibility and softness. Therefore, it is more competitive with vinyl and rubber products, especially for electrical products. Furthermore, m the copolymer can be processed like a thermoplastic material which exhibited an excellent toughness in low temperature and stress scratch resistance. [48, 49]

3. Ethylene-Butene Copolymer (EBC)

Ethylene-butene copolymer (EBC) elastomer is synthesized from gas phase polymerization in highly active catalyst SiO_2 or Zn-Cl_2/AlR_3/Alcohol, $TiCl_4$, Ti (oBu) $_4$/$MgCl_2$, which has the properties of copolymerization in site to catalyze the gas phase polymerization of ethylene and butene. This elastomer copolymer keeps the properties of thermoplastic and elastomer's properties both. The ethylene-butene copolymer elastomer has a high degree of the branch, low density, and low cost per unit volume compared with ethylene-propylene rubber due to the elastomer thermoplastic properties of the copolymer even without vulcanization and can be recycled without decreasing physical and processing properties. [50]

4. Background of study

4.1. E-Beam Irradiation

There are several crosslinking methods used in the chemical industry, like chemical cross-linking, silane cross-linking, peroxide cross-linking, UV cross-linking, and irradiation cross-linking. Electron-Beam irradiation leading to polymer cross-linking has many advantages in comparison with other methods. Firstly, the

processing condition is not taking place during polymer parts production like injection molding or extrusion. It is not affected by cross-linking since it applies after the processing. Furthermore, the process of cross-linking is extremely fast and can use in a straightforward way to the possibility of changing the degree of cross-linking by irradiation dose. Moreover, the E-Beam irradiation is considered the cleanest and most environmentally friendly cross-linking method since it does not involve other chemicals. Only energy electrons are used to perform. [51] A shower of fast-moving electrons strikes the polymer for up to 5 cm as it passes through the beam. The fast electrons ionize the long-chain molecules into the polymer. The ionized polymer chains connect, and the cross-linked polymer matrix is created. The polymer matrix has improved physical properties compared to the original material. The e-beam radiation could increase the Heat resistance creep resistance, and low-temperature impact strength can be enhanced. The simulation of E-beam irradiation and the dose of the application shows in Figure1. The irradiation of the polymer could affect the behavior of the polymer. The effectiveness of irradiation could be depending on many factors as polymer structure and dose applied. The E-beam irradiation mainly depended on physical aspect (like Tg, crystallinity), chemical structure, molecule weight, polymer configuration; the amount used environmental parameters and condition (nitrogen, air, temperature), the geometry of the polymer sample (i.e., the thickness of sample), and addition of cross-linking agent. [41, 51]

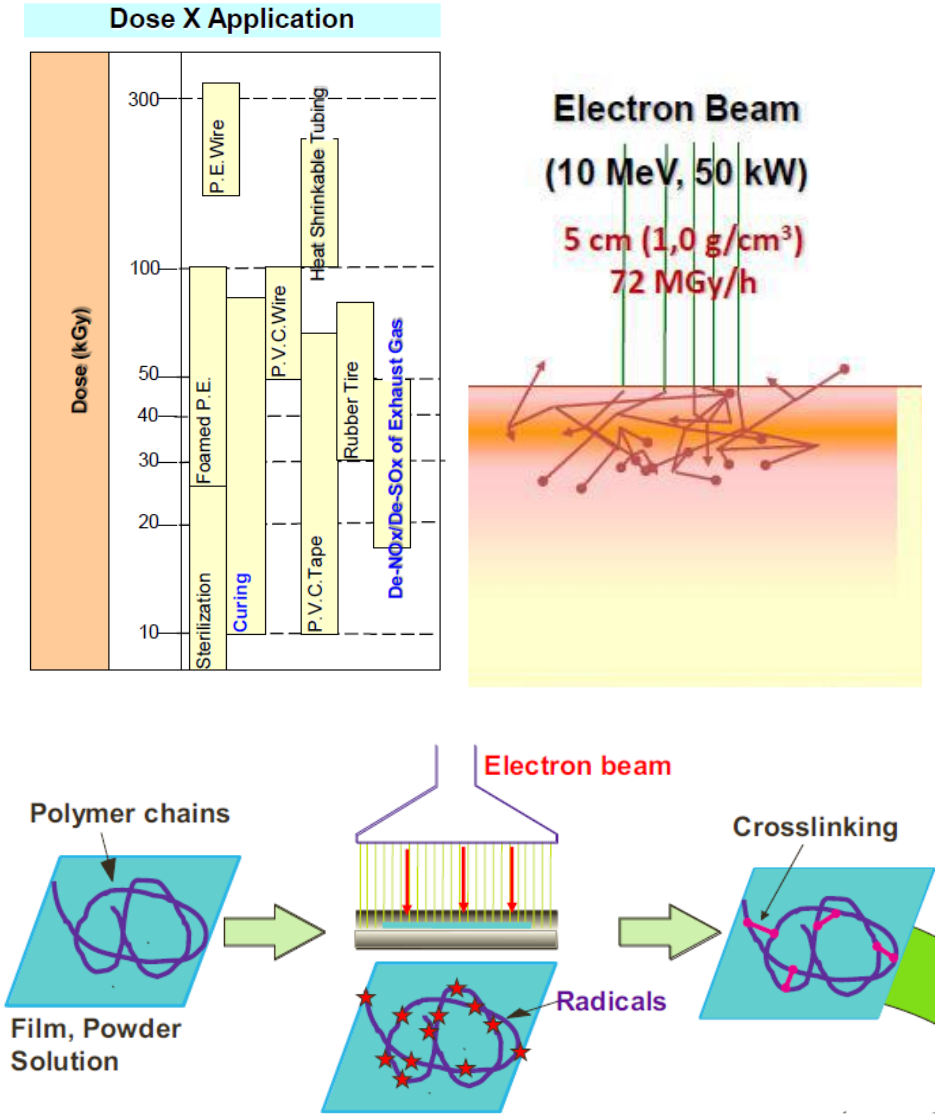

Figure 1. The simulation of E-beam irradiation and the dose of the application

During the ionizing irradiation, polymers can cross-link, be grafted, or degrade. [41, 42] Mateev *et al*. investigated the effect of e-beam irradiation on the gel formation process of EVA/PE films in range 40-250kGy when the significant change in gel content occurred in range 40-170kGy [43]. This fact and our experience from our previous experiments [44] influenced our range of e-beam radiation, being this time 60, 120, and 180 KGy.

4.2. Dynamic mechanical analysis (DMA)

The dynamical mechanical analysis (DMA) is one of the essential tools in the polymer laboratory, which is based on the oscillatory deformations to measure the mechanical response goes back to Poynting (1909) [52-54], who is conducted the first oscillatory experiment to measure the elasticity of a material. The DMA test found less use up to the sixties when commercial instruments became more user-friendly. These early instruments were slow and limited. Today, several companies have developed mighty DMA's. They are mainly used to measure the glass transition temperature and modules [55].

Dynamic mechanical analysis (DMA) is a technique that enables the two components E' and E'', which together are known as the complex tensile modulus, E*, to be measured. In DMA, the stress or strain described in Figure 2 is applied to the specimen in an oscillatory manner that is usually described as sinusoidal. However, the exact nature of the deformation depends on the particular instrument used for the measurements.

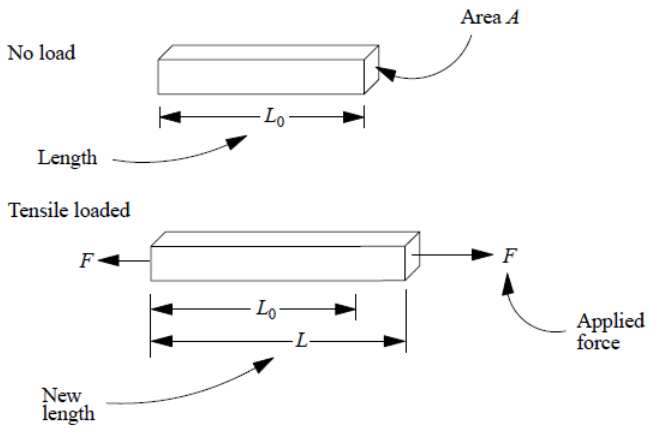

Figure 2. A specimen at rest and in a tensile-loaded condition

A sample is held under sufficient tension with the same wave as the material's viscoelastic nature; these properties are out of phase by an amount or angle, δ, the phase lag. For an ideal elastic material, δ is zero, and the stress and strain are in phase. For a Newtonian liquid, if it could be so tested, δ would be 90°. For viscoelastic materials, δ is between 0 and 90°. These components of the modulus can be represented as two vectors that are 90° out of phase with each other, as described in Figure 3.[54]

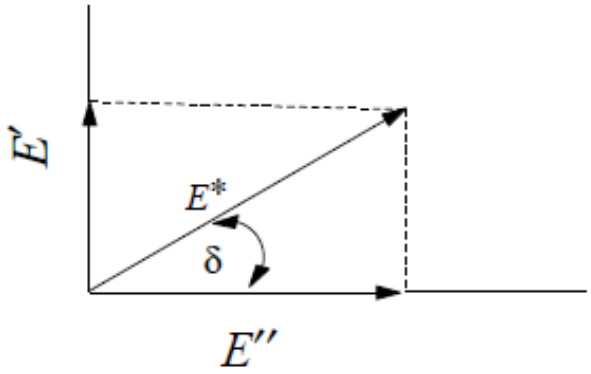

Figure 3Vector represents the components, E' and E'', of the complex shear modulus, E, and the phase angle, δ.*

To understand the storage and loss components of a material, consider a rubber ball dropped from some height onto a hard, elastic surface. The ball will bounce up and down with a decreasing size as each succeeding bounce occurs until it is finally at rest.

The ball's elastic nature causes it to return to the release point using stored energy, but the ball's viscous nature results in it losing energy as heat to the surroundings; consequently, the ball reaches a height somewhat less than the original measurement. The motion is gradually damped until finally, the ball ceases to bounce. [56]

4.3. Creep

When polymers are subjected to stress, they undergo deformations by conformational changes (smaller and larger-scale molecular rearrangements) and viscoelastic flow. To analyze the viscoelastic response in creep and relaxation experiments, spring and dashpot elements are frequently used. The spring behaves precisely like a metal spring, stretching instantaneously under stress and holding the load, whereas the plunger immersed in the dashpot filled with a Newtonian liquid moves at a rate proportional to the stress. On removing the stress, there is no recovery.

The time dependence of viscoelastic response is similar to the time dependence of reactive electrical circuits, and identical ordinary differential equations can describe both in time. A convenient way of developing these relations while also helping visualize molecular motions employs "spring-dashpot" models. These mechanical analogs use "Hookean" springs, depicted in Figure 4 and described by:

$$\sigma = k\mathcal{E}$$

Where σ and Ɛ are analogous to the spring force and displacement, and the spring constant k is identical to Young's modulus E; k, therefore, has units of N/m^2. The spring models the instantaneous bond deformation of the material, and its magnitude will be related to the fraction of mechanical energy stored reversibly as strain energy.

Figure 4. Hookean spring (left) and Newtonian dashpot (right).

The ideal spring obeys Hooke's law, and the liquid in the dashpot follows Newton's law of viscosity

$$\sigma = \eta \cdot \frac{d\varepsilon}{dt} \quad (1)$$

The two most straightforward arrangements of dashpots and springs are the Kelvin-Voigt and the Maxwell configuration, shown in Figure 4.

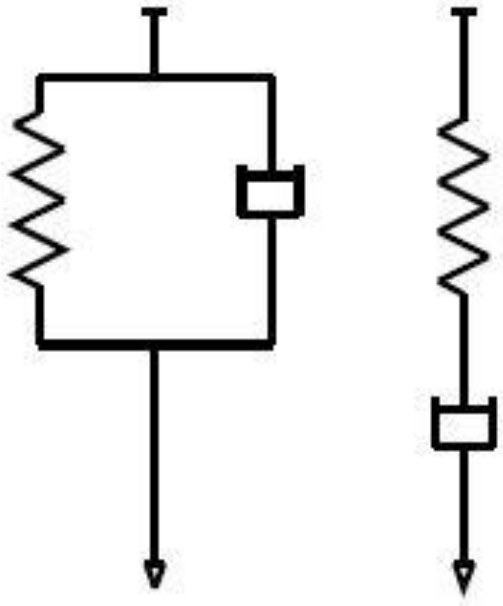

Figure 5. Kelvin (left) and Maxwell (right) configuration

In the Maxwell configuration, both the spring and the dashpot are connected in series. Both elements are subjected to the same stress in this configuration but are permitted an independent strain.

$$\sigma_s = \sigma_s \quad (2)$$

$$\varepsilon_t = \varepsilon_D + \varepsilon_S \quad (3)$$

Where the subscript D indicates the damper, and the subscript S indicates the spring. The basic equation for the strain rate in the Maxwell model is

$$\frac{d\varepsilon}{dt} = \frac{1}{E}.\frac{d\sigma}{dt} + \frac{\sigma}{\eta} \quad (4)$$

In the Kelvin-Voigt configuration, the two elements are connected in parallel, and both components are subjected to the same strain but different stress:

$$\sigma_t = \sigma_D + \sigma_S \quad (5)$$

$$\varepsilon_D = \varepsilon_S \quad (6)$$

The basic equation for the stress in the Kelvin-Voigt model is

$$\sigma = E \cdot \varepsilon + \eta \cdot \frac{d\varepsilon}{dt} \quad (7)$$

The two formations of dashpots and springs behave very differently in a creep experiment. A stress is applied to ends of elements, and strain (creep) is observed as a function of time. The viscoelastic response of the two models is shown below.

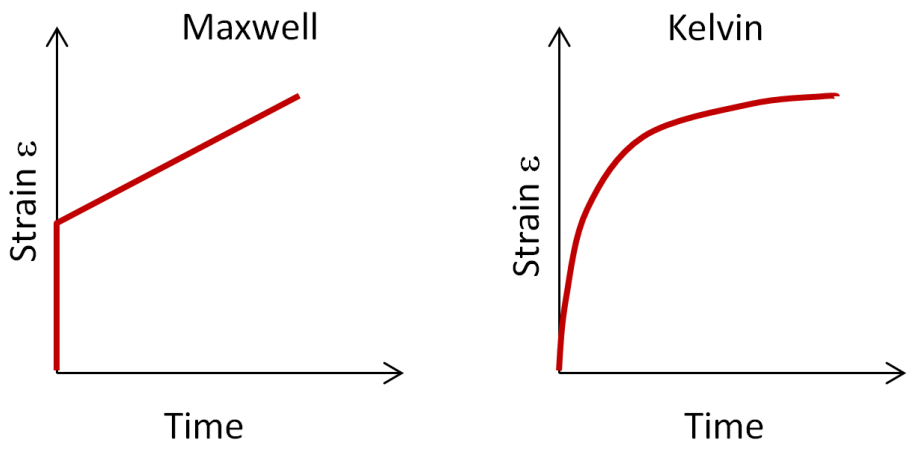

Figure 6. The viscoelastic response of the Maxwell (left) and Kelvin (right)

The spring of the Maxwell arrangement response immediately, as illustrated by the vertical line in the graph above, is left. The height of the jump is

$$\varepsilon_0 = \frac{\sigma_0}{\mathrm{E}} \quad (8)$$

While the spring remains at a constant extension or strain, the dashpot's plunger pulls out at a constant rate. The rate of strain is given by

$$\frac{d\varepsilon}{dt} = \frac{\sigma_0}{\eta} \quad (9)$$

Therefore, the effect of sudden stress is

$$\varepsilon(t) = t \cdot \frac{\sigma_0}{\eta} + \frac{\sigma_0}{E} \quad (10)$$

Which is $t \cdot \frac{\sigma_0}{\eta}$ the irreversible and $\frac{\sigma_0}{E}$ the reversible strain response. The initial reaction is identical with the spring response because the dash-pot does not restrict the spring movement in the Maxwell element in series. In contrast, the dash-pot simulates the liquid-like behavior at large observation times.

The Kelvin-Voigt model shows very different behavior. Since the dashpot and the spring are parallel, the strain in each component are identical. In this configuration, the dashpot slowly bears all the stress initially and gradually transfers it to the spring. The differential equation for creep deformation is

$$\frac{\sigma_0}{\eta} = \frac{\varepsilon}{\lambda} + \frac{d\varepsilon}{dt} \quad (11)$$

With $\lambda = \frac{\eta}{E}$ This linear differential equation has the solution:

$$\varepsilon(t) = \frac{1}{E} \cdot \left[1 - \exp\left(-\frac{t}{\lambda}\right)\right] \quad (12)$$

Some viscoelasticity problems can be solved with the Maxwell and Kelvin-Voigt arrangements alone. However, more often, they are combined with more complex configurations to describe the creep and relaxation behavior of polymeric materials more accurately. [57]

In a creep experiment, the stress is increased suddenly from zero to a value of σ_0 at $t = 0$. The result is interpreted in terms of creep compliance.

$$j = \frac{\Upsilon(t)}{\sigma_0} \quad (13)$$

Rheological behavior such as creep can be observed for many engineering materials such as metals, polymers, ceramics, concrete, soils, rocks, ice, etc.

Understanding the creep behavior of a material is essential in design and manufacturing. This can lead to dimensional instability of the product and a failure at applied constant stresses that are significantly lower than the ultimate tensile

strength. Creep is a slow continuous deformation of a material under constant stress. In general, creep can be described in three terms. In the first stage, which is the primary screen, the material undergoes deformation at a decreasing rate. The second stage is the second stage, which proceeds at a constant rate. Furthermore, finally, the tertiary stage that happens at an increasing rate and termination in fracture. [58]

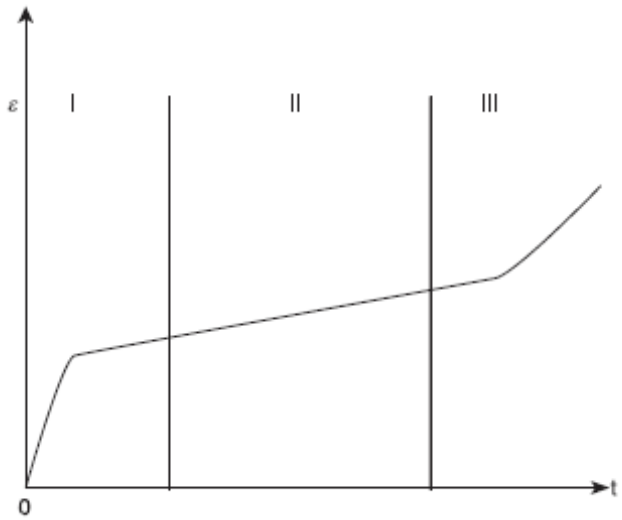

Figure 7. Creep stages

An immediate strain (ε_0) related to the applied stress is detected after the stress, and this is followed by a progressive increase in the strain, as shown in Figure 8b. The total strain at any instant of time is represented as the sum of the instant elastic strain and the creep strain, i.e.,

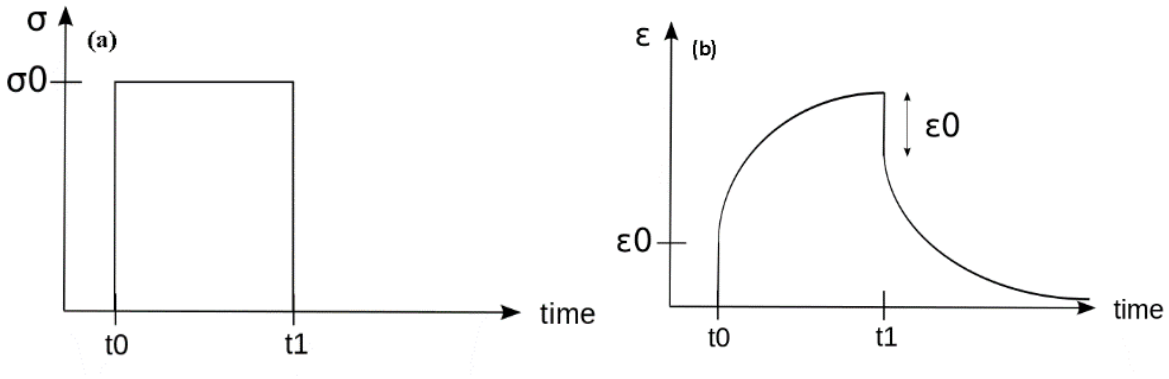

Figure 8. Creep: (a) application of constant stress; (b) strain response.

$$\varepsilon(t) = \varepsilon(0) + \varepsilon(c) \quad (14)$$

Creep compliance is the ratio of the total strain ε (t) to the applied constant stress $\sigma_{0,}$ which is given by:

$$j(t) = \frac{\varepsilon\,(t)}{\sigma_0} \quad (15)$$

The shear creeps compliance J(t) is strictly defined as the change in the strain as a function of time under the instant application of constant stress and provides a means to measure the capacity of a material to flow in response to suddenly applied stress. [59]

Linear viscoelastic models are used for non-Newtonian materials. All linear viscoelastic models are made up of linear springs and linear dashpots. The liner viscosity is a combination of spring and dashpot model, while the spring presents the elastic portion, and the dashpot presents the vicious portion. The scheme of the four-element model gives in Figure 9.

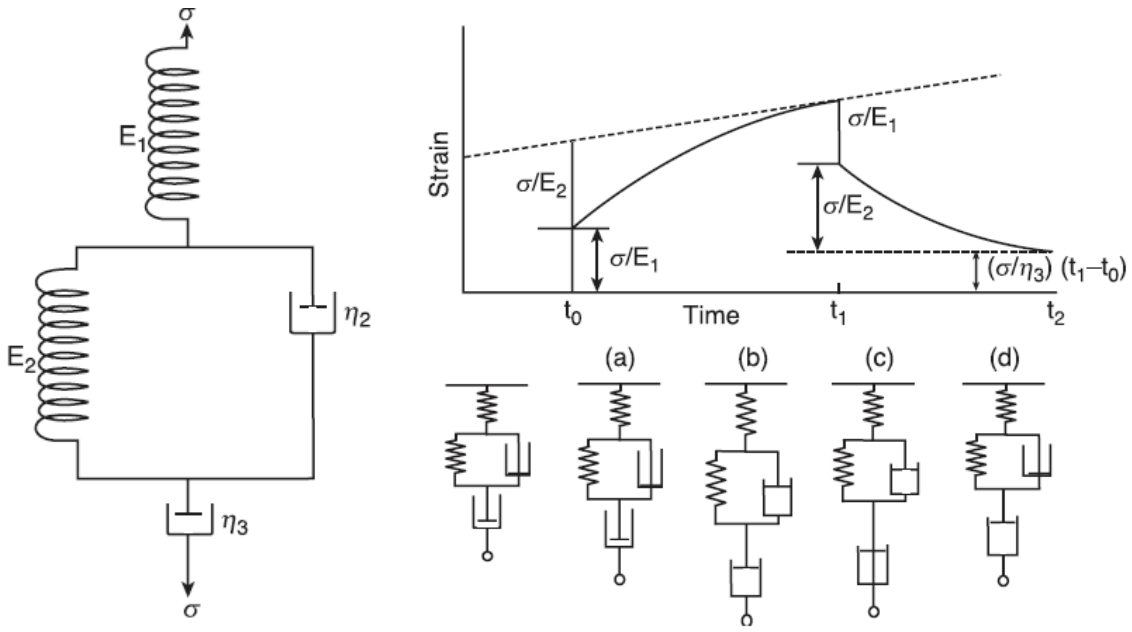

Figure 9. Creep-recovery behavior of a four-element model

The creep response can be obtained by adding the creep response of Kelvin and Maxwell's elements in the combine to obtain:

$$\varepsilon(t) = \sigma_0 \left[\frac{1}{\mathrm{E}_0} + \frac{1}{E_1}\left(1 - e^{-\frac{t}{\tau}}\right) + \frac{1}{\eta}\right] \quad (16)$$

$$\tau = \frac{\eta}{E} \quad (17)$$

Where E_0 and η are the modulus and viscosity of the Maxwell spring and dashpot, respectively; E is the modulus and viscosity of the Kelvin spring, respectively; σ_0 is the initially applied stress; τ is the retardation time taken to produce 63.2% or $(1 - e^{-1})$ of the total deformation in the Kelvin unit.

Here, the behavior shown represents the most general behavior possible for a viscoelastic material, instant elasticity, delayed elasticity, and flow.

4.4. Frequency Sweep

Storage modulus (G′) and loss modulus (G″) is calculated as a function of shear strain (γ %). In the frequency sweep test, a small amplitude oscillatory shear, $\dot{\gamma} = \gamma_o \sin(\omega t)$ is applied to the samples. Resulting shear stress is calculated as:

$$\sigma(\mathrm{t}) = \gamma_o[G'(\omega)\sin(\omega t) + [G''(\omega)\cos(\omega t)] \quad (18)$$

And G′, G″ and dynamic viscosity (η*), which measured as a function of angular frequency (ω) in the range of 0.1–100 rad/s at a strain value in the linear viscoelastic region.

4.5. Dependence of losing factor (tan δ)

Dependence of loss factor (tan δ) and complex viscosity |η*| of the samples on frequency are a model to observe the viscoelastic compound negative slope's behavior in the Tan δ curve is a normal behavior of viscoelastic. In contrast, the positive slope refers to the elastic response of the viscoelastic samples dominating this elastic behavior.

$$\tan\delta = \frac{G''}{G'} \quad (19)$$

The dynamic viscosity is defined by [60]

$$\eta'' = \frac{G'}{\omega} \quad (20)$$

And the elastic part of the complex viscosity:

$$\eta' = \frac{G''}{\omega} \quad (21)$$

$$|\eta^*| = \left(\eta'^2 + \eta''^2\right)^{\frac{1}{2}} \quad (22)$$

The power-law equation is written as:

$$|\eta^*| = k\omega^n \quad (23)$$

Where $|\eta^*|$ is complex viscosity, k is a sample-specific pre-exponential factor, ω is the oscillation frequency in the frequency sweep test, and n is the shear-thinning exponent, which can be directly calculated from the logarithmic plot of complex viscosity $|\eta^*|$ vs. frequency (ω) as

$$log|\eta^*| = \log k + n\log(\omega) \quad (24)$$

The shear-thinning exponent, n, is the straight-line slope obtained by plotting log $|\eta^*|$ vs. log ω. [20, 61, 62]

4.6. Theoretical Models to Describe the Molecular Behavior

There are several theoretical models to describe the molecular behavior of filled composites. The earliest theory was Einstein's hydrodynamic theory for the viscosity of colloidal suspensions. Einstein model describes an increase of viscosity due to the addition of rigid spherical particles. This model was modified for nonspherical particles, such as fibers. In fibers, the length to diameter (L/D) aspect ratio plays an important role. [63, 64]. Guth and Gold generalized Einstein's by replacing the viscosity with elastic modulus. However, different shapes and sizes of fibers can lead to an unexplained and unpredictable modulus and aggregates in the matrix. The modified equation of Guth and Smallwood [65]

Guth and Gold's model is shown in Equation 25. The equation is designed for spherical particles [66].

Gm=unfilled modulus

$$\frac{Gc}{Gm} = (1 + \ 2.5\Phi \ + 14.1\Phi^2) \quad (25)$$

Where: Gc = Shear modulus of the composite

Gm = shear modulus of the gum

Φ = volume fraction of the filler

Calculation of volume fraction (ΦA) from weight fraction w_A

$$w_A = \frac{m_A}{m_A + m_B} \quad (26)$$

Furthermore, since:

$$V_A = \frac{m_A}{\varrho_A} \quad (27)$$

So

$$\phi_A = \frac{V_A}{V_A + V_B} = \frac{\frac{m_A}{\varrho_A}}{\frac{m_A}{\varrho_A} + \frac{m_B}{\varrho_B}} \cdot \left[\frac{\frac{1}{m_A + m_B}}{\frac{1}{m_A + m_B}}\right]$$

$$= \frac{\frac{m_A}{\varrho_A \cdot (m_A + m_B)}}{\frac{m_A}{\varrho_A \cdot (m_A + m_B)} + \frac{m_A}{\varrho_A \cdot (m_A + m_B)}} = \frac{\frac{w_A}{\varrho_A}}{\frac{w_A}{\varrho_A} + \frac{w_B}{\varrho_B}} \quad (28)$$

Thus reinforcement factor $\frac{Gc}{Gm}$ is dependent only on the volume fraction of spherical filler in a lower concentration. At a higher concentration of the filler, it is observed that the reinforcement factor increases rapidly more than predicted by the equation. This is attributed to network formation or organization of filler particles

into chain-like structures. To account for the "accelerated stiffening" caused by these chains- like or non-spherical fillers. Guth-Smallwood shape factor (f) for non-spherical particles and since the f>1, the reinforcement factor will increase rapidly by increasing the fiber content.

$$\frac{Gc}{Gm} = (1 + 0.67\, f\, \Phi + 1.62 f^2 \Phi^2) \quad (29)$$

Where: f = shape factor

4.7. Thermal conductivity

The Fitch (1935) method is used to determine composites' conductivity [29], where the specimen is a sandwich between a warm source and a steady temperature metal barrel as a heat sink. The schematic of the instrument used for thermal conductivity measurement can be seen in Fig 10.

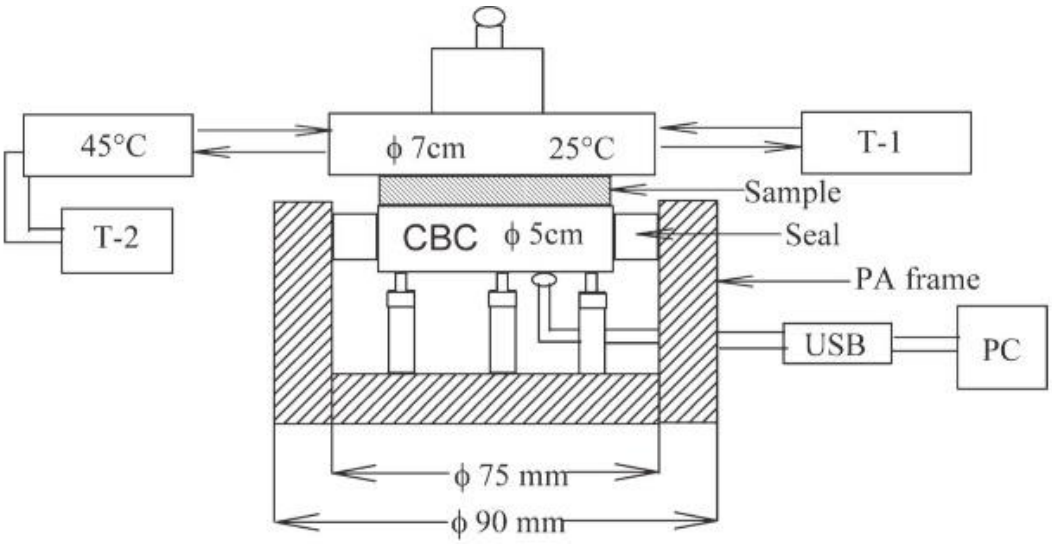

Figure 10. Schematic diagram of the apparatus used for thermal conductivity measurement

The dependence of temperature on time is described with the following equation. [67]

$$-K\frac{dt}{d\tau} = \frac{S\lambda(t - t_2)}{\delta} + B(t - t_2) \quad (29)$$

Where,

T_2 =45°C

T_1 =25°C

K = the central brass cylinder heat capacity which is 317.5 J/k in our work

S = sample area (m^2)

λ = thermal conductivity (W m^{-2} K^{-1})

T = EBC/CF temperature (°C)

T_1 = hollow brass cylinder temperature 25 (°C)

T_2 = CBC initial temperature (°C)

δ = specimen thickness (m)

B = coefficient accounting for a heat loss (J s^{-1} K^{-1})

τ= time (s)

B is calculated according to

$$B=\alpha S_z \quad (30)$$

Where

α = heat transfer coefficient (W m^{-2} K^{-1})

Sz = heat loss area (m^2).

By solving Eq. 3:

$$T = T_1 - (T_1 - T_2) * e^{|-(A_1 - A_2)\tau|} \quad (31)$$

Where:

$$A_1 = \frac{S.\lambda}{\delta.K} \ , A_2 = \frac{B}{K} \quad (32)$$

However, equation 5 can be simplified with exponential growth with three parameters as:

$$y = y_0 + ae^{(-bx)} \quad (33)$$

The coefficient b is obtained from the nonlinear regression.

4.8. Electric conductivity

Electrically conductive composites with a thermoplastic matrix are considered an essential group of relatively inexpensive materials for special applications such as sensors, detectors [68]. Conductivity in a highly insulating matrix is achieved by the admixtures of conductive additives, for example, fine metal powders or conductive polymers. [69] Carbon-based filters (carbon black, graphite, or carbon fibers) are the most frequently used conductive fillers because of their high conductivity, relatively low price, and good ultimate and processing properties. [8, 70]

Tensile deformation and a gauge factor of the composite were determined by a two-point technique to measure the electric resistance and strain. In this research, the change of electrical resistance is defined as [67]

$$\Delta R = \frac{\mathrm{R} - \mathrm{R_0}}{\mathrm{R_0}} \quad (34)$$

Where

R_0= the initial electrical resistance of the sample before the first elongation

R= the resistance during elongating

And elongation is defined as:

$$\varepsilon = \frac{L - L_0}{L_0} \quad (35)$$

Where L_0 represents the initial length of the specimen while L is the length during stretching experienced.

Slobodian et al. has studied the effect of Multi-walled carbon nanotubes (MWCNTs) on polyurethane. They investigated that the local contact forces between nanotubes probably decreased during elongation, allowing a worse contact of nanotubes and increasing their contact resistance. Also, the distance between contacts may increase during elongation due to nanotubes' evoked relative motion, which corresponds to nanotube segments' higher intrinsic resistance between contacts. Finally, the elongation may also straighten the nanotubes, which results in fewer contacts between nanotubes. Since the contact points may act as parallel resistors, their decreasing number causes an enhancement of MWCNT network resistance [71].

Nevertheless, Abot *et al*. found out that carbon nanotube yarns' addition exhibits negative piezo impedance used for sensing purposes. They found that, when the CNT yarns are deformed, the yarn's forces are sustained and transmitted through the nanotube contact points. They thus determine the electrical connectivity between the nanotubes. As the CNTyarn is subjected to tension, the nanotubes that comprise the

yarn are brought closer together, reducing the voids between them. As the nanotubes come into closer contact, the electrical resistance decreases as the interfacial resistance decreases [19].

Naghashpour and Van Hoa have done the electromechanical of glass fiber/epoxy composite laminated by carbon nanotube sensors. The researchers investigated that reduction in thickness was thought to reduce the distance between the crossing CNTs. This would reduce the tunneling resistance between the crossing CNTs and reduce the through-thickness electrical resistance (TTER). However, an increase in TTER was observed, which can be the separation of CNTs due to the lengthwise load, as shown in Figure 11b [72].

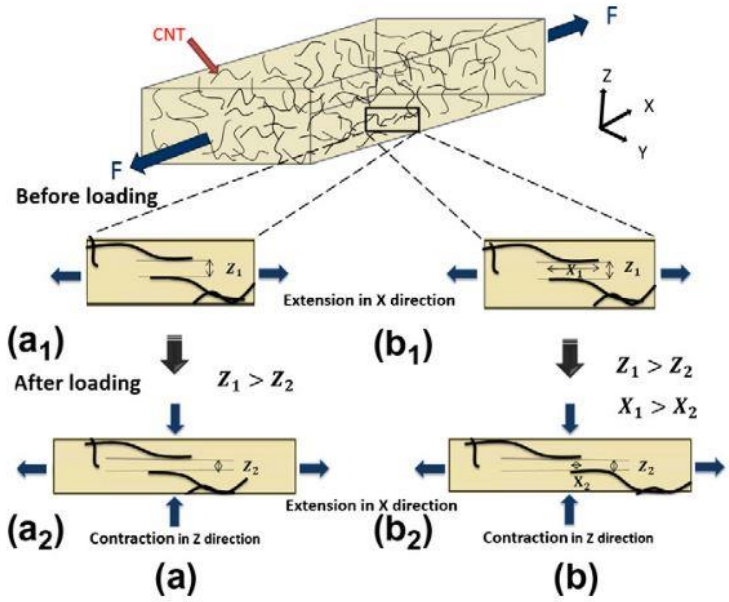

Figure 11. Poisson coupling reduces the laminate thickness. Schematic illustrating (a) reduction of the tunneling distance between crossing CNTs (a1 and a2 before and after loading) and (b) one possible explanation for the increase in TTER (b1 and b2 before and after loading).

4.9. Gel content

An electron beam cross-linked gel contents are obtained by calculating the insoluble cross-linked material after extracting the solvent. A tiny amount of cross-linked material is wrapped in a stainless steel cage and placed in a boiling solvent[73]. The gel content is calculated as the percent ratio of the final weight to the sample's initial weight multiplied by one hundred.

5. Experiment:

Electron beam irradiation

Electron beam irradiation was applied at room temperature in BGS Beta-Gama-Service Gmbh, Germany. The process is controlled not to surpass 50 °C. The source of radiation is toroid electron accelerator Rhodotron (10 MeV, 200kW). The irradiation is applied in a tunnel on a moderately moving conveyor with the irradiation dosage ranging from 60 to 180 KGy (30 KGy per pass) with 3m/min belt speed and 10 mA with 78 cm sample distance from the scanner for 2-second irradiation.

5.1. Optical microscopy

Carbon fiber's dimensions are evaluated with optical microscopy using an Olympus RX41 microscope (Tokyo, Japan) to calculate the aspect ratio (L/D length over diameter) of carbon fiber in the composite.

5.2. Gel content

The gel contents of electron-beam cross-linked EVA samples were obtained by calculating the insoluble cross-linked material after extracting the solvent according

to ASTM D2765-01. A small amount of cross-linked material (about 0.15 g) was wrapped in a stainless steel cage and placed in boiling xylene solvent for 6 h with 1 wt.% of an antioxidant. The sample was weighted after the evaporation of the solvent. Finally, the gel content was calculated as the percent ratio of the final weight to the sample's initial weight multiplied by one hundred.

To calculate the starting gel dose and the radiation chemical yield of crosslinking and scission, the widely accepted Charlesby-Pinner equation was used

$$s + \sqrt{s} = \frac{p_0}{q_0} + \frac{1}{q_0 P_n D} \quad (36)$$

$$In\ plot \quad s + \sqrt{s} \quad vs.\ \frac{1}{D}: \quad intercept = \frac{p_0}{q_0},\ \ slope = \frac{1}{q_0 P_n}$$

Where p_0 and q_0 are the chain scission and crosslinking density per unit dose in kGy^{-1} respectively, P_n is the average number degree of polymerization before irradiation, and D is the irradiation dose in KGy

5.3. Electric resistance

The electrical resistance changes of change in strain-relaxation cycles were analyzed with precise weight using the two-point technique. The test was done using various forces (1, 2, 3, 4, 5 N) for 5 minutes to measure the strain and electric resistance change in time. The change of resistance was measured with the Vernier LabQuest Interface System (VLQIS) connected to the Differential Voltage Probe and the Wheatstone bridge with sampling frequency 200Hz.

5.4. Dynamic Mechanical Analysis (DMA)

METTLER Toledo Switzerland performed the dynamic mechanical analysis. Samples with dimensions of 11 × 11 × 0.5 mm were tested for creep-relaxation, stress-strain, and frequency sweep. The stress-strain was performed in a force range 0 to 2 N with a 0.4 N/min force rate at 150C. The creep relaxation was measured in three steps. At first, the sample is placed in the DMA machine for 1 min at 150 °C under 0.05 N. The sample was then under the creep test for 5 min at 150 °C under 1 N force. Finally, the force dropped to 0.05 N for 5 min at 150 °C for relaxation. The frequency sweep test was done at 150 °C with a preload force of 0.1 N in the frequency range 0.1 to 100 Hz by 10 steps per decade with 10 μm displacement.

5.5. Thermal conductivity

The process of measurement and the instrument are explained below. At first, the 5 cm diameter central brass cylinder (CBC) is bound to reach t_2 =45°C with another chamber's assistance related to an indoor water regulator by elastic hoses with a water thermostat with 0.1°C accuracy. This takes about 3 minutes to reach a suitable temperature. Then the hot chamber is quickly removed. The sample with a 5 cm diameter is placed on top of CBC with a second brass cylinder on the top with a weight of 100g, which is connected to a second water thermometer with the temperature set to 25° C.

The heat transfer from the hot CBC to the cold cylinder while going throw the sample. The CBC temperature is reducing quickly. The CBC data is collected every 5 s for 30 min by a thermocouple associated with a National Instruments information obtaining hardware (NI USB-9211A, Portable USB-Based DAQ (Data Acquisition))

for Thermocouples software and following to the computer using the USB port. [74] The data was analyzed using LabVIEW signal Express 2.5.

6. Materials

6.1. Long Carbon Fiber

The fiber is produced by treating an acrylic fiber precursor, with pyrolysis, surface treatment, and sizing processes. Each bobbin of Torayca (Toray Carbon Fibers America) from Japan carbon fiber is protected against dust and packed in the container to prevent damage during transportation. This never twisted fiber is used in the high tensile application. The specification of fiber is given in table 2.

Table 2. Carbon fiber properties

Tensile Strength	2,450 MPa
Tensile Modulus	125 GP
Strain	2.1%
Density	1.8 g/cm3
Filament Diameter	7 µm

6.2. Carbon Black fiber

The conductive Carbon Black (KETJENBLACK EC300J) with the composition of 10wt% polycarbonate with 99.95% purity is used for this study were purchased from Akzo Nobel Polymer Chemicals Ltd. Shanghai, PR China, with a bulk density of 0.125-0.145 g/cm^3 and apparent density of 2.26 g/cm^3, pore volume (DBP) 310-

345 ml/100 g and 3.9Ω·cm. This CB is mainly used as an electro-conductive filler used in resin compounds, electro-conductive battery materials, paint, colorant, and toner.

6.3. Ethylene-vinyl acetate (EVA)

Ethylene-vinyl acetate with trade name Supreme Ultra FL 00328 was used. ExxonMobil Chemical Belgium supplied it (Antwerp Belgium) the melt flow index (MFI) is 3.0 g/10 min and density 0.951 g/cm^2; with 28 wt.% of vinyl acetate.

6.4. Ethylene-Butene Copolymer (EBC)

Ethylene-butene copolymer (ENR 7467) was purchased from DOW Engage® chemical company in the USA with specific properties like ultimate tensile strength 2 MPa, tensile elongation of 600%. The melt flow index (MFI) is 1.2 dg/min and 0.862 g/ cm^3

6.5. Preparation of materials:

Ethylene-vinyl acetate and Ethylene butyl copolymer with carbon fiber were mixed and homogenized with different concentrations (5, 10, 15, 20, 25 wt.%) using a two-roll mill at 150 °C for 5 min. Following, a sheet with a thickness of 0.5 mm was prepared by compression molding at 150 °C and 10 MPa for 5 min preheating and 5 min pressing. Finally, the cold press was used for 10 min with 10 MPa pressure. In the end, the prepared samples were cut into the dumbbell shape for the creep test. The porosity density was measured according to Archimedes method ASTM B962-15 and was found to be less than 1% which is acceptable.

The same process is performed for Ethylene butyl copolymer and carbon black.

6.6. Electron-beam irradiation

Electron-beam irradiation was applied at room temperature in BGS Beta-Gama-Service Gmbh, Germany. The process was controlled not to surpass 50 °C. The source of radiation was toroid electron accelerator Rhodotron (10 MeV, 200kW). The irradiation was applied in a tunnel on a moderately moving conveyor with the irradiation dosage ranging from 60 to 180 KGy (30 KGy per pass) with 3 m/min belt speed and 10 mA with 78 cm sample distance from the scanner for 2-second irradiation.

6.7. Dynamic mechanical analysis (DMA)

METTLER Toledo Switzerland performed the dynamic mechanical analysis. Samples with dimensions of 11×11×0.5 mm were tested for creep-relaxation, stress-strain, and frequency sweep. The stress-strain was performed in a force range 0 to 2N with a 0.4 N/min force rate at 150 °C.

The creep relaxation was measured in three steps. At first, the sample was placed in the DMA machine for 1 min at 150°C under 0.05 N. The sample was then under the creep test for 5 min at 150 °C under 1N force. Finally, the force dropped to 0.05 N for 5 min at 150 °C for relaxation.

The frequency sweep test was done at 150 °C with a preload force of 1 N in the frequency range 0.1 to 100Hz by 10 steps per decade with 10 μm displacement. Higher frequency than 100 Hz is not recommended as all the specimen sizes except the one with 1 mm thickness are not useful due to their higher demand of displacement which the piezoelectric actuator is not capable of providing [75]

6.8. Gel content

The gel contents of electron-beam cross-linked EVA samples were obtained by calculating the insoluble cross-linked material after extracting the solvent according to ASTM D2765-01. A small amount of cross-linked material (about 0.15 g) was wrapped in a stainless steel cage and placed in boiling xylene solvent for 6 h with 1 wt.% of an antioxidant. The sample was weighted after the evaporation of the solvent. Finally, the gel content was calculated as the percent ratio of the final weight to the sample's initial weight multiplied by one hundred.

6.9. Optical microscopy

Dimensions of carbon fibers were evaluated by optical microscopy using an Olympus RX41 microscope (Tokyo, Japan) to calculate the aspect ratio (L/D length over diameter) of carbon fibers in the composite.

6.10. Size-exclusion chromatography

The molecular weight measurement was performed at 160 °C on a Polymer Laboratories PL 220 high-temperature chromatograph (Polymer Laboratories, Varian Inc., Church Stretton, Shropshire, England) equipped with three 300 mm x 7.5 mm PLgel Olexis columns and a differential refractive index detector. 1,2,4-trichlorobenzene (TCB) was used as eluent, stabilized with butylhydroxytoluene (BHT) (Ciba, Basel, Switzerland) as an antioxidant. A mobile phase flow rate of 1 mL min^{-1} was used, and the volume of 200 mL was injected. The sample was prepared to a concentration of 0.5 mg mL^{-1} in TCB. Narrowly distributed polyethylene standards (Polymer Standards Service GmbH, Mainz, Germany) were used for calibration purposes.

6.11. Electric resistance

For electrical characterization, several methods are used. The two-point probe method using a digital multimeter and four-point probe method using Hall effect measurements is more common[76]. However, due to four-probe measurement limitations during the starching, the change EBC/CB's electrical resistance change in strain-relaxation cycles was analyzed with precise weight using the two-point probe technique. Two single-terminal electrodes are attached to the surface of the conductive structure called the two-point probe technique. A DC or AC source current is then connected through the two electrodes, and the subsequent voltage over the same electrodes is estimated. The electrical resistance between these two electrodes is then determined, according to Ohm's law.

To increase the results' reliability, copper plates used as electrodes were attached to the sample, dissolved the backing adhesive, flooded into butanone solution, and then washed using tap water. After drying and cleaning copper plates, the pellets were sandwiched with upper and lower Ag's electrodes using silver paint around the surface of dumbbell specimens. The test was done using various forces (1, 2,3,4,5 N) for 5 min to measure the strain and electric resistance change in time. When the samples were ready, an electrical circuit powered by a DSC power source was applied to the DC source was used for the tests for its simplicity. However, it is worth to mention that in reality, 1 kHz is commonly used to prevent polarization inaccuracy. The change of resistance was measured with the Vernier LabQuest Interface System (VLQIS) connected to the Differential Voltage Probe and the Wheatstone bridge with sampling frequency 200Hz.

7. Influence of carbon fibers on ethylene-vinyl acetate (EVA)

The influence of carbon fibers and radiation on shear stress creep compliance and frequency sweep of ethylene-vinyl acetate (EVA) was investigated by dynamic mechanical analysis. The addition of carbon fiber into EVA leads to a significant increase in shear stress (see Figure 12). This behavior is similar to the one reported by Das *et al*. [77].

The shear stress of the EVA composites with a content of 20 wt.% of carbon fiber has the highest value. In contrast, the pure EVA has the lowest shear stress at the same shear strain (such as at 0.10 strain, the values are about 0.004 and 0.007 MPa for 0 and 20 wt.% of CF, respectively), due to the improved interfacial action [78]. Hamid *et al*. reported that fiber could significantly improve stiffness by hindering the matrix [79].

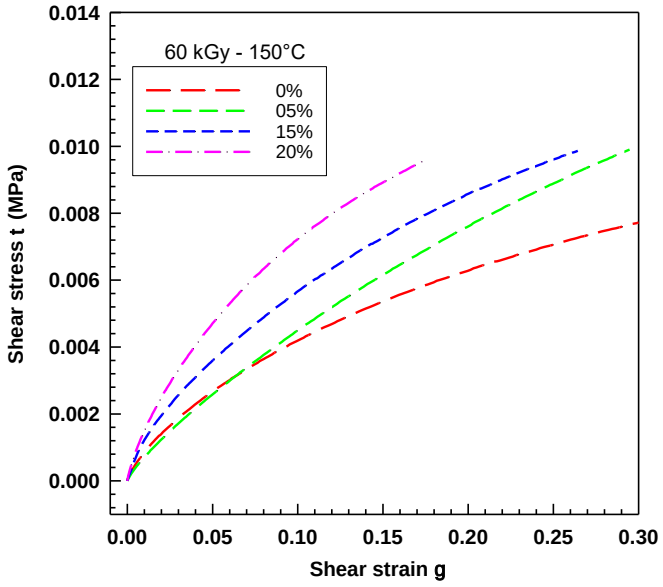

Figure 12. Shear stress-strain curves of EVA/CF composites

The increase of shear modulus as a function of increasing CF content is illustrated in Fig 12. The highest values of G' were found for the sample irradiated by 180 KGy. These results are in agreement with other scientists. An increase in G' due to an increasing volume fraction of carbon nanotubes was reported, e.g., by Potschke *et al*. [80]. An increase in G' values at 0.1 rad s^{-1} due to increasing e-beam radiation for ethylene-octene copolymer was reported, e.g., by Poongavalappil *et al.* [81].

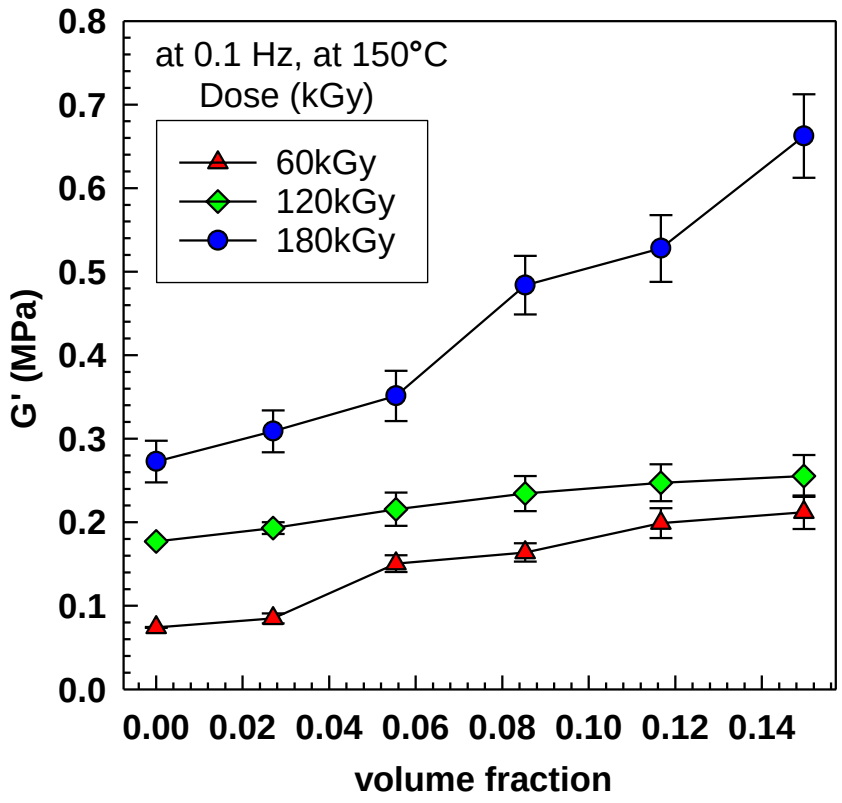

Figure 13. Experimental relative G' at 150 °C at frequency 0.1 rad/s

To calculate the relative G' increase, it is necessary to calculate the fiber's volume fraction in the composite. The volume fraction is calculated according to equation 28, while the densities of CF and EVA 328 are 1.80 g/cm^3 and 0.951 g/cm^3, respectively.

The densities of the composites were calculated according to these equations:

$$V_A + V_B = V_{comp} \quad (37)$$

$$\rho = \frac{m}{V}, \; V = \frac{m}{\rho} \quad (38)$$

$$\frac{m_A}{\rho_A} + \frac{m_B}{\rho_B} = \frac{m_{comp}}{\rho_{comp}} \quad (39)$$

$$w_A = \frac{m_A}{m_{comp}} \;\; , \;\; w_B = \frac{m_B}{m_{comp}}, \;\; w_A + w_B = 1 \quad (40)$$

$$\frac{m_A}{\rho_A} + \frac{m_B}{\rho_B} = \frac{m_{comp}}{\rho_{comp}} \cdot \left[\frac{\frac{1}{m_{comp}}}{\frac{1}{m_{comp}}} \right]$$

$$\frac{w_A}{\rho_A} + \frac{w_B}{\rho_B} = \frac{1}{\rho_{comp}}$$

$$\rho_{comp} = \frac{1}{\frac{w_A}{\rho_A} + \frac{w_B}{\rho_B}}$$

Densities of the composites and volume fraction are listed in Table 3. These values are in a good agreement (within $\pm 3\%$) to the experimentally obtained values (by pycnometer).

Table 3. Shear modulus in Experimental, Guth- Smallwood for spherical and non-spherical filler equation

Wa	**Φa**	**Density (g/cm3)**	**Experimental at 0.1 Hz**	**G =Gm (1+ 2.5Φ +14.1Φ2)**	**Gc =Gm (1 +0.67 f Φ +1.62f 2Φ2)**
0	0	0.951	0.074	0.074	0.074
0.05	0.02705	0.97	0.0849	0.07977	0.1100

0.1	0.05545	1	0.1505	0.08747	0.1847
0.15	0.08528	1.02	0.1638	0.09737	0.3040
0.20	0.11667	1.05	0.1990	0.10979	0.4748
0.25	0.14974	1.08	0.2119	0.14974	0.7044

The volume fraction, density of each composite, experimental (see Fig.14), Guth – Gold for spherical, and Guth-Smallwood for non-spherical particles are calculated according to equation 29 shown in Table 3.

Many attempts have been made to incorporate interactions between neighboring particles to predict predictions at higher volume fractions. Most of these models add one or more terms to a polynomial series expansion of the amplification factor. One of the most cited models of this class is the Guth and Gold [1938], which can be seen in Equation 25.

One of the most used models of this type is the Guth model developed for rod-like shapes characterized by the ratio of the length to the particles' width or the filler aggregate structures into which the particles cluster. This model attempts to account for the fact that particle aggregation (clustering) has a significant impact on stiffness at higher volume fractions (i.e. vf > 0.15); in practice, *f* is typically between 4 and 10 which essentially makes this model similar to the Guth-Gold model but with a much higher coefficient on the quadratic term, thus further amplifying the aggregation or “shape” effect at higher volume fractions according to Equetion 29. To illustrate the modulus of EVA-CF composite, the aspect ratio of

carbon fiber should be determined. Fig.3 shows the comparison between the experimental modulus with Guth-Gold for spherical and Guth-Smallwood for non-spherical particles. It indicates that the non-spherical Guth-Smallwood is closer to the experimental data at lower concentrations; however, the Guth-Gold model is closer is closer in higher concentration.

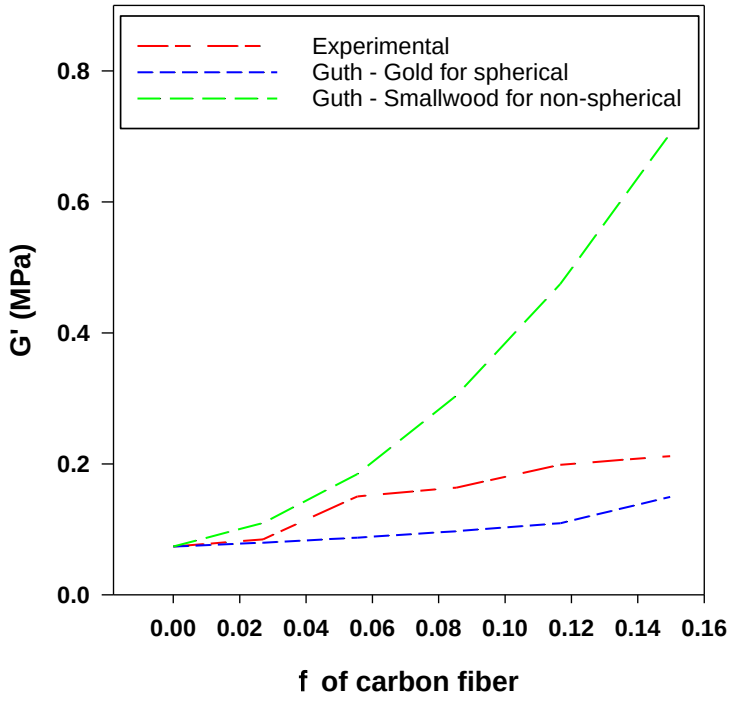

Figure 14. Prediction of modules with Guth- Smallwood for spherical and non-spherical filler vs. experimental

The correlation of experimental increase in modulus with theoretical predictive models was well illustrated, e.g., by Mandal *et al*. [82]. The statistical data of the aspect ratio for EVA/CF composite are shown in Fig.15b. This data was obtained from various electronic microscope photographs of EVA in Fig.15a having different CF contents, i.e., 5-20wt%.

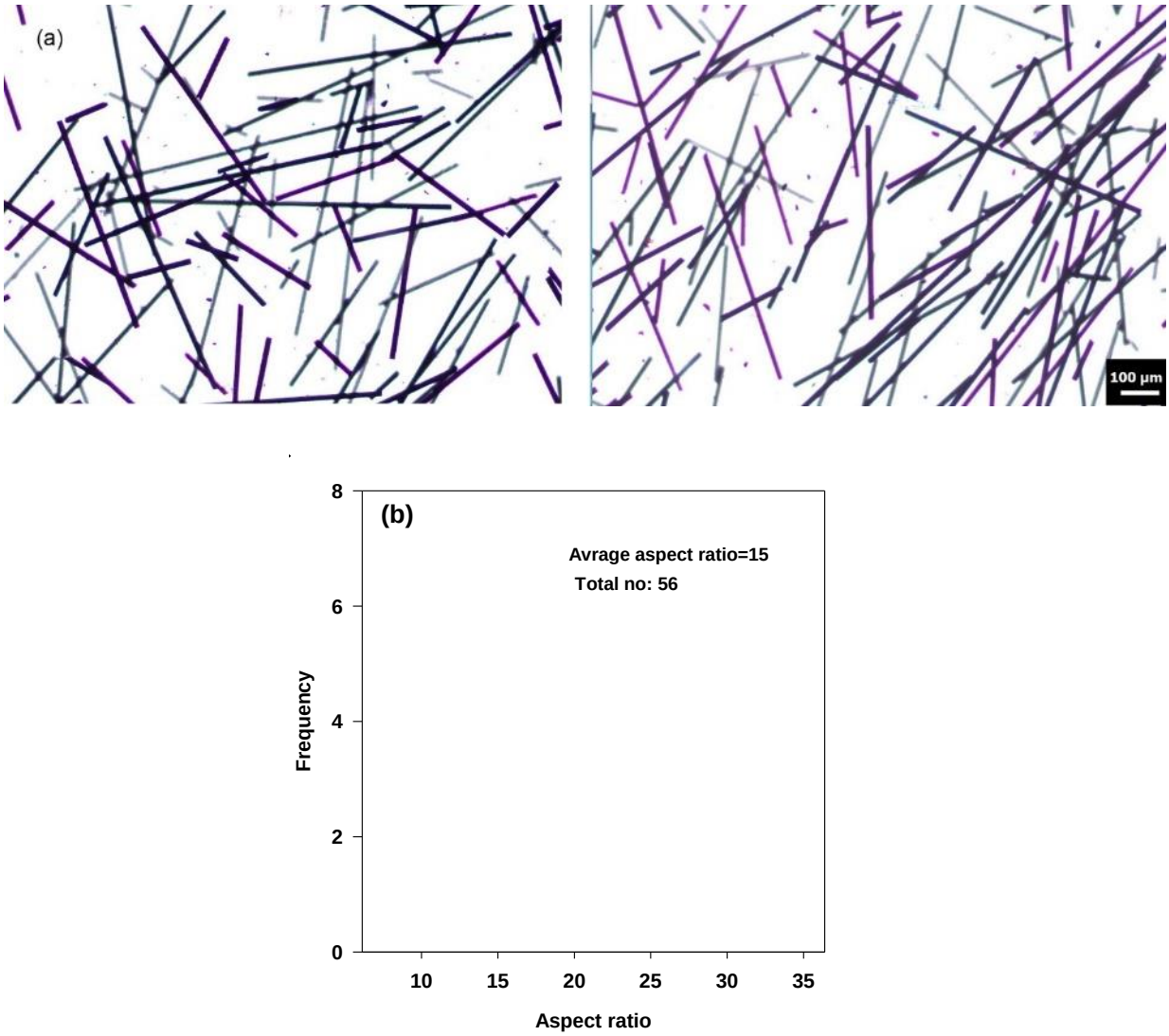

Figure 15. a) Optical microscope image of EVA-CF, b) Histograms of the aspect ratio of carbon fiber in EVA-CF composites

The effect of irradiation dose on shear stress at 0.03 shear strain is visible in Fig16 b. It is also common throughout the rubber industry to observe M100 modules and M300 of the modulus (at 100 and 300% elongation), and our choice was the stress at 0.03 shear strain. The graph indicates that EVA with a higher dose exhibited higher shear stress because EVA with a higher dose contains more radiation cross-links than the lower dose. It was observed that the shear stress of EVA with 5 wt. % of carbon fiber was following an exponential rise with R^2=0.999 regression. As demonstrated

in Fig16 a, an addition of CF fiber with a higher radiation dose can enhance the shear stress, since CF as a filler and crosslinking can improve the stiffness by restricting the movement of the matrix [83, 84]. Improvements in physical and mechanical properties of electron beam irradiation cross-linked EVA foams were also reported by Rezaian *et al*. [85]. Mechanical changes of electron-beam irradiated EVA film were reported by Matsui *et al*. [86].

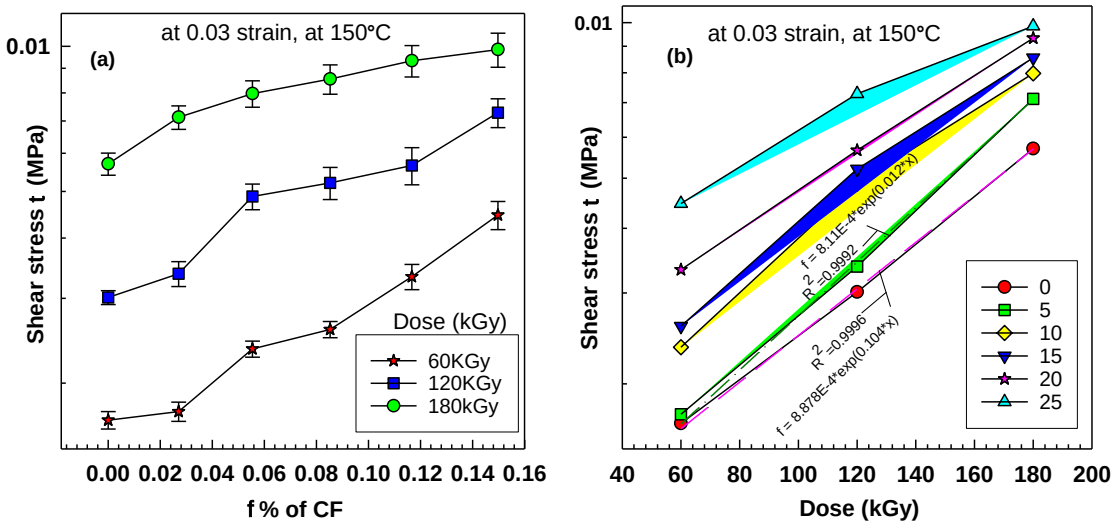

Figure 16. a) Shear stress vol.fr. Of CF b) shear stress–dose curves of EVA/CF composites

The development of creep in time is shown in Fig17 a. The addition of carbon fiber to EVA causes a reduction of the creep. It indicates that the addition of 20 wt. % of CF caused almost three times lower creep compared to pure EVA. The graph also shows that the creep decreases with the addition of carbon fiber, and the rate of the creep (slope) decreases from 26 to 11 for pure EVA and 20 wt. % of carbon fibers, respectively. Fig17 b suggests a systematic decrease in creep with increasing the CF fibers' content after 5 min and after recovery observed after 10 min. Our

results follow the trend of other researchers. Creep reduction due to Nanofillers' addition was reported, e.g., by Shokrieh *et al*. [87].

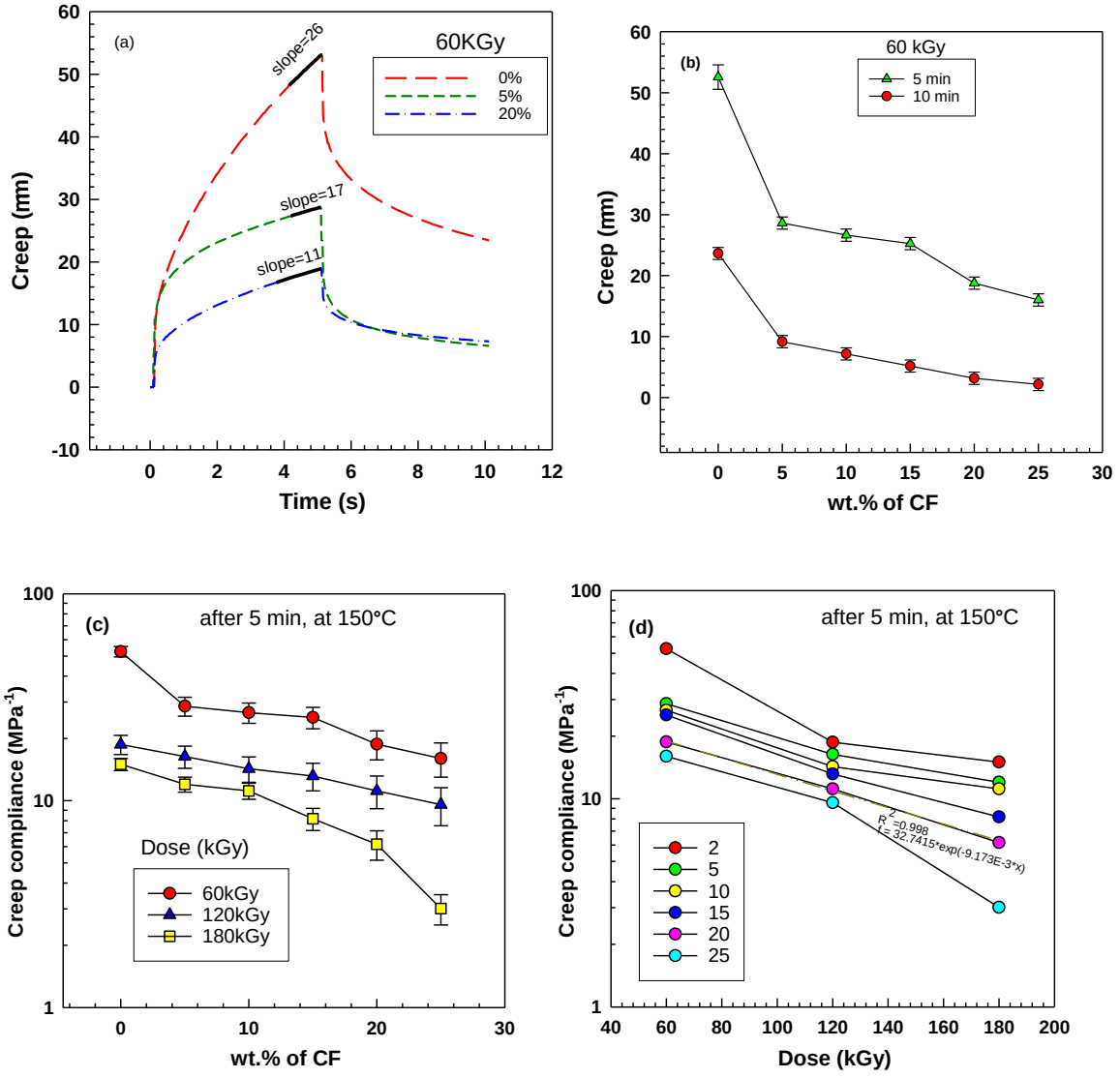

Figure 17. a) creep–time b) creep (recovery)–wt. % curves of EVA/CF composite at 150 °C as a function of. c) wt. % of CF and d) dose (KGy) after 5 min.

Figs17 c,d shows the sensitivity of creep to CF content and radiation dose. The graph (Figure 17d) indicates a significant decrease in creep with a radiation dose (KGy). It shows that EVA composite with a dose of 180 KGy has nearly seven times lower creep than a dose of 60 KGy, which is caused by crosslinking. We have found

an exponential decrease in creep compliance with increasing radiation levels in our previous study of the ethylene-octane copolymer [88]. Creep reduction with an increasing level of cross-linking (by the addition of peroxide) was also reported by Theravalappil *et al*. [53].

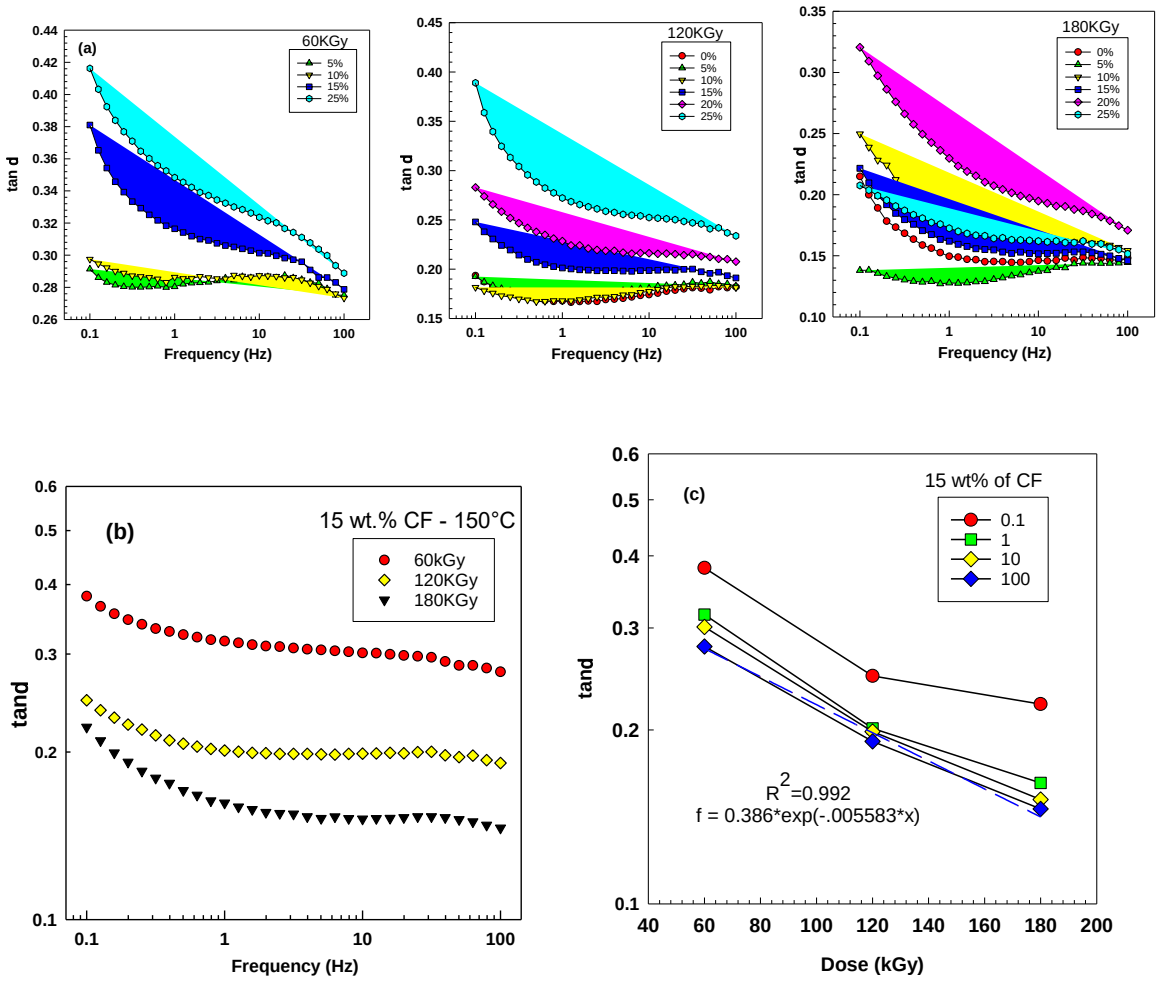

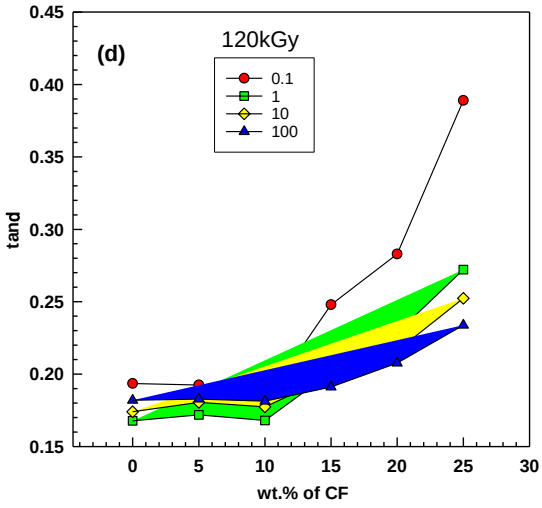

Figure 18. tan δ at 150 °C. a, b as a function of frequency, c)Dose 0.1 rad/s, d) of CF content

Fig.18 shows the tan δ vs. frequency, dose, and CF content. The graph indicates that the addition of fiber to EVA will increase the tan δ. The tan δ for EVA composite (120 KGy) with 25% CF content is nearly 0.4, while the pure EVA is around 0.2, followed by 0.25 and 0.3 for 15% and 20%, respectively. A decrease of tan δ value with increasing cross-linking levels due to the addition of peroxide was reported, e.g., by Poongavalappil *et al*. [52]. Tan δ values have dropped by raising the radiation level from 60 KGy to 180 KGy. That is caused by an increase in molecular weight, which hinders the free flow of the material. It is also evident that the tan δ of the composites decreases significantly with increasing frequency, as shown in Fig.18a and b. The influence of frequency on the tan δ is complex. The chain motion can be restricted with the change of the external force, and the internal friction is low at low frequency; so, the tan δ is low. While in our cross-linked EVA system, the CF has caused increase in tan δ McNally et al. (79) reported a decrease in tan δ values due to carbon nanotubes' addition uncross-linked PE. Figure 18c indicates the tan δ

change with the dose at all frequencies. It shows that with an increase of the dose, tan δ is decreasing for all frequencies.

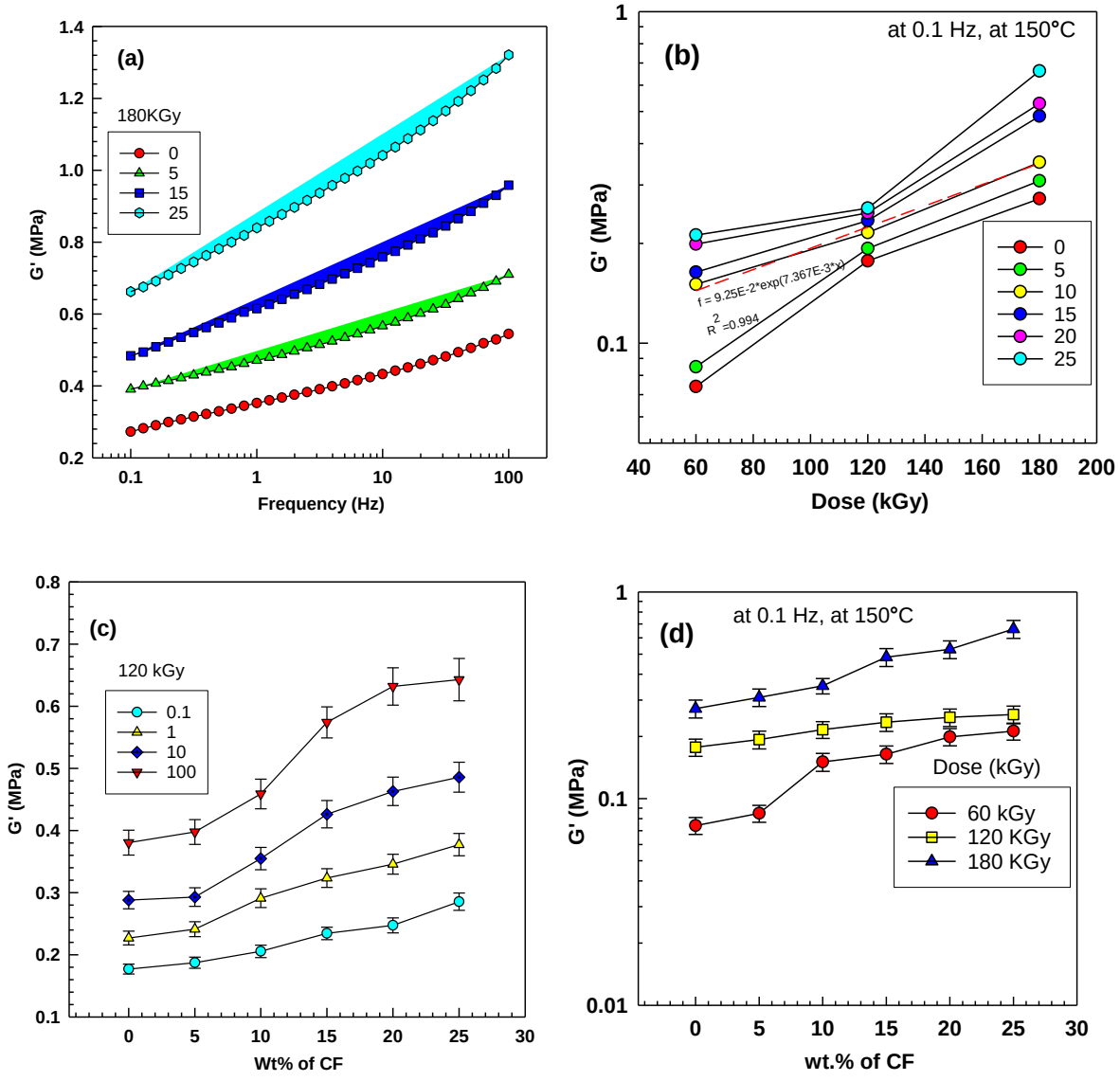

Figure 19. Shear modulus (real part) G' at 150 °C. a, b as a function of frequency, c and d for frequency 0.1 rad/s as a function of c)dose, d) carbon fiber content

Fig.19 shows the G' increases after irradiation. The increase of G' was observed in the irradiation dose-ranging 60-180 KGy. For the EVA 25 wt. % of carbon fiber, the increase of G' was higher. The highest increase of G' was found for EVA 25 wt.

% of carbon fiber (in the range 20-67 kPa). For the range of 60, 120, and 180 KGy, the G' values for pure EVA were 8, 17, and 28 KPa, respectively, and for EVA 15 wt. % of carbon fiber, they were 16, 23, and 43 kPa. An increase in G' due to the cross-linking was reported, e.g., by Mussatti and Macosko [89]. It has also been observed that fiber has an increased influence at a higher frequency. An increase in G' value due to the increasing level of carbon nanotubes was reported, e.g., by Potschke *et al*. [80, 90], and also due to the increasing level of graphene, e.g., by Kim and Macosko [91] or by Varghese *et al*. [92].

Calculation of G parameters according to Charlesby-Pinner equation [44, 93]

To calculate Charlesby-Pinner parameters, it is necessary to have molecular weight and gel content data for various levels of irradiation.

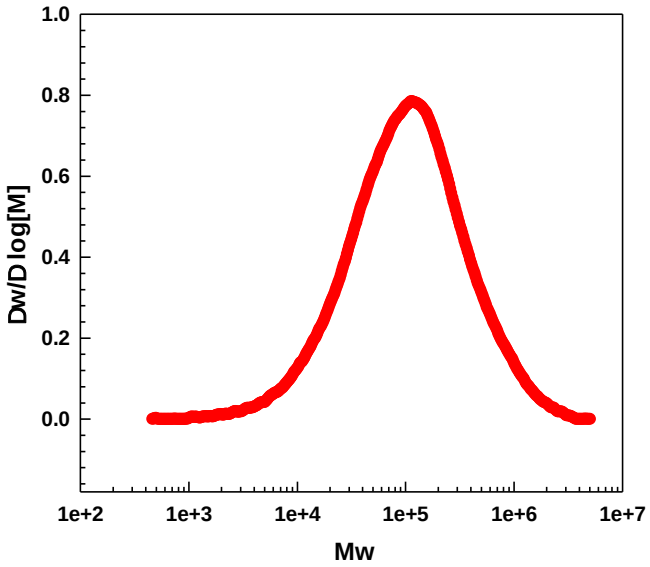

Figure 20. The molecular weight distribution of EVA

Figure 20 depicts the EVA molecular weight distribution using gel permeation chromatography (GPC). The graph shows that EVA's molecular weight in this study

is 300 to 5000000 g/mol. The peak position is around 100000 g/mol. The results from the GPC test are listed in Table 4.

Table 4.GPC results of EVA 328

Sample Name	Mp	Mn	Mw	Mz	Mz+1	PD
	g/mol					
EVA 328	113000	43400	196000	625000	1286000	4.5

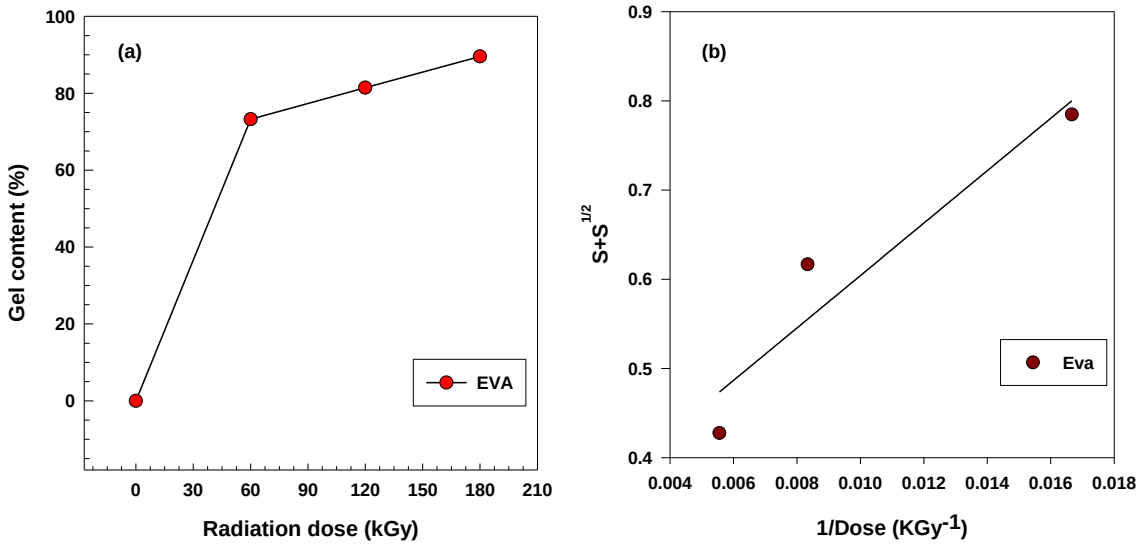

Figure 21. a) Gel content results for three radiation cross-linked EVA b) Charlesby–Pinner analysis

Fig.21 shows that increasing the radiation dose to 60 KGy caused an insoluble 3D network with gel content being 72 wt.%. In the radiation range 60–180 KGy, the gel content is increasing only moderately, as shown in Figure 21 for 72%, 81%, and 89%, respectively, which could be ascribed to the increase in molecular weight and

cross-linking. These results are in good agreement with Sharif *et al*. [94], who studied radiation effects on LDPE, EVA, and their blends.

Figure 21b was used in Charlesby-Pinner calculation, as shown below.

Calculation of the degree of polymerization

EVA 328 MFI=3, Vinyl acetate= 28%

$$etylen = -CH_2 - CH_2 -, \quad M_{ET} = 2 \cdot C + 4 \cdot H = 2 \cdot 12.011 + 4 \cdot 1.008 = 28.054\ g/mol$$

$$vinyl\ acetate = -CH_2 - CH(O - CO - CH_3) -, \quad M_{VA} = 4 \cdot C + 2 \cdot O + 6 \cdot H = 4 \cdot 12.011 + 2 \cdot 15.9994 + 6 \cdot 1.008 = 86.09\ g/mol$$

$$wt.fraction\ of\ vinyl\ acetate\ w_{VA} = \frac{28}{100} = 0.28$$

$$wt.fraction\ of\ ethylene\ w_{ET} = 1 - w_{VA} = 1 - 0.28 = 0.72$$

$$molar\ fraction\ of\ vinyl\ acetate = x_{VA}$$

$$x_{VA} = \frac{\frac{w_{VA}}{M_{VA}}}{\frac{w_{VA}}{M_{VA}} + \frac{w_{ET}}{M_{ET}}} = \frac{\frac{0.28}{86.09}}{\frac{0.28}{86.09} + \frac{0.72}{28.054}} = 0.1124717$$

$$molar\ fraction\ of\ ethylene = x_{ET} = 1 - x_{VA} = 1 - 0.1124717 = 0.8875283$$

$$average\ molecular\ weight\ of\ repeating\ unit$$

$$M_{ET-OCT} = x_{ET}M_{ET} + x_{VA}M_{VA} = 0.8875 \cdot 28.054 + 0.1125 \cdot 86.09 = 34.58\ g/mol$$

$$Polymerization\ degree = P_n = \frac{M_{nEVA}}{M_{ET-VA}} = \frac{43400}{34.58} = 1255$$

Charlesby-Pinner equation

$$s + \sqrt{s} = \frac{p_0}{q_0} + \frac{1}{q_0 P_n D} \quad (41)$$

$$In\ plot \quad s + \sqrt{s} \quad vs.\ \frac{1}{D}: \quad intercept = \frac{p_0}{q_0},\ \ slope = \frac{1}{q_0 P_n}$$

$$In\ case\ of\ EVA-28: \quad intercept = 0.3103,\ \ slope = 39.38$$

$$then \quad \frac{p_0}{q_0} = 0.3103 \quad and \quad \frac{1}{q_0 P_n} = 39.38$$

$$q_0 = \frac{1}{slope \cdot P_n} = \frac{1}{29.38 \cdot 1255} = 0.000027121$$

$$then \quad p_0 = q_0 \cdot intercept = q_0 \cdot \frac{p_0}{q_0} = 0.000027121 \cdot 0.3103$$

$$= 0.0000084156$$

$$s + \sqrt{s} = \frac{G(S)}{2G(X)} + \frac{4.82 \times 10^6}{G(X) M_n D} \quad (42)$$

$$then \quad \frac{G(S)}{2G(X)} = \frac{p_0}{q_0}$$

$$\frac{G(X)}{G(S)} = \frac{1}{2\frac{p_0}{q_0}} = \frac{1}{2 \cdot 0.3103} = 1.6113$$

$$slope = \frac{4.82 \times 10^6}{G(X) M_n}$$

$$G(X) = \frac{4.82 \times 10^6}{slope \cdot M_n} = \frac{4.82 \times 10^6}{29.3832 \cdot 43400} = 3.7797$$

$$in\ tercept = \frac{G(S)}{2G(X)}$$

$$G(S) = 2 \cdot G(X) \cdot intercept = 2 \cdot 3.7797 \cdot 0.3103 = 2.3456$$

Table 5. Calculation of Charlesby-Pinner parameters

wt.% of Vinyl acetate	**wt. fraction of vinyl acetate**	**wt. fraction of ethylene**	**molar fraction of vinyl acetate**	**molar fraction of ethylene**	**MET-VA**	**Mn**	**Pn**
28	0.28	0.72	0. 8875	0.1125	34.58	43400	1255

slope	p_0/q_0	q_0	p_0	G(X)/G(S)	G(X)	G(S)
29.38	0.3103	2.7121E-05	8.4156E-06	1.6113	3.7797	2.3456

All the essential parameters are listed in Table 5. Parameters G(X) =3.78 and G(S) =2.35 mean that both cross-linking and chain scission occur during e-beam irradiation. The ratio of the parameters G(X)/G(S) =1.61 indicates that cross-linking prevails over the scission for this copolymer. The ratio G(X)/G(S)=1.61 is comparable to our previous results on ethylene-octene copolymer with 30 wt.% of octene [95] when the ratio was 1.77.

8. Influence of Carbon black on ethylene butene copolymer (EBC)

The influence of Carbon black and force on shear stress, creep compliance, frequency sweep, and electromechanical study of the ethylene butene copolymer (EBC) was investigated by Dynamic Mechanical Analysis (DMA).

Figure 22 indicates the effect of force and CB content on creep after 5 min of EBC/CB composite. The creep of the composites with a content of 25 wt% of carbon fiber has the lowest value for almost four times compared to the pure EBC, which has the highest creep. Furthermore, increasing the force could increase creep due to the improved interfacial action between the copolymer and the fiber [78]. Additionally, stiffness could be improved by fiber's addition by hindering the matrix material [79]. Moreover, stiffness could be improved by fiber's addition by hindering the matrix material [79].

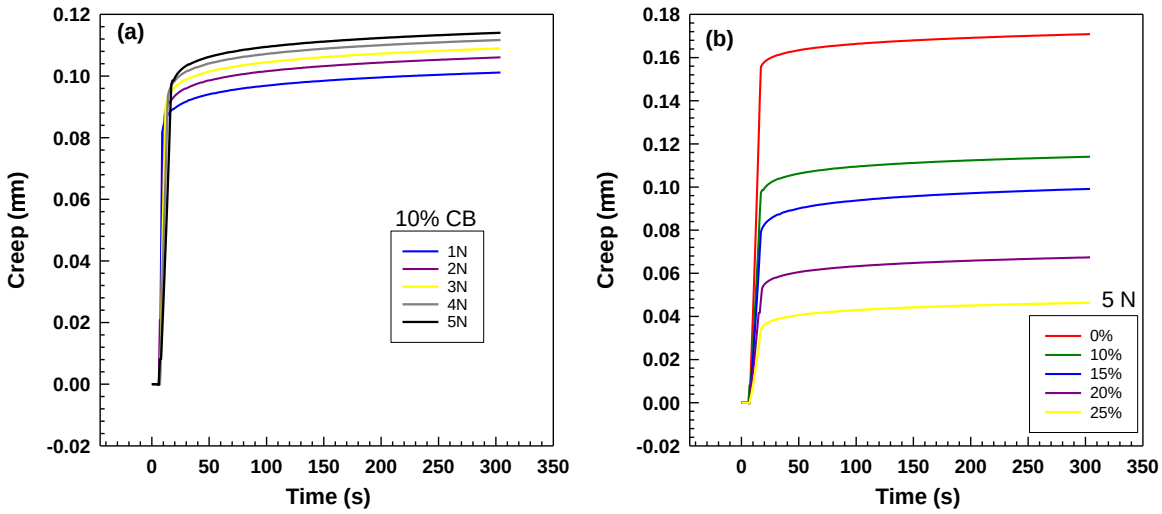

Figure 22. creep–time for a) 10% wt. CB b) 5N curves of EBC/CB composite at 25 °C for different concentration and stress

The stress and creep compliance was measured as a function of CB loading and forces in Figure 23.

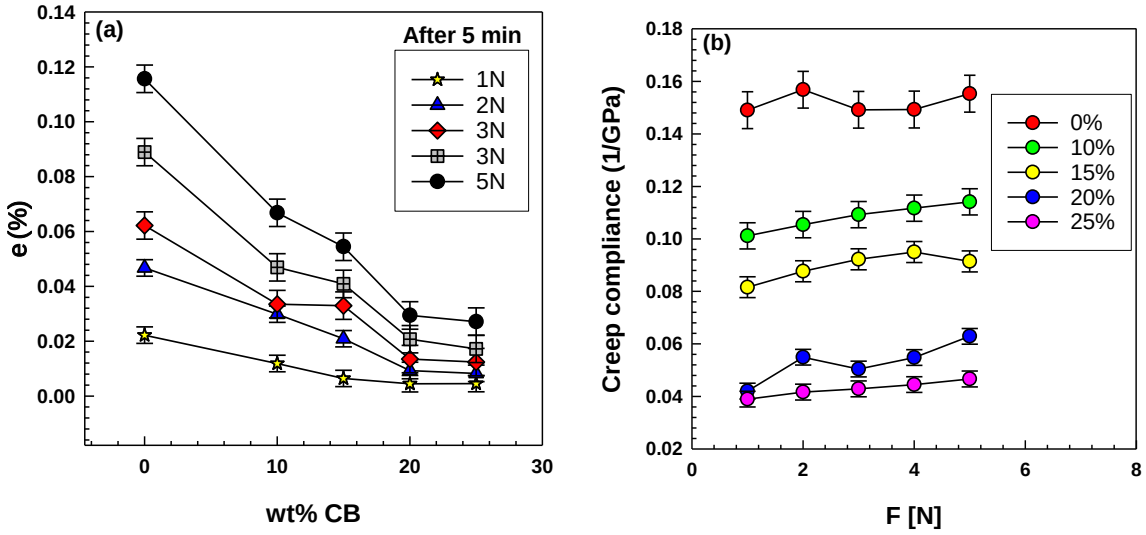

Figure 23. a) Strain vs. CB concentration for different force after 5 min b) creep compliance vs. force for different loading of CB content.

Table 6. Shear modulus G of EBC/CB composite at 0.01% shear strain

CB content (wt. %)	Shear modulus G (MPa)
0	1.720 ± 0.08
10	7.414 ± 0.35
15	8.902 ± 0.38
20	13.670 ± 0.52
25	15.305 ± 0.71

It shows that elongation (ε) significantly decreased by increasing the CB content up to 20% wt. On the other hand, there is not much difference from 20% wt to 25 % wt as the fiber looks well dispersed, and the filler covers the matrix. It also indicates that increasing the force up to 5 N could increase elongation six times due to the butene polymer composite's rubber behavior. The creep compliance graph shows that the addition of carbon black to the matrix decreases the creep compliance due to the significant interaction between the fiber and matrix, which leads to the increased modulus.

Stress-strain tensile curves from DMA tests are shown in Figure 24. The Figure shows that the addition of CB from 0% wt. to 25% wt. to EBC would increase the modules Pa. Table 6 shows the modulus change by the addition of CB fiber at 0.01 shear strain [96] as mathematical representations rely on the linearity of response of both elastic and viscous components. It shows that by increasing the CB content to the matrix, the Young modulus would increase from 7.414 for 10 wt% Pa to 15.305 for 25 wt%. Savetlana et al. reported that the addition of 20 wt%carbon black to the natural rubber could increase the modulus for 18 times from 2.5 to 47 MPa because of the reinforcing potential from flexible filler formation network and strong polymer-filler coupling. The principal factors determined the capability of reinforcement were (i) Van der walls force between CB and polymer, (ii) the chemical cross-link of polymer into the filler surface due to the free radical reaction

between carbon atoms in filler and polymer, and (ii) the mechanical interlocking of the polymer on to the filler surface.[97] Moreover, it looks like increasing fiber content. The copolymer composite tend to acts more brittle, which might be because of the quality of the fibers dispersion and good interaction between carbon black and ethylene butene copolymer. This is the global result of an efficient load transfer from the matrix to the first, strong chemical interactions and second, geometric interactions, such as the high specific surface area between the carbon black surface and the ethylene butane copolymer segments.[98-100] It has been established by numerous studies that addition of carbon base fibers exhibit a significant increase in modulus as compared to the matrix resin. As mentioned earlier, this is mainly due to the fact that functionalization improves both dispersion and stress transfer.

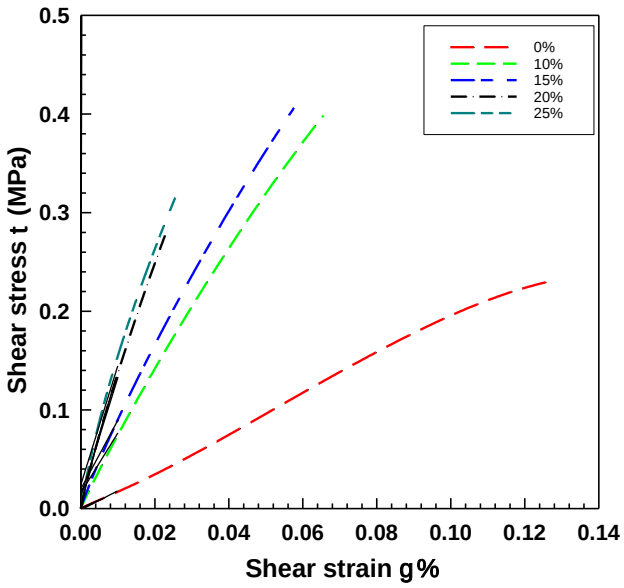

Figure 24. Representative tensile stress-strain curves for EBC/CB for different concentrations.

The electric resistance vs. force is shown in Figure 24b. In this test, the electrical resistance was measured with a variety of loads for 5 min. However, the addition of CB up to 10% would not affect resistance. It might be related to the low concentration of carbon black in the matrix caused by disassociation between CB particles. That could decrease the resistance to almost zero. There are two types of electrical conduction in the EBC/CB that can happen. “Contact" or "tunneling" mechanism. Conductive fillers are physically in contact with each other and form a conducting network in the contact mechanism. However, the electron's mobility has tunneled between the neighboring conductive fillers, which are separated by the polymeric layers in the tunneling mechanism [49, 101].

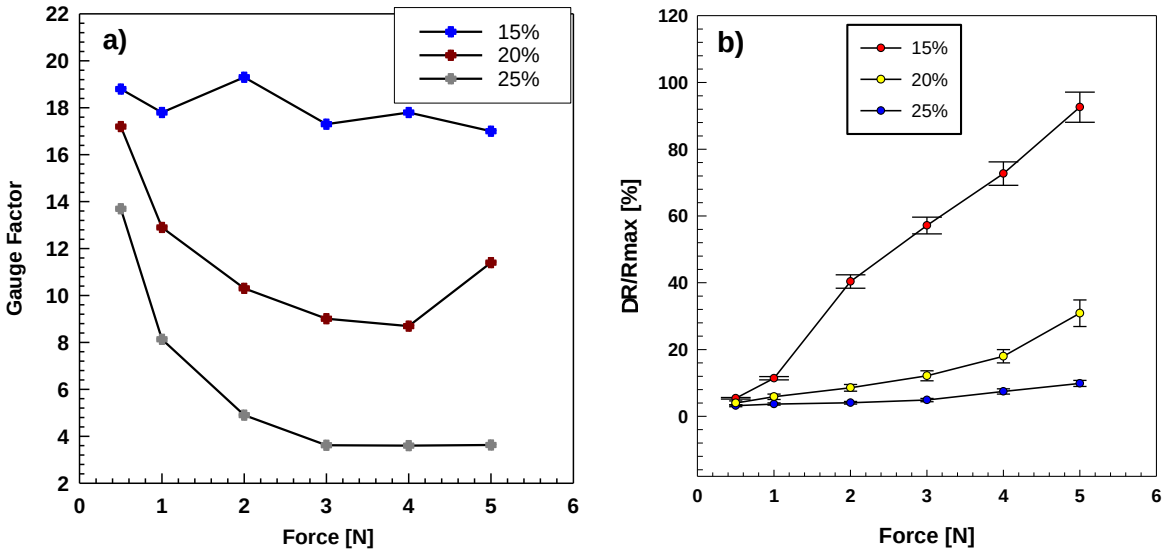

Figure 25. A) Gauge factor b) Change of electrical resistance vs. force for different concentrations of CB.

Costa *et al*. [102] reported that the piezoresistive polymer blends gauge factor (GF) values ranging from 5 to 80. The gauge factor can be defined as [35, 103]

$$G = \frac{1}{\varepsilon}\left(\frac{\Delta R}{R_0}\right) \quad (42)$$

Where R0 is initial resistance, ΔR is the change of resistance and ε is a strain. For a composite with strain-independent conductivity behavior, the following relationship is generally followed:[23]

$$\frac{\Delta R}{R_0} = \varepsilon\,(2 + \varepsilon\,) \quad (43)$$

Figure 25a indicates the gauge factor for different CB concentrations under force between 4 and 20, which is around five times higher than conventional metal gauge. It shows that the addition of CB to EBC could decrease the gauge factor with force.

The gauge factor is around two at low strain, but it may be as high as 1300 for carbon nanotube /epoxy composite [104]. However, the most reported value is below 100 [102, 103, 105].

The addition of CB from 15Wt% to 25wt% leads to increased resistance dramatically, increasing interaction, and contacting the CB particles. Moreover, increasing the force leads to a decrease in the thickness of the sample. It caused an increase in the interaction of CB particles.

Storage modulus (G′) and loss modulus (G″) was tested as a function of shear strain (γ %).

In the frequency sweep test, a small amplitude oscillatory shear,$\dot{\gamma} = \gamma_o \sin(\omega t)$ was applied to the samples. Resulting shear stress was recorded as:

$$\sigma(\mathrm{t}) = \gamma_o[G'(\omega)\sin(\omega t) + [G''(\omega)\cos(\omega t)] \quad (44)$$

G′, G″ and dynamic viscosity (η∗) were measured as a function of angular frequency (ω) in the range of 0.1–100 rad/s at a strain value in the linear viscoelastic region [106, 107].

Figure 26 indicates the storage modulus (G') and loss modulus (G'), Tan δ, and complex viscosity $|\eta^*|$ of the samples as a frequency function.

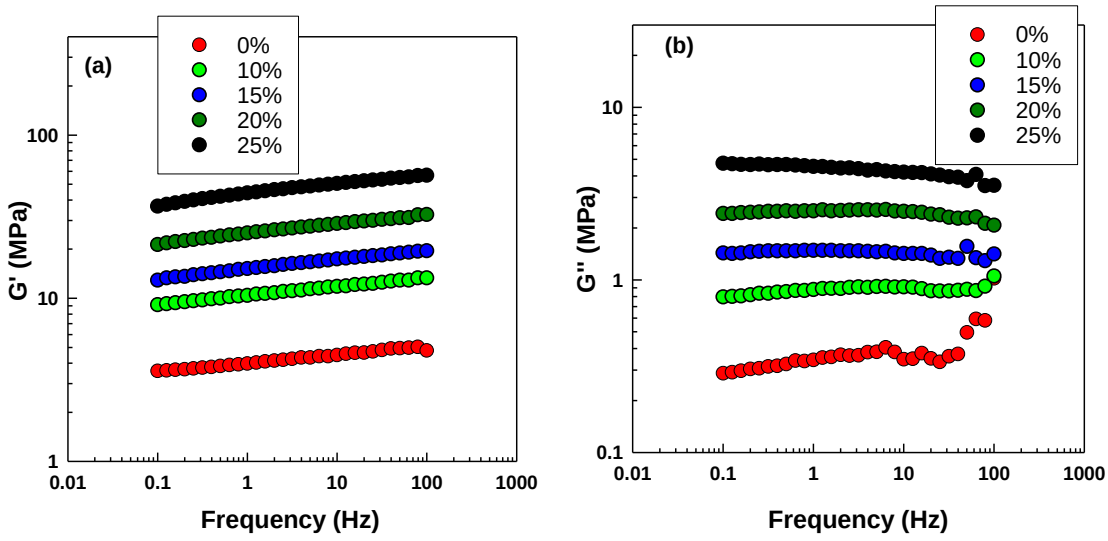

Figure 26. (a) G', (b) G", as a function of frequency composites for different CB content for EBC/CB

It is observed that the loose modulus (G') is more sensitive than G''. It is well known that the storage modulus with the changes of CB content.

There is no significant change in storage modulus observed for EBC/CB up to 20 percent because there is no interfacial interaction between CB fiber and EBC. However, EBC with 25% wt. content will decrease the storage modulus up to 30% from 5 to 3.5 MPa for the entire frequency rate.

On the other hand, it can be observed that G' is increased significantly by increasing the frequency. It also can be observed that the addition of CB up to 25% wt. could increase G' up to 3 times.

Dependence of loss factor (tan δ) and complex viscosity $|\eta^*|$ of the samples on frequency are given in Figure 27. Tan δ curves of the polymer copolymer with CB decreased with increasing frequency.

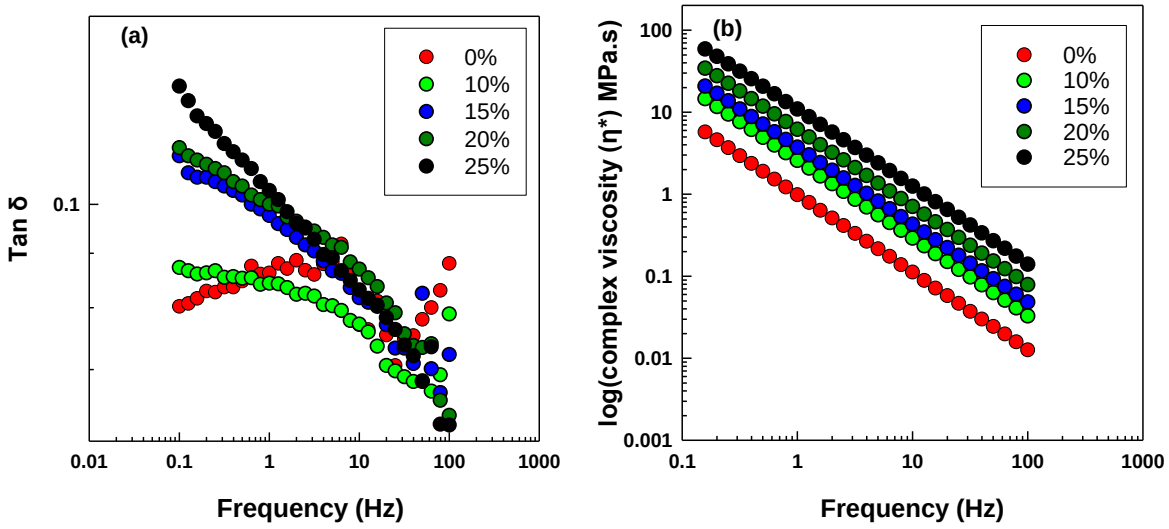

Figure 27. (a) tan δ (b) $|\eta^*|$ as a function of frequency composites for different CB content for EBC/CB

The negative slope in the Tan δ curve is a normal behavior of viscoelastic. In contrast, the positive slope refers to the elastic response of the viscoelastic samples dominating this elastic behavior.

$$\tan \delta = \frac{G''}{G'} \; Eq \quad (44)$$

Figure 27b. $|\eta^*|$ curves with frequency region were fitted by the power-law model to determine the shear-thinning phenomena.

The dynamic viscosity is calculated according to the equation 45.

$$|\eta^*| = k\omega^n \quad (45)$$

$$log|\eta^*| = \log k + n\log(\omega) \qquad (46)$$

The shear-thinning exponent, n, is the straight-line slope obtained by plotting log $|\eta^*|$vs. log ω [20, 61, 62].

The volume fraction of the carbon black (Φ) is calculated according to the equation 47.

$$\phi = \frac{V_A}{V_A + V_B} = \frac{\frac{m_A}{\varrho_A}}{\frac{m_A}{\varrho_A} + \frac{m_B}{\varrho_B}} = \frac{\frac{m_A}{\varrho_A \cdot (m_A + m_B)}}{\frac{m_A}{\varrho_A \cdot (m_A + m_B)} + \frac{m_A}{\varrho_A \cdot (m_A + m_B)}}$$

$$= \frac{\frac{w_A}{\varrho_A}}{\frac{w_A}{\varrho_A} + \frac{w_B}{\varrho_B}} \qquad (47)$$

While the density of CB and EBC is 2.26 g/cm^3 and 0.862 g/cm^3, respectively. The volume fraction is shown in Table 7.

The van Gurp-Palmen (vGP) plot, which plots phase angle δ° versus complex modulus $|G^*|$, is sensitive to polydispersity and long-chain branching (95, 96).

The complex modulus $|G^*|$ is reported:

$$"|G^*| = (G'^2 + G''^2)^{1/2} \quad (48)$$

Table 7. Power-law factors determined from the |η|vs. log ω*

ϕ% CB	**Composite Density g/cm^3**	**k**	**ω**
0	0.862	-0.19512 ± 0.087	-0.94834
4.07	0.92	0.21998 ± 0.0103	-0.94573
6.31	0.95	0.382447 ± 0.0183	-0.94187
8.71	0.98	0.600717 ± 0.0284	-0.9416
11.28	1.02	0.84419 ± 0.0325	-0.93966

As shown in Figure 28, van Gurp-Palmen curves of EBC/CB show that the addition of CB to the EBC would increase. The blend shows the vGP plot predicted for linear polymers, i.e., a plateau at b = 7° in the low IG* I region.

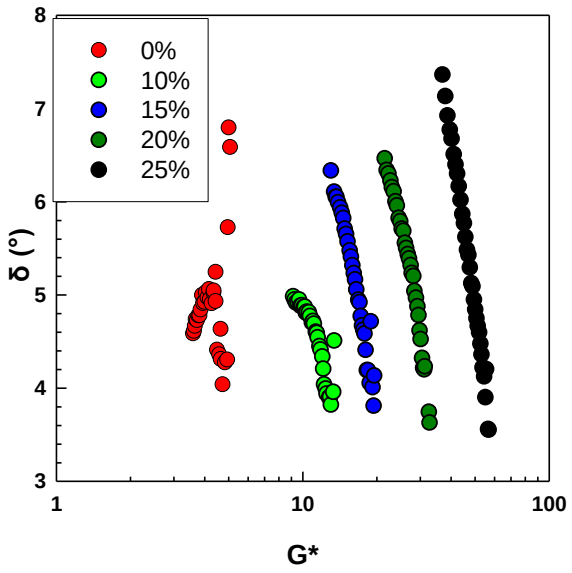

Figure 28. vGP of EBC for different CB content

The graphs show that addition CB content could increase δ ̊from 3.5° to 7°. Several studies have been reported about vGP, which have been similar tend peak followed by a downward tendency [108-111].

9. Influence of Carbon fiber on ethylene butene copolymer (EBC)

The electrical, mechanical, and thermal conductivity of ethylene butene copolymer (EBC) composites with carbon fibers were studied. EBC/carbon-fiber composites can be utilized as an electro-mechanical material capable of changing its electric resistance with mechanical strain. Carbon fibers were introduced to EBC with different concentrations (5-25 wt. %).

Electrical conductivity

Tensile deformation and gauge factors were determined by a two-point technique to measure the electric resistance as a function of the strain. In this research, according to questions 34 and 35.

The composite samples with the various CF (5, 10, 15, 20, and 25 wt. %) were deformed by the tensile stress with increasing stress (0.442, 0.884, 1.325, and 1.768, and 2.219 MPa) respectively. Micrograph of optical microscopy from EBC carbon fiber for 15 wt. % and 25 wt. % can be seen in Figure 29.

Figure 29 shows the fracture morphologies of EBC with 15 wt. % and wt. 25% of carbon fiber. The optical microscopy examination indicated that the fibers were homogeneously distributed in the EBC composites. It was also observed that at low fiber contents, 15 wt. %, fewer fibers were lying on the surface in comparison with the 25 wt. % of carbon fiber

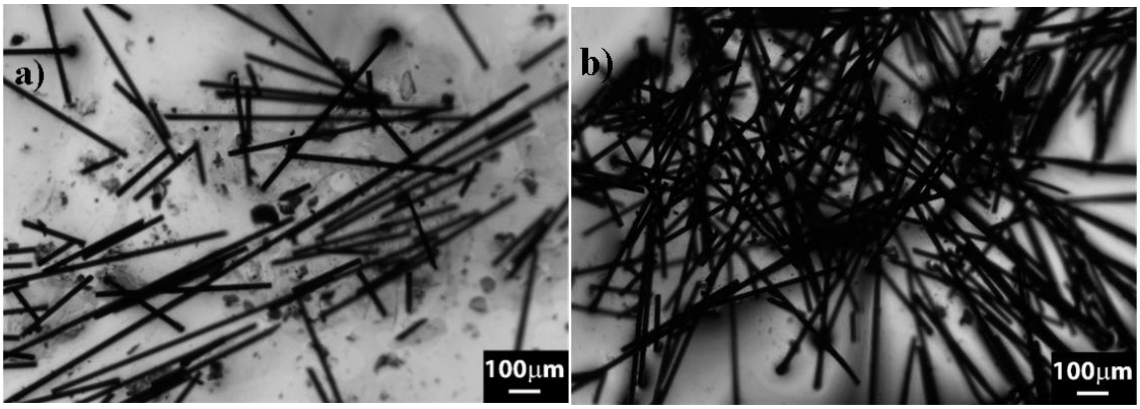

Figure 29. Micrographs from optical microscopy (a) ethylene-butene -copolymer (EBC) and carbon fiber (CF) with 15 wt.% (b) ethylene-butene copolymer (EBC) and carbon fiber (CF) 25 wt.%.

. The composite with 25 wt.% carbon fiber had higher fiber agglomerates because of low dispersion caused by excess filler [112].

The strain caused by tensile stress, and the change of electrical resistance was measured. The change of electric resistance of EBC with 5% and 10% of carbon fibers could not be measured. There being zero conductivity because of the low concentration of CF. It was also observed that the EBC composite with 15% of carbon fiber had a low chance of electrical resistance with a change of strain due to the low content of carbon fibers, which might be because of the lower amount of fiber and resistivity of carbon fiber during the deformation. Furthermore, it is observed in Figure 3 that EBC/CF with 25 wt. The % resistance change is increasing with deformation, as increasing the connection between carbon fibers.[71, 74, 113]. The number of fibers in EBC/CF 15 wt. % is much lower than 25 wt.% that could be measured only up to 0.884 MP. The Figure shows that five cycles increase of tensile strain up to 2.935 MPa for 25 wt. % and four steps up to 1.768 MPa for 15 wt. % of CF. By opening the circles in the graph, the relevant resistance changes, while solid

circles signify strain values. Figure 30 shows that EBC/CF 25 wt. % is also conductive at the peak strain of about 16% once the resistance change is about 4500%.

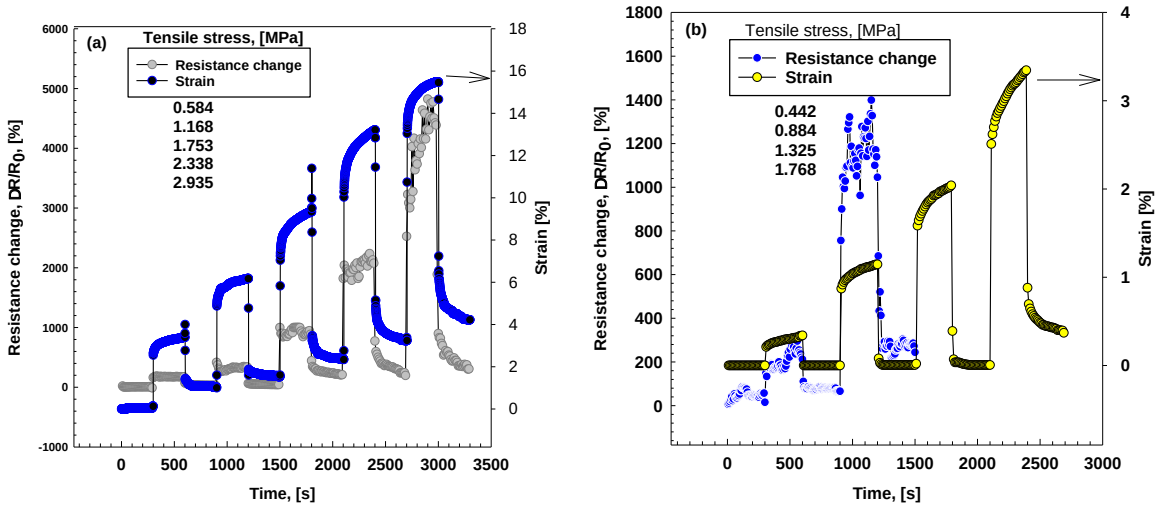

Figure 30. Relative resistance change, Δ R/R0, and the strain, ε, of a) EBC/CF 25 wt.% b) EBC/CF 15 wt.%.

The relative resistance increases with strain continually with no gap. It is no longer common in the conductive particulate mixture when a point of very high resistance is touched the higher strain. Furthermore, the mixtures' resistance returns almost to unload state to the value of 0 and 3 percent for 15 wt. % and 25 wt. %, respectively, as can see in Figure 31.

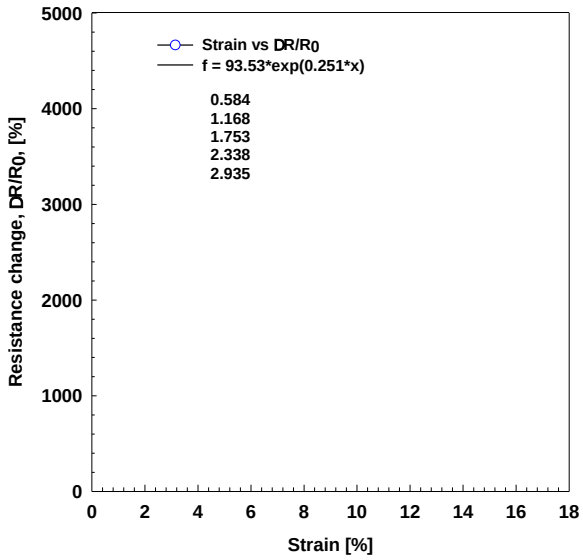

Figure 31. Resistance change vs. strain for EBC/CF 25 wt. % composite in loading/unloading

Figure 32 indicates the gauge factor for EBC/CF 25 wt. %. The gauge factor rises with strain values around 50 and starts deformation and growth as much as 300 at a 16% strain. This is a remarkable growth that keeps EBC/CF mixture within the variety of mixture of substances and strain gauges with excellent sensitivity to tensile deformation.

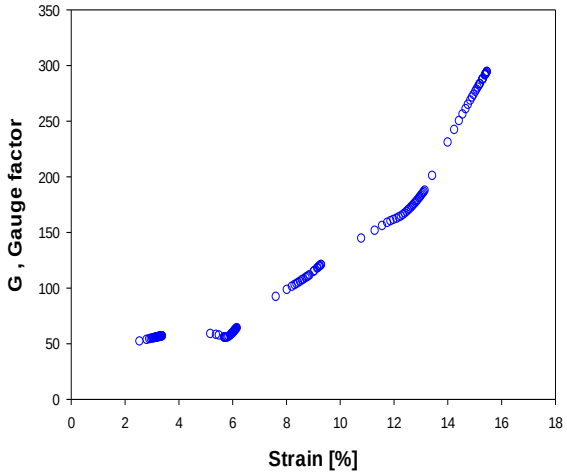

Figure 32. Strain dependence of gauge factor GF of EBC/CF 25 wt. %

Thermal conductivity

The dependence of temperature on time is described with the equation 51.[67]

$$T = T_1 - (T_1 - T_2) * e^{|-(A_1 - A_2)\tau|} (49)$$

Where:

$$A_1 = \frac{S\lambda}{\delta K} \ (50), A_2 = \frac{B}{K} \ (51)$$

However, equation 51 can be simplified with exponential growth with three parameters as:

$$y = y_0 + ae^{(-bx)} \qquad (52)$$

The coefficient b is obtained from the nonlinear regression. The calculation of the thermal conductivities of EBC/CF is shown in Table 8 and Figure 33.

Table 8. The thermal conductivity Parameters of EBC/CF

CF %	b	A1	λ (W m^{-2} K^{-1})	R^2
0	0.0015611	0.0012981	0.1952	0.999976
5	0.0019353	0.0016723	0.2266	0.999961
10	0.0020541	0.00179114	0.2413	0.999968
15	0.0021213	0.00185826	0.2477	0.999968
20	0.0023160	0.002053	0.2635	0.999979

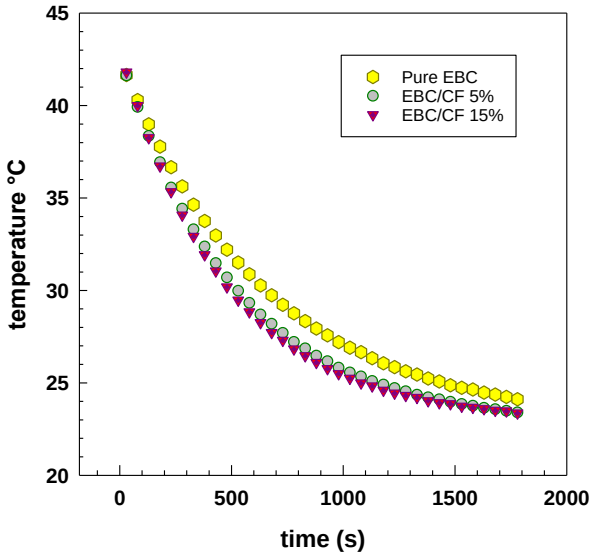

Figure 33. Thermal conductivity measurement: temperature vs. time for EBC/CF for different concentration of carbon fiber content with the initial temperature of 45°C

Figure 34 shows that the thermal conductivities of the EBC/CF composites increased with increasing CF.

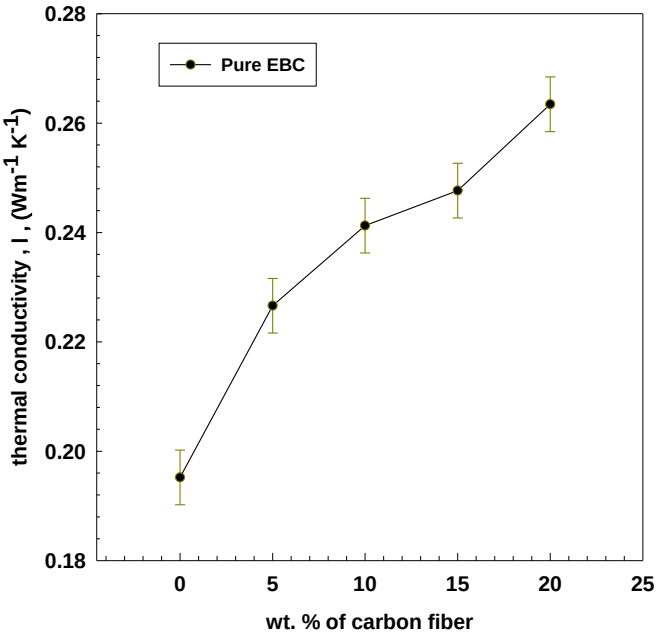

Figure 34. Thermal conductivity as a function of the carbon fiber content

The highest measured thermal conductivity was 0.263 W m−1 K−1 for an EBC/CF 20 wt.% increase of 35% compared with pure EBC.

The uniform distribution of CF had a large effect on the growth in thermal and electric conductivity. Since CF has high conductivity for both heat and electricity, the CF loading in EBC increased the mixture's thermal and electric conductivities [67, 114].

10. Conclusions

The influence of carbon fibers and radiation on shear stress creep compliance and frequency sweep of ethylene-vinyl acetate (EVA) was investigated by dynamic mechanical analysis. The linear viscosity and electromechanical properties of Ethylene Butene copolymers filled with electric conductive Carbon Black and Carbon fiber are investigated.

Ethylene-vinyl acetate and Ethylene butyl copolymer with carbon fiber were mixed and homogenized with different concentrations (5, 10, 15, 20, 25 wt.%) using a two-roll mill at 150 °C for 5 min. Following, a sheet with a thickness of 0.5 mm was prepared by compression moldings at 10 MPa with 5 min. The same process is performed for Ethylene butyl copolymer and carbon black.

The EVA-CF composites were found to have higher shear modulus for given shear strain by adding filler and increasing irradiation due to the interaction between the matrix and fiber and increasing the molecular weight irradiation due to crosslinking. It was also observed that tan δ decreased with increasing doses from 60 to 180 KGy for 0.1 to 100 Hz frequencies. There was a dramatic decrease in creep with increasing CF content and increasing irradiation, which confirmed the high interaction and raised cross-linking level. The analysis of unsolvable gel content confirmed the effect of irradiation on cross-linking since the radiation dose up to 180 KGy increased the amount of insoluble gel.

The linear viscosity and electromechanical properties of Ethylene Butene copolymers filled with electric conductive Carbon Black are investigated. The

dynamic mechanical viscosity and modulus found to be increased with the addition of Carbon Black into Ethylene Butene copolymer. Moreover, the electrical resistance is growing with Carbon Black content due to the interaction and contact between the particles. The elongation (ε) significantly decreases by increasing the CB content regarding the well disperses and hardening effect of CB.

These work results establish manufacturing elastic strain sensors' potential using an economical and multipurpose method, with potential flexible electronics products.

Observations from optical microscopy indicated a relatively good dispersion of carbon fibers in the matrix and the length of the fibers was preserved. The electromechanical testing showed that the composite's straining led to a change in its macroscopic electrical resistance. The EBC/CF composites had high degree of sensitivity of electric resistivity to strain, and the changes were reversible. Therefore, the results indicate the composite's good potential to be used as an electrical strain sensor. We found out that the mixtures exhibit an increase in thermal conductivity with loading carbon fiber due to the high intrinsic phonon spectrum mismatch between polymer material and fillers, leading to increased heat transfer.

11.List of Abbreviations

CB	Carbon Black
CF	Carbon fiber
DMA	Dynamic Mechanical Analysis
E	Modulus
EBC	Ethylene-butene copolymer
EVA	Ethylene-vinyl acetate
G”	Loss modulus
G’	Storage modulus
Gc	Shear modulus of the composite
Gm	Shear modulus of the gum
J(t)	Creep compliance
k	Sample specific pre-exponential factor
KGy	Kilo Gray
MgCl2	Magnesium chloride
n	Shear thinning exponent
PAN	Poly acrylonitrile
SiC	Silicon carbide

SoO2	Silicon dioxide
Tg	Glass transition
Ti(oBu)4	Titanium butoxide
TiCl4	Titanium tetrachloride
Zn-Cl2	Zinc chloride
H	Viscosity
η*	Complex viscosity,
Σ	Stress
ω	Oscillation frequency
Φ	Volume fraction of the filler
τ	Deformation

12. List of Tables

13. List of Figures:

Refrence:

1. Liu, H., et al., *Electrically conductive polymer composites for smart flexible strain sensors: a critical review.* Journal of Materials Chemistry C, 2018. **6**(45): p. 12121-12141.
2. Kim, K.-H., et al., *Enhancement of linearity range of stretchable ultrasensitive metal crack strain sensor via superaligned carbon nanotube-based strain engineering.* Materials Horizons, 2020. **7**(10): p. 2662-2672.
3. Akhtar, I. and S.-H. Chang, *Highly aligned carbon nanotubes and their sensor applications.* Nanoscale, 2020.
4. Ke, K., Z. Sang, and I. Manas-Zloczower, *Stretchable elastomer composites with segregated filler networks: effect of carbon nanofiller dimensionality.* Nanoscale Advances, 2019. **1**(6): p. 2337-2347.
5. Capiati, N.J. and R.S. Porter, *The concept of one polymer composites modelled with high density polyethylene.* Journal of Materials Science, 1975. **10**(10): p. 1671-1677.
6. Essabir, H., et al., *Mechanical and Thermal Properties of Polymer Composite Based on Natural Fibers: Moroccan Luffa Sponge/High Density Polyethylene.* Journal of Biobased Materials and Bioenergy, 2015. **9**(3): p. 350-357.
7. Song, J.B., et al., *Electromagnetic interference properties of carbon nanofiber-reinforced acrylonitrile-styrene-acrylate/natural graphite composites.* Journal of Applied Polymer Science, 2017. **134**(43).
8. Slobodian, P., P. Riha, and R. Olejnik, *Electromechanical Sensors Based on Carbon Nanotube Networks and Their Polymer Composites*, in *New Developments and Applications in Sensing Technology*, S.C. Mukhopadhyay, A. Lay-Ekuakille, and A. Fuchs, Editors. 2011, Springer Berlin Heidelberg: Berlin, Heidelberg. p. 233-251.
9. Kasgoz, A., D. Akin, and A. Durmus, *Effects of size and shape originated synergism of carbon nano fillers on the electrical and mechanical properties of conductive polymer composites.* Journal of Applied Polymer Science, 2015. **132**(30).
10. Iqbal, A., et al., *The effect of filler concentration on the electrical, thermal, and mechanical properties of carbon particle and carbon fiber-reinforced poly(styrene-co-acrylonitrile) composites.* Polymer Composites, 2007. **28**(2): p. 186-197.
11. Matabola, K., et al., *Single polymer composites: A review*. Vol. 44. 2009. 6213-6222.
12. Hemanth, R., M. Sekar, and S. Bheemappa, *Effects of fibers and fillers on mechanical properties of thermoplastic composites*. Vol. 2. 2014. 28-35.
13. Li, J. and F. Sun, *The effect of nitric acid oxidization treatment on the interface of carbon fiber-reinforced thermoplastic polystyrene composite.* Polymer-Plastics Technology and Engineering, 2009. **48**(7): p. 711-715.
14. Tiwari, S., J. Bijwe, and S. Panier, *Gamma radiation treatment of carbon fabric to improve the fiber-matrix adhesion and tribo-performance of composites.* Wear, 2011. **271**(9-10): p. 2184-2192.

15. Pusch, J. and B. Wohlmann, *Chapter 2 - Carbon Fibers*, in *Inorganic and Composite Fibers*, B. Mahltig and Y. Kyosev, Editors. 2018, Woodhead Publishing. p. 31-51.

16. Mohd Radzuan, N.A., et al., *The effect of milled carbon fibre filler on electrical conductivity in highly conductive polymer composites.* Composites Part B: Engineering, 2017. **110**: p. 153-160.

17. Jin, F.L., S.Y. Lee, and S.J. Park, *Polymer matrices for carbon fiber-reinforced polymer composites.* Carbon Letters, 2013. **14**(2): p. 76-88.

18. Harea, E., et al., *Electrical conductivity degradation of fatigued carbon black reinforced natural rubber composites: Effects of carbon nanotubes and strain amplitudes.* Express Polymer Letters, 2019. **13**(12): p. 1116-1124.

19. Abot, J.L., T. Alosh, and K. Belay, *Strain dependence of electrical resistance in carbon nanotube yarns.* Carbon, 2014. **70**: p. 95-102.

20. Durmuş, A., et al., *Intercalated linear low density polyethylene (LLDPE)/clay nanocomposites prepared with oxidized polyethylene as a new type compatibilizer: Structural, mechanical and barrier properties.* European Polymer Journal, 2007. **43**(9): p. 3737-3749.

21. Chand, S., *Review Carbon fibers for composites.* Journal of Materials Science, 2000. **35**(6): p. 1303-1313.

22. Bautista-Quijano, J.R., et al., *Strain sensing, electrical and mechanical properties of polycarbonate/multiwall carbon nanotube monofilament fibers fabricated by melt spinning.* Polymer, 2016. **82**: p. 181-189.

23. Chen, S., et al., *Polymer-Enhanced Highly Stretchable Conductive Fiber Strain Sensor Used for Electronic Data Gloves.* Advanced Materials Technologies, 2016. **1**(7): p. 1600136.

24. Costa, P., S. Ribeiro, and S. Lanceros-Mendez, *Mechanical vs. electrical hysteresis of carbon nanotube/styrene-butadiene-styrene composites and their influence in the electromechanical response.* Composites Science and Technology, 2015. **109**: p. 1-5.

25. Feng, C. and L.Y. Jiang, *Micromechanics Modeling of Bi-Axial Stretching Effects on the Electrical Conductivity of CNT-Polymer Composites.* International Journal of Applied Mechanics, 2015. **7**(1).

26. Lebedev, O.V., S.G. Abaimov, and A.N. Ozerin, *Modeling the effect of uniaxial deformation on electrical conductivity for composite materials with extreme filler segregation.* Journal of Composite Materials, 2019.

27. Slobodian, P., et al., *Compressive stress-electrical conductivity characteristics of multiwall carbon nanotube networks.* Journal of Materials Science, 2011. **46**(9): p. 3186-3190.

28. D'Aloia, A.G., et al., *Electrical, mechanical and electromechanical properties of graphene-thermoset polymer composites produced using acetone-DMF solvents.* Polymers, 2018. **10**(1): p. 82.

29. Matzeu, G., et al., *A temperature sensor based on a MWCNT/SEBS nanocomposite.* Sensors and Actuators A: Physical, 2012. **178**: p. 94-99.

30. Yang, H., et al., *Strain-sensitive electrical conductivity of carbon nanotube-graphene-filled rubber composites under cyclic loading.* Nanoscale, 2019. **11**(2): p. 578-586.

31. Fiorillo, A., C. Critello, and S. Pullano, *Theory, technology and applications of piezoresistive sensors: A review.* Sensors and Actuators A: Physical, 2018. **281**: p. 156-175.

32. Sanli, A., et al., *Piezoresistive characterization of multi-walled carbon nanotube-epoxy based flexible strain sensitive films by impedance spectroscopy.* Composites Science and Technology, 2016. **122**: p. 18-26.

33. Zhu, Z.H., *Piezoresistive Strain Sensors Based on Carbon Nanotube Networks Contemporary approaches related to electrical conductivity.* Ieee Nanotechnology Magazine, 2015. **9**(2): p. 11-23.

34. Ferreira, A. and S. Lanceros-Mendez, *Piezoresistive response of spray-printed carbon nanotube/poly(vinylidene fluoride) composites.* Composites Part B-Engineering, 2016. **96**: p. 242-247.

35. Biccai, S., et al., *Negative gauge factor piezoresistive composites based on polymers filled with MoS2 nanosheets.* ACS nano, 2019.

36. Gaska, K., et al., *Mechanical Behavior of Melt-Mixed 3D Hierarchical Graphene/Polypropylene Nanocomposites.* Polymers, 2020. **12**(6): p. 1309.

37. Wang, Z. and D.E. Smith, *Numerical analysis on viscoelastic creep responses of aligned short fiber reinforced composites.* Composite Structures, 2019. **229**: p. 111394.

38. Srivatsava, M. and P.S.R. Sreekanth, *Experimental characterization of dynamic mechanical properties of hybrid carbon-Kevlar reinforced composite with sandwich configuration.* Materials Today: Proceedings, 2020. **27**: p. 931-935.

39. Sabet, M., H. Soleimani, and S. Hosseini, *Graphene impact of the LDPE characteristics.* Polymer Bulletin, 2020. **77**(1): p. 459-474.

40. George, J.J. and A.K. Bhowmick, *Fabrication and Properties of Ethylene Vinyl Acetate-Carbon Nanofiber Nanocomposites.* Nanoscale Research Letters, 2008. **3**(12): p. 508-515.

41. Makuuchi, K. and S. Cheng, *Radiation processing of polymer materials and its industrial applications*. 2012: John Wiley & Sons.

42. Ramarad, S., et al., *Improved crystallinity and dynamic mechanical properties of reclaimed waste tire rubber/EVA blends under the influence of electron beam irradiation.* Radiation Physics and Chemistry, 2017. **130**: p. 362-370.

43. Mateev, M. and S. Karageorgiev, *The effect of electron beam irradiation and content of EVA upon the gel-forming processes in LDPE-EVA films.* Radiation Physics and Chemistry, 1998. **51**(2): p. 205-206.

44. Svoboda, P., *Influence of Branching Density in Ethylene-Octene Copolymers on Electron Beam Crosslinkability.* Polymers, 2015. **7**(12): p. 2522-2534.

45. Fitzer, E., *Pan-based carbon fibers—present state and trend of the technology from the viewpoint of possibilities and limits to influence and to control the fiber properties by the process parameters.* Carbon, 1989. **27**(5): p. 621-645.

46. Council, N.R., *High Performance Synthetic Fibers for Composites*. 1992, Washington, DC: The National Academies Press. 148.

47. Fink, J.K., *Handbook of Engineering and Specialty Thermoplastics: Polyolefins and Styrenics*. 2010: John Wiley.

48. Liu, Z.Q., et al., *A Geometry Effect of Carbon Nanomaterials on Flame Retardancy and Mechanical Properties of Ethylene-Vinyl Acetate/Magnesium Hydroxide Composites.* Polymers, 2018. **10**(9).

49. Varghese, A.M., et al., *Effect of Graphene on Polypropylene/Maleic Anhydride-graft-Ethylene–Vinyl Acetate (PP/EVA-g-MA) Blend: Mechanical, Thermal, Morphological, and Rheological Properties.* Industrial & Engineering Chemistry Research, 2018. **57**(23): p. 7834-7845.

50. Quan, D.P., X.G. Fan, and H.H. Wang, *Structure and mechanical properties of ethylene-butene copolymers.* Chemical Research in Chinese Universities, 2002. **18**(1): p. 52-55.

51. Manas, D., et al., *The Effect of Irradiation on Mechanical and Thermal Properties of Selected Types of Polymers.* Polymers, 2018. **10**(2): p. 158.

52. Poongavalappil, S., et al., *Cross-linking kinetics study and high temperature mechanical properties of ethylene-octene copolymer (EOC)/dicumylperoxide(DCP) system.* European Polymer Journal, 2011. **47**(10): p. 1949-1955.

53. Theravalappil, R., et al., *Creep and Dynamic Mechanical Analysis Studies of Peroxide-Crosslinked Ethylene-Octene Copolymer.* Macromolecular Materials and Engineering, 2012. **297**(8): p. 761-767.

54. Menard, K.P. and N. Menard, *Dynamic mechanical analysis.* Encyclopedia of Analytical Chemistry: Applications, Theory and Instrumentation, 2006: p. 1-25.

55. Menard, K.P. and N.R. Menard, *Dynamic mechanical analysis in the analysis of polymers and rubbers.* Encyclopedia of polymer science and technology, 2002: p. 1-33.

56. Hill, L.W., *Dynamic Mechanical and Tensile Properties*, J. Koleske, Editor. 2012, ASTM International: West Conshohocken, PA. p. 624-636.

57. Roylance, D., *Engineering viscoelasticity.* Department of Materials Science and Engineering–Massachusetts Institute of Technology, Cambridge MA, 2001. **2139**: p. 1-37.

58. Guedes, R.M., *Creep and fatigue in polymer matrix composites*. 2010: Elsevier.

59. Tweedie, C.A. and K.J. Van Vliet, *Contact creep compliance of viscoelastic materials via nanoindentation.* Journal of Materials Research, 2006. **21**(6): p. 1576-1589.

60. Macosko, C.W., *Rheology principles, measurements, and applications.* 1994.

61. Durmus, A., A. Kasgoz, and C.W. Macosko, *Linear low density polyethylene (LLDPE)/clay nanocomposites. Part I: Structural characterization and quantifying clay dispersion by melt rheology.* Polymer, 2007. **48**(15): p. 4492-4502.

62. Mussatti, F.G. and C.W. Macosko, *Rheology of network forming systems.* Polymer Engineering & Science, 1973. **13**(3): p. 236-240.

63. Qian, J.W., et al., *A novel method for estimating unperturbed dimension [eta](theta) of polymer from the measurement of its [eta] in a non-theta solvent.* European Polymer Journal, 2001. **37**(7): p. 1403-1407.

64. Jayanarayanan, K., S. Thomas, and K. Joseph, *Effect of blend ratio on the dynamic mechanical and thermal degradation behavior of polymer–polymer composites from low density polyethylene and polyethylene terephthalate.* Iranian Polymer Journal, 2016. **25**(4): p. 373-384.

65. Jha, V., et al., *Modeling of the effect of rigid fillers on the stiffness of rubbers.* Journal of Applied Polymer Science, 2008. **107**(4): p. 2572-2577.

66. Rezende, C.A., et al., *Natural rubber-clay nanocomposites: Mechanical and structural properties.* Polymer, 2010. **51**(16): p. 3644-3652.

67. Svoboda, P., et al., *A study on electrical and thermal conductivities of ethylene–octene copolymer/expandable graphite composites.* Polymer Engineering & Science, 2012. **52**(6): p. 1241-1249.

68. Chodák, I., M. Omastová, and J. Pionteck, *Relation between electrical and mechanical properties of conducting polymer composites.* Journal of Applied Polymer Science, 2001. **82**(8): p. 1903-1906.

69. Omastova, M., et al., *Electrical properties and stability of polypyrrole containing conducting polymer composites.* Synthetic Metals, 1996. **81**(1): p. 49-57.

70. Bengtsson, P., et al., *ELECTRICAL NOISE CHARACTERISTICS OF CARBON BLACK-FILLED LINEAR LOW-DENSITY POLYETHYLENE NEAR THE PERCOLATION-THRESHOLD.* Polymer Engineering and Science, 1993. **33**(9): p. 573-580.

71. Slobodian, P., et al., *Enhancing effect of KMnO4 oxidation of carbon nanotubes network embedded in elastic polyurethane on overall electro-mechanical properties of composite.* Composites Science and Technology, 2013. **81**: p. 54-60.

72. Naghashpour, A. and S. Van Hoa, *In situ monitoring of through-thickness strain in glass fiber/epoxy composite laminates using carbon nanotube sensors.* Composites Science and Technology, 2013. **78**: p. 41-47.

73. Chauvet, J., J.M. Asua, and J.R. Leiza, *Independent control of sol molar mass and gel content in acrylate polymer/latexes.* Polymer, 2005. **46**(23): p. 9555-9561.

74. Slobodian, P., et al., *Pre-Strain Stimulation of Electro-Mechanical Sensitivity of Carbon Nanotube Network/Polyurethane Composites.* Ieee Sensors Journal, 2016. **16**(15): p. 5898-5903.

75. Esmaeeli, R., et al., *Designing a New Dynamic Mechanical Analysis (DMA) System for Testing Viscoelastic Materials at High Frequencies.* Modelling and Simulation in Engineering, 2019. **2019**: p. 7026267.

76. Loh, K. and S. Nagarajaiah, *Innovative developments of advanced multifunctional nanocomposites in civil and structural engineering*. 2016: Woodhead Publishing.

77. Das, A., et al., *Modified and unmodified multiwalled carbon nanotubes in high performance solution-styrene-butadiene and butadiene rubber blends.* Polymer, 2008. **49**(24): p. 5276-5283.

78. Yu, K.J., et al., *Modification of the Interfacial Interaction between Carbon Fiber and Epoxy with Carbon Hybrid Materials.* Nanomaterials, 2016. **6**(5).

79. Hamid, Y., A. Abu Bakar, and N. Deirram, *Mechanical and Morphological Properties of Waste Eurycoma longifolia Fiber/Montmorillonite Reinforced Poly(vinyl chloride) Hybrid Composites.* Journal of Applied Polymer Science, 2013. **128**(2): p. 1170-1175.

80. Potschke, P., T.D. Fornes, and D.R. Paul, *Rheological behavior of multiwalled carbon nanotube/polycarbonate composites.* Polymer, 2002. **43**(11): p. 3247-3255.

81. Poongavalappil, S., et al., *Study on the influence of electron beam irradiation on the thermal, mechanical, and rheological properties of ethylene-octene copolymer with high comonomer content.* Journal of Applied Polymer Science, 2013. **128**(5): p. 3026-3033.

82. Mandal, S. and S. Alam, *Studies on the mechanical, thermal, and morphological properties of poly(ether ether ketone)/poly(ether sulfone)/barium titanate nanocomposites: Correlation of experimental results with theoretical predictive models.* Journal of Applied Polymer Science, 2012. **126**(2): p. 724-733.

83. Oliani, W.L., et al., *Study of the morphology, thermal and mechanical properties of irradiated isotactic polypropylene films.* Radiation Physics and Chemistry, 2010. **79**(3): p. 325-328.

84. Matthews, K.H., et al., *Gamma-irradiation of lyophilised wound healing wafers.* International Journal of Pharmaceutics, 2006. **313**(1-2): p. 78-86.

85. Rezaeian, I., et al., *Improvements of physical and mechanical properties of electron beam irradiation-crosslinked EVA foams.* Polymers for Advanced Technologies, 2009. **20**(5): p. 487-492.

86. Matsui, T., M. Shimoda, and Y. Osajima, *Mechanical Changes of Electron-Beam Irradiated Ethylene Vinyl-Acetate Copolymer (Eva) Film .1.* Polymer International, 1992. **29**(2): p. 85-90.

87. Shokrieh, Z., M.M. Shokrieh, and Z. Zhao, *A modified micromechanical model to predict the creep modulus of polymeric nanocomposites.* Polymer Testing, 2018. **65**: p. 414-419.

88. Svoboda, P., et al., *Electron beam crosslinking of ethylene-octene copolymers.* Polymer, 2015. **81**: p. 119-128.

89. Mussatti, F.G. and C.W. Macosko, *Rheology of Network Forming Systems.* Polymer Engineering and Science, 1973. **13**(3): p. 236-240.

90. Potschke, P., et al., *Rheological and dielectrical characterization of melt mixed polycarbonate-multiwalled carbon nanotube composites.* Polymer, 2004. **45**(26): p. 8863-8870.

91. Kim, H. and C.W. Macosko, *Processing-property relationships of polycarbonate/graphene composites.* Polymer, 2009. **50**(15): p. 3797-3809.

92. Varghese, A.M., et al., *Effect of Graphene on Polypropylene/Maleic Anhydride-graft-Ethylene Vinyl Acetate (PP/EVA-g-MA) Blend: Mechanical, Thermal, Morphological, and Rheological Properties.* Industrial & Engineering Chemistry Research, 2018. **57**(23): p. 7834-7845.

93. Turgis, J.D. and X. Coqueret, *Electron beam sensitivity of butyl acrylate copolymers: effects of composition on reactivity.* Macromolecular Chemistry and Physics, 1999. **200**(3): p. 652-660.

94. Sharif, J., S.H.S.A. Aziz, and K. Hashim, *Radiation effects on LDPE/EVA blends.* Radiation Physics and Chemistry, 2000. **58**(2): p. 191-195.

95. Svoboda, P., *High-temperature study of radiation cross-linked ethylene-octene copolymers.* Polymer Bulletin, 2017. **74**(1): p. 121-144.

96. Capela, C., S. Oliveira, and J. Ferreira, *Mechanical behavior of high dosage short carbon fiber reinforced epoxy composites.* Fibers and Polymers, 2017. **18**(6): p. 1200-1207.

97. Savetlana, S., et al., *The effect of carbon black loading and structure on tensile property of natural rubber composite.* IOP Conference Series: Materials Science and Engineering, 2017. **223**: p. 012009.

98. Hamid, Y., A.A. Bakar, and N. Deirram, *Mechanical and morphological properties of waste Eurycoma longifolia fiber/montmorillonite reinforced poly (vinyl chloride) hybrid composites.* Journal of Applied Polymer Science, 2013. **128**(2): p. 1170-1175.

99. Hamid, Y., P. Svoboda, and D. Svobodova, *Influence of Electron Beam Irradiation on High-Temperature Mechanical Properties of Ethylene Vinyl Acetate/Carbon Fibers Composites.* Journal of Vinyl and Additive Technology, 2020. **26**(3): p. 325-335.

100. Le, T.-T., *Prediction of tensile strength of polymer carbon nanotube composites using practical machine learning method.* Journal of Composite Materials, 2020: p. 0021998320953540.

101. Yousefi, N., et al., *Highly aligned graphene/polymer nanocomposites with excellent dielectric properties for high-performance electromagnetic interference shielding.* Advanced Materials, 2014. **26**(31): p. 5480-5487.

102. Costa, P., et al., *Piezoresistive polymer blends for electromechanical sensor applications.* Composites Science and Technology, 2018. **168**: p. 353-362.

103. Bhandari, S., *Polymer/Carbon Composites for Sensor Application*, in *Carbon-Containing Polymer Composites*, M. Rahaman, D. Khastgir, and A.K. Aldalbahi, Editors. 2019, Springer Singapore: Singapore. p. 503-531.

104. Anand, S.V. and D.R. Mahapatra, *Quasi-static and dynamic strain sensing using carbon nanotube/epoxy nanocomposite thin films.* Smart Materials and Structures, 2009. **18**(4): p. 045013.

105. Zhou, J. and Y.-L. Hsieh, *Conductive Polymer Protonated Nanocellulose Aerogels for Tunable and Linearly Responsive Strain Sensors.* ACS Applied Materials & Interfaces, 2018. **10**(33): p. 27902-27910.

106. Adefisan, O.O. and A.G. McDonald, *Evaluation of the strength, sorption and thermal properties of bamboo plastic composites.* Maderas. Ciencia y tecnología, 2019. **21**(1): p. 3-14.

107. Arulmurugan, M., et al., *Impact of BaSO 4 filler on woven Aloevera/Hemp hybrid composite: Dynamic mechanical analysis.* Materials Research Express, 2019.

108. López-Barrón, C. and C. Macosko, *Rheology of compatibilized immiscible blends with droplet-matrix and cocontinuous morphologies during coarsening*. Vol. 58. 2014. 1935-1953.

109. Trinkle, S., P. Walter, and C. Friedrich, *Van Gurp-Palmen Plot II – classification of long chain branched polymers by their topology.* Rheologica Acta, 2002. **41**(1): p. 103-113.

110. Rulduà, M.L.M., et al., *Procesado en fundido de PLA reforzado con nanofibras de celulosa a partir de un masterbatch preparado de forma sostenible.* Materiales Compuestos, 2019. **3**(3): p. 107-111.

111. Delgado, D.E., et al., *Validation of quartz crystal rheometry in the megahertz frequency regime.* Journal of Polymer Science Part B: Polymer Physics, 2019.

112. Sanchez-Garcia, M.D., E. Gimenez, and J.M. Lagaron, *Morphology and barrier properties of solvent cast composites of thermoplastic biopolymers and purified cellulose fibers.* Carbohydrate Polymers, 2008. **71**(2): p. 235-244.

113. Slobodian, P., et al. *Improving sensitivity of the polyurethane/CNT laminate strain sensor by controlled mechanical preload*. in *IOP Conference Series: Materials Science and Engineering*. 2016. IOP Publishing.

114. Ren, L., et al., *Enhanced thermal conductivity for Ag-deposited alumina sphere/epoxy resin composites through manipulating interfacial thermal resistance.* Composites Part A: Applied Science and Manufacturing, 2018. **107**: p. 561-569.

Acknowledgement

This works has been supported by the Internal Grant Agency (IGA/FT/2017/007) of the Tomas Bata University in Zlin)

14. Resume:

Mr Yasin Hamid 06/09/1985

Brno -Czech Republic Contact no.: +420731755523

Email: Hamid@utb.cz

Past Educational Details

1.	PhD student in Polymer Engineering	Tomas Bata in Zlin	2014-2021
2.	West Pomeranian University of Technology	IAESTE Internship	2017
3.	Center of Polymer System in Zlin	Researcher (Part-time)	2017-2018
4.	Master of science polymer technology	University Technology Malaysia	2009-2012
5.	Bachelor of polymer engineering	Mahshahr Azad University	2004 - 2008

Special Skills: (Polymer Field)

Experience with inspection of Motors, Pumps , Steam Turbine case , MCC, Shipping , NDT Experience with thermoplastic and thermoset materials like EVA, PE, PP, etc.,

Ability to work with two roll mill, hot press, Extruder, Brabender, Cutter (machinery) Ability to work and analysis with DSC, SEM, XRD, FTIR, DMA

Polymer testing instrument like a universal testing machine (tensile, stress-strain, module)

Other qualification

1	MATLAB programming	2009
2	Navigate your career, Lets chat	2010
3	Navigate your career, Mind mapping	2010
5	Piping and PDMS (Advance)	2014

Scientific Researchs:

Hamid, Yasin & Bakar, Aznizam & Deirram, Nayeleh. (2012). Mechanical and Morphological Properties of Waste Eurycoma longifolia Fiber/Montmorillonite Reinforced Poly (vinyl chloride) Hybrid Composites. *Journal of Applied Polymer Science*. 128. 10.1002/APP.38401.

HAMID, Yasin, Petr SVOBODA (FT) a Dagmar SVOBODOVÁ. Influence of electron beam irradiation on high-temperature mechanical properties of ethylene vinyl acetate/carbon fibers composites. *Journal of Vinyl and Additive Technology* [online]. 2019 [cit. 2021-02-02]. ISSN 1083-5601. Dostupné z: https://onlinelibrary.wiley.com/doi/epdf/10.1002/vnl.21747.

HAMID, Yasin a Petr SVOBODA. Investigation of the influence of carbon black on the rheology and electromechanical properties of ethylene butene copolymer. *Materials Research Express* [online]. 2020, vol. 7, iss. 12 [cit. 2021-02-02]. ISSN 2053-1591. Dostupné z: https://iopscience.iop.org/article/10.1088/2053-1591/abd19c.

HAMID, Yasin a Petr SVOBODA. A study on thermal and electrical conductivities of ethylene-butene copolymer composites with carbon fibers, *International polymer processing,*

Awards: Best student award 2012 from University Technology Malaysia

Language Proficiency:

English: Advance

Arabic: Native

Persian: Native

Czech: Basic

Computer skills:

Microsoft Office Applications (Word, Excel and PowerPoint), MATLAB, Sigma plot, software and hardware, data analysis, Internet

15. Appendix

15.1. Influence of carbon fibers on ethylene vinyl acetate (EVA)

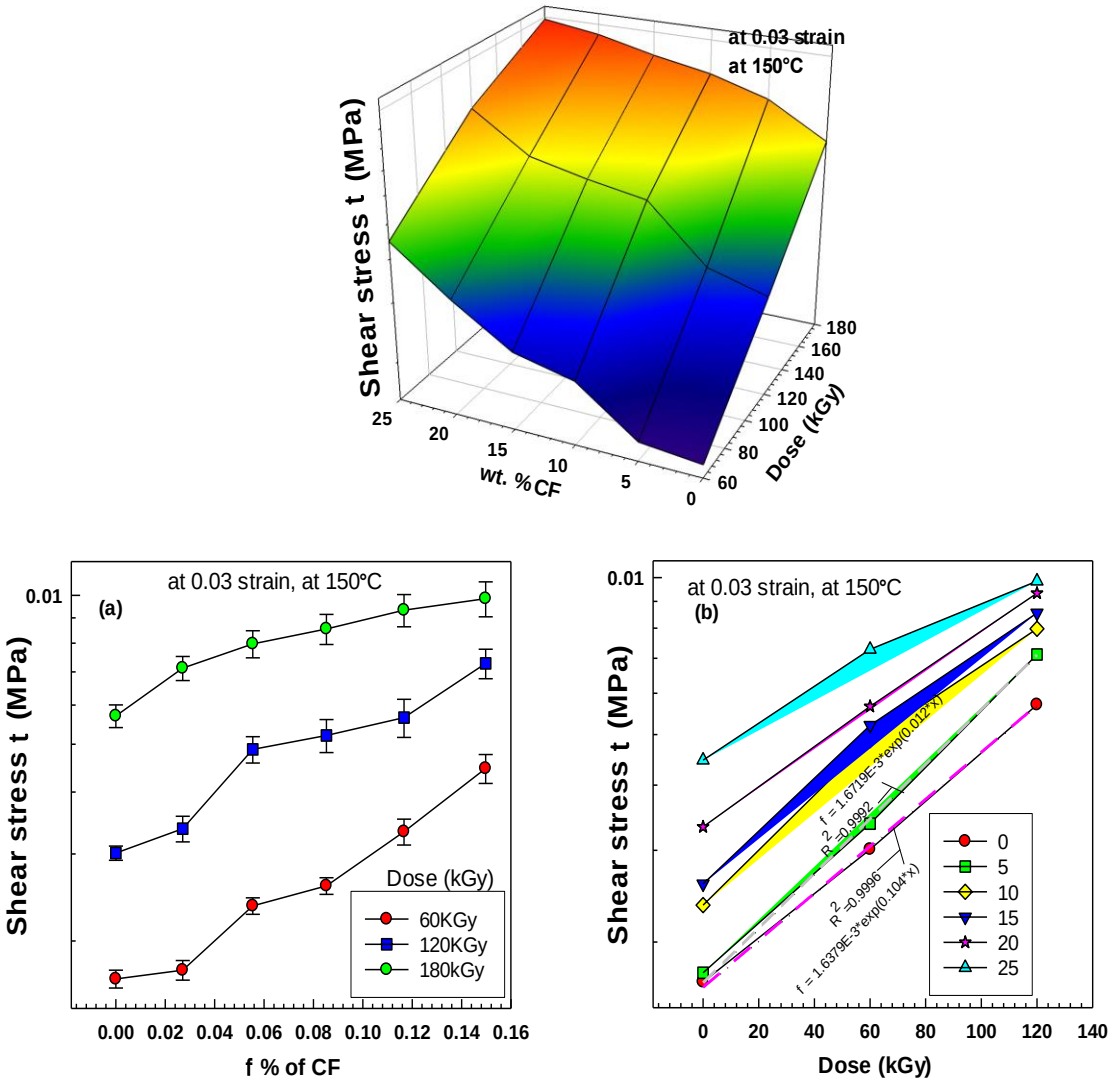

(a) Shear stress vol.fr. Of CF b) shear stress–dose curves of EVA/CF composites

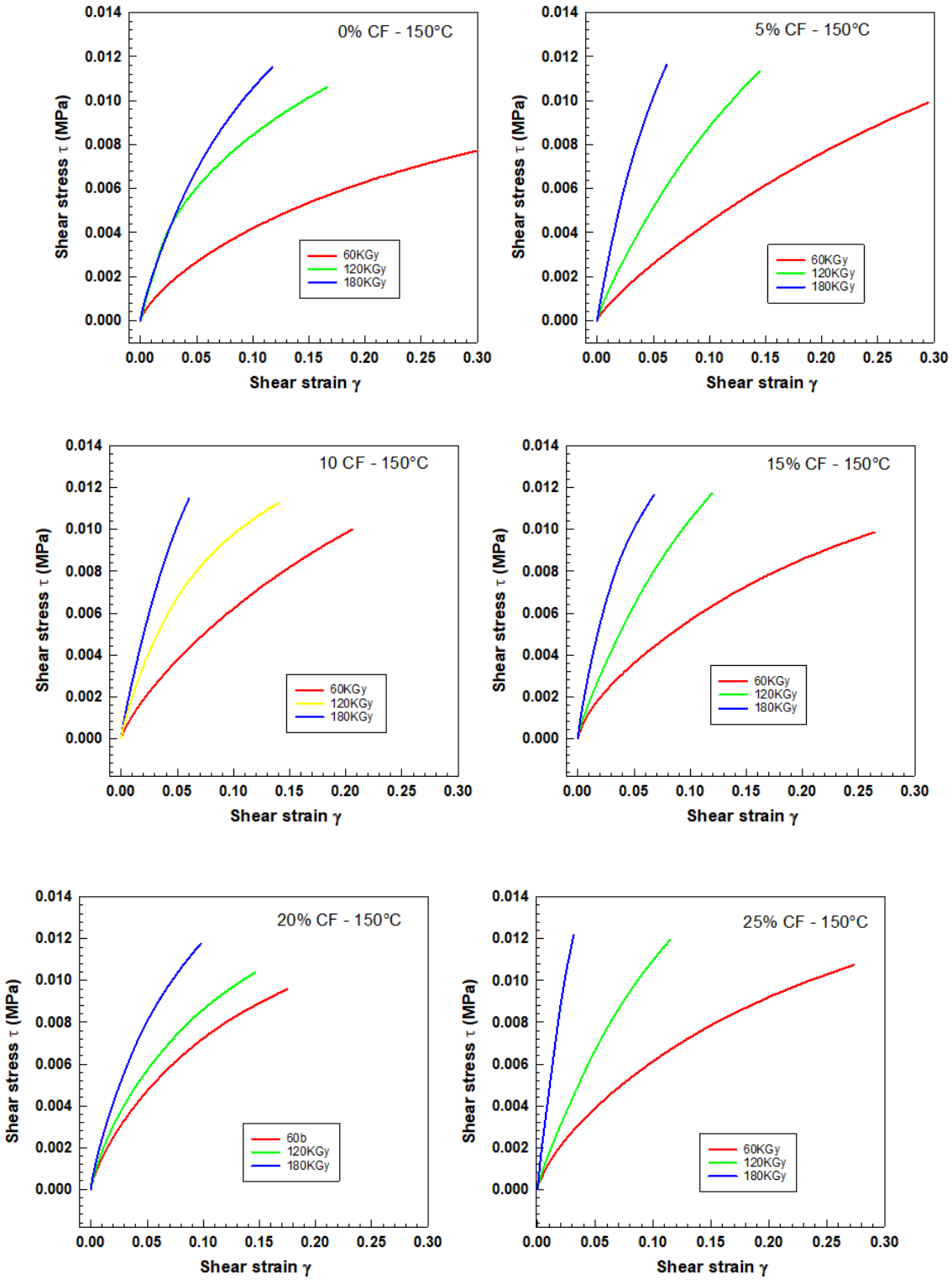

Shear stress-strain curves of EVA/CF composites increasing Dose KGy

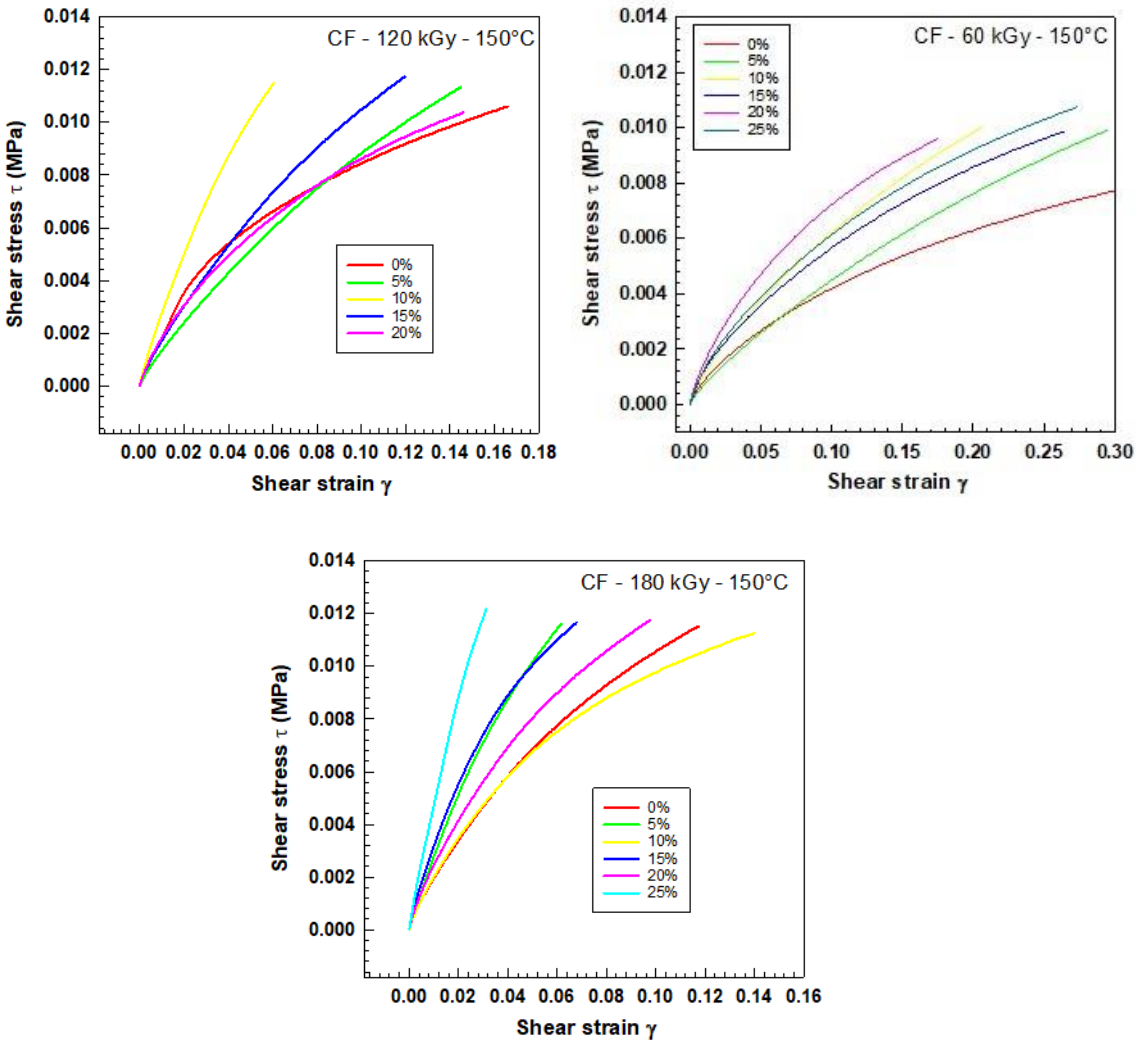

Shear stress-strain curves of EVA/CF composites increasing CF

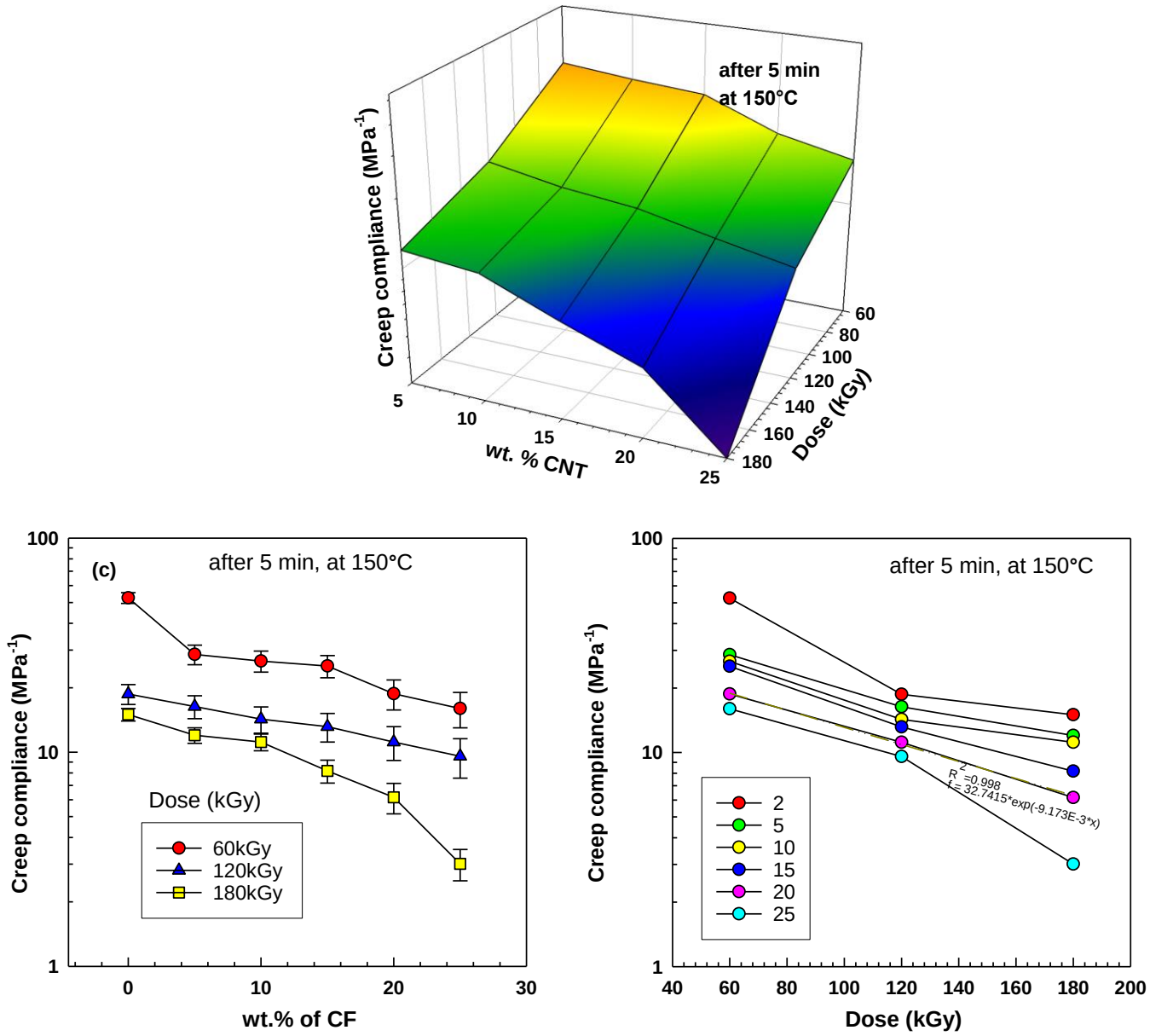

Creep vs wt. % of CF and dose (KGy) after 5 min.

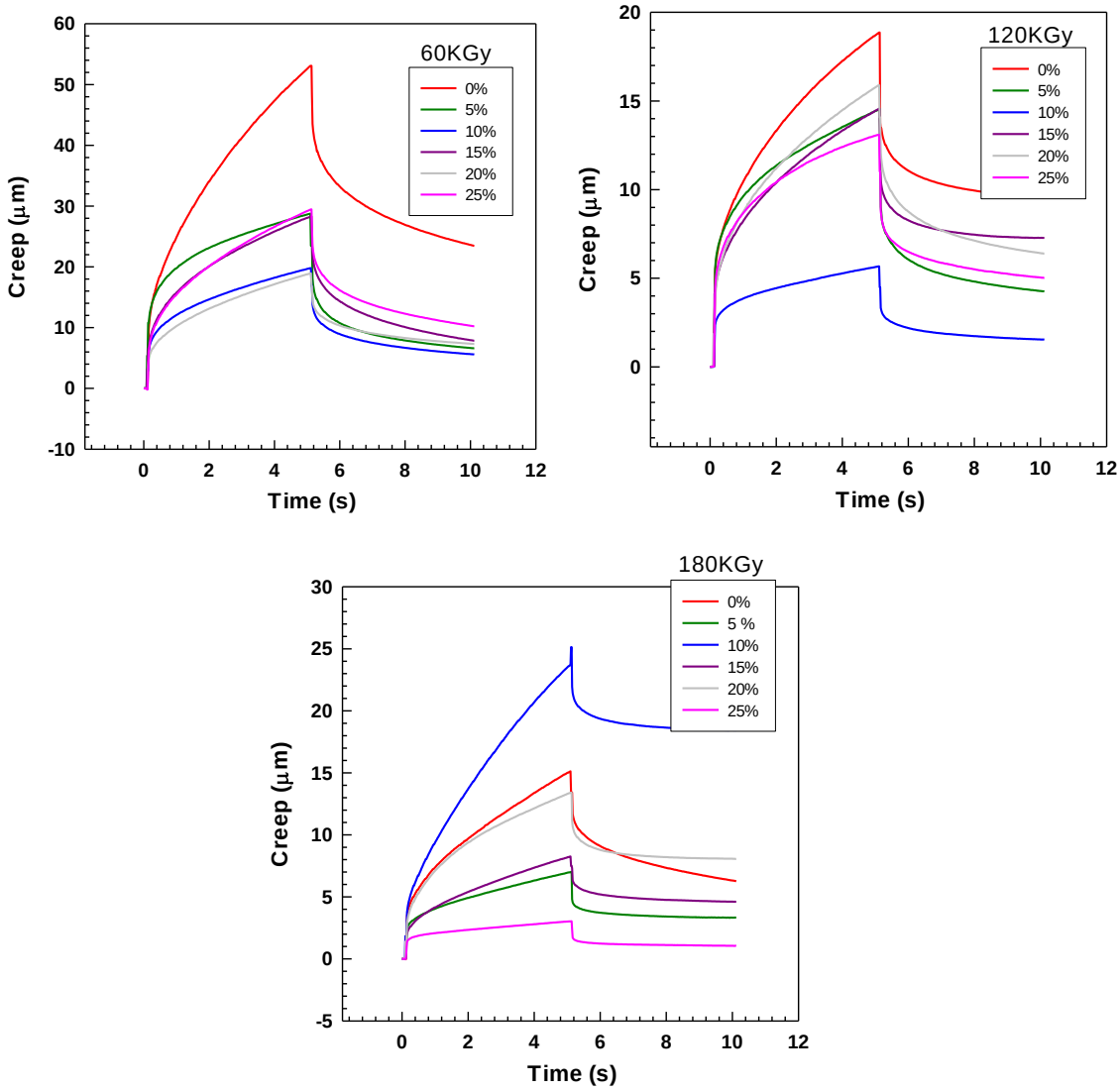

Creep–time for different wt. % and Dose (KGy)

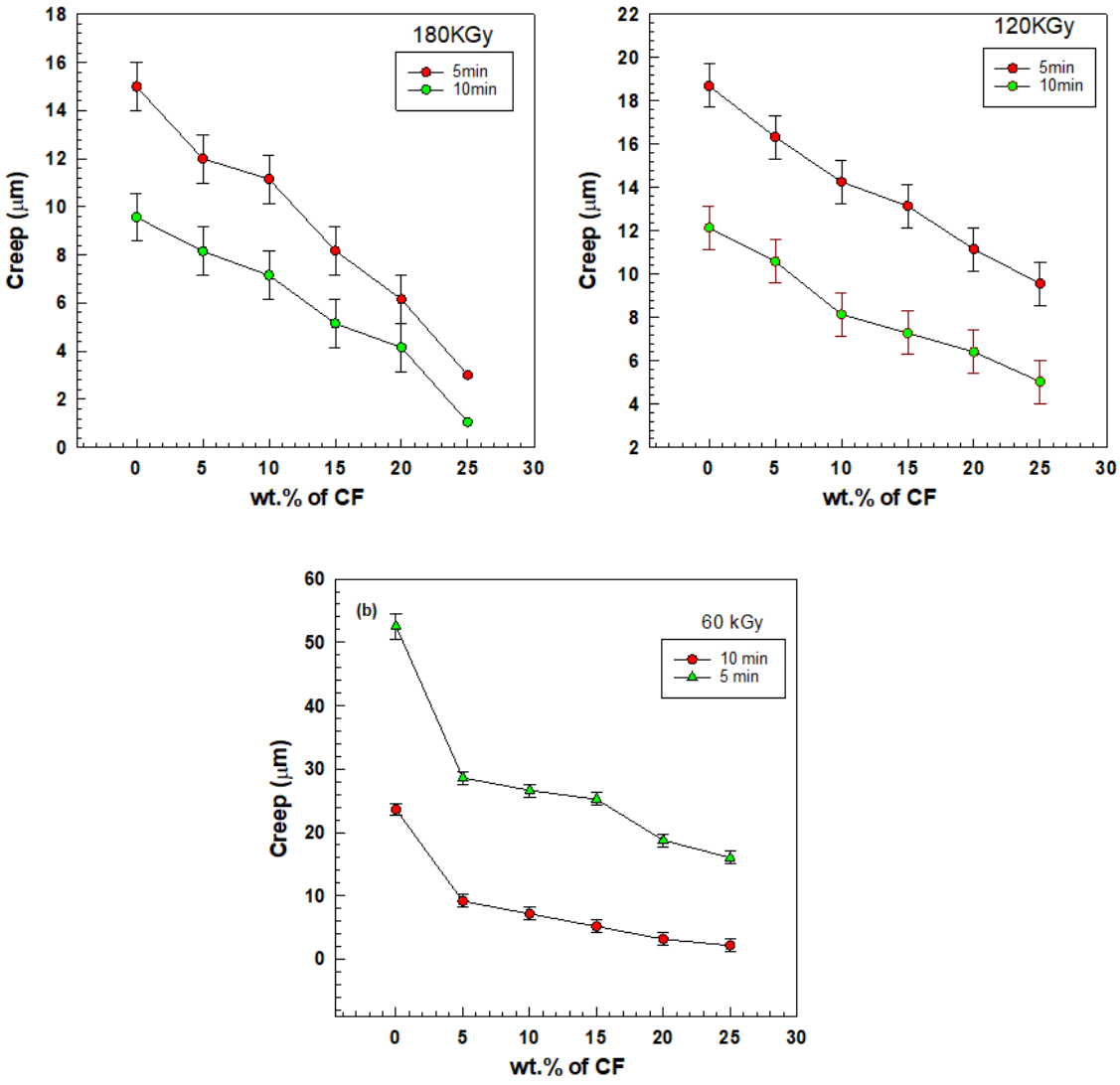

Creep (recovery)–wt. % curves of EVA/CF composite at 150 °C as a function of Dose (KGy) after 5 and 10 minuets

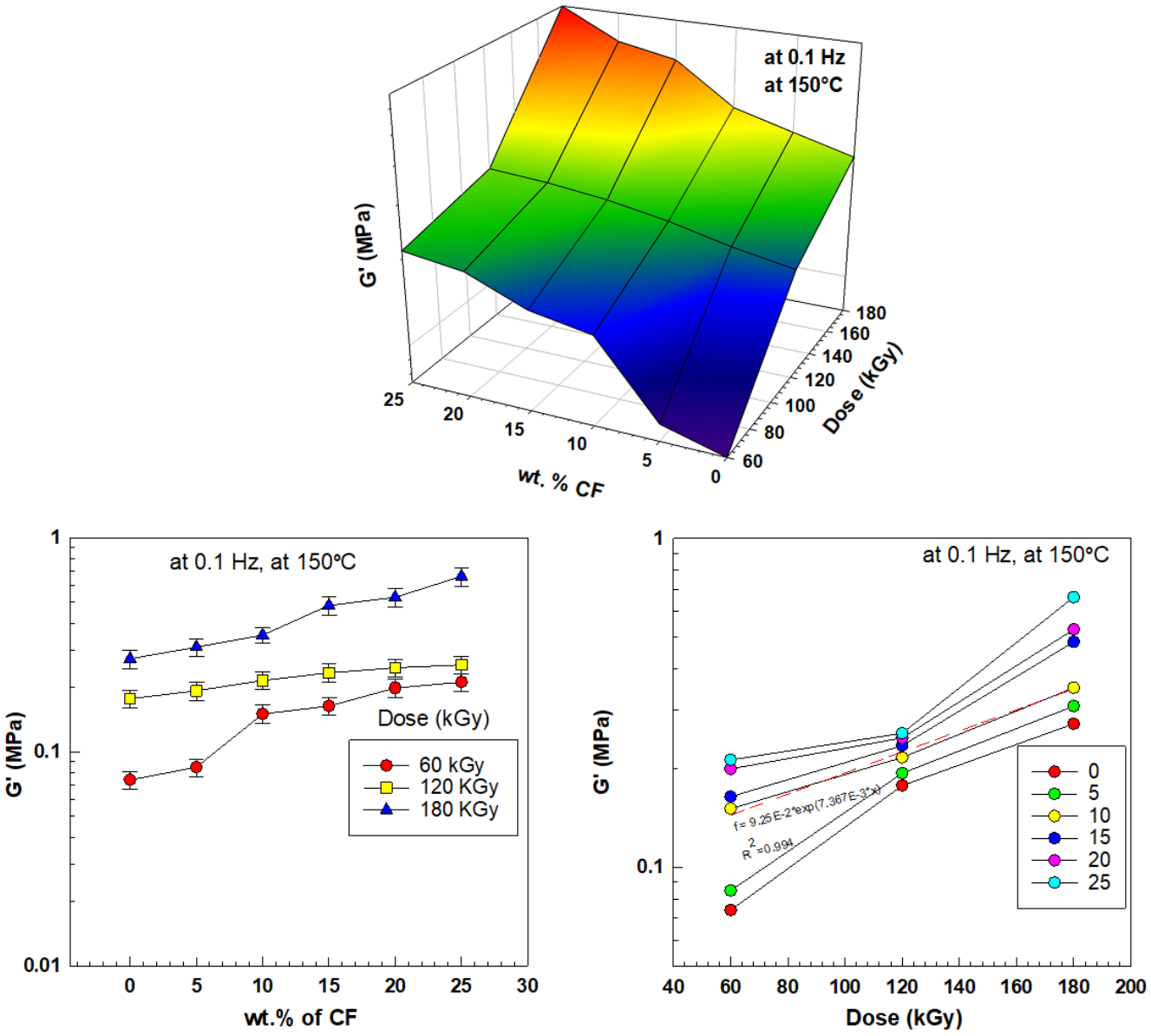

Shear modulus (real part) G' at 150 °C as a for frequency 0.1 rad/s as a function of carbon fiber and Dose (KGy)

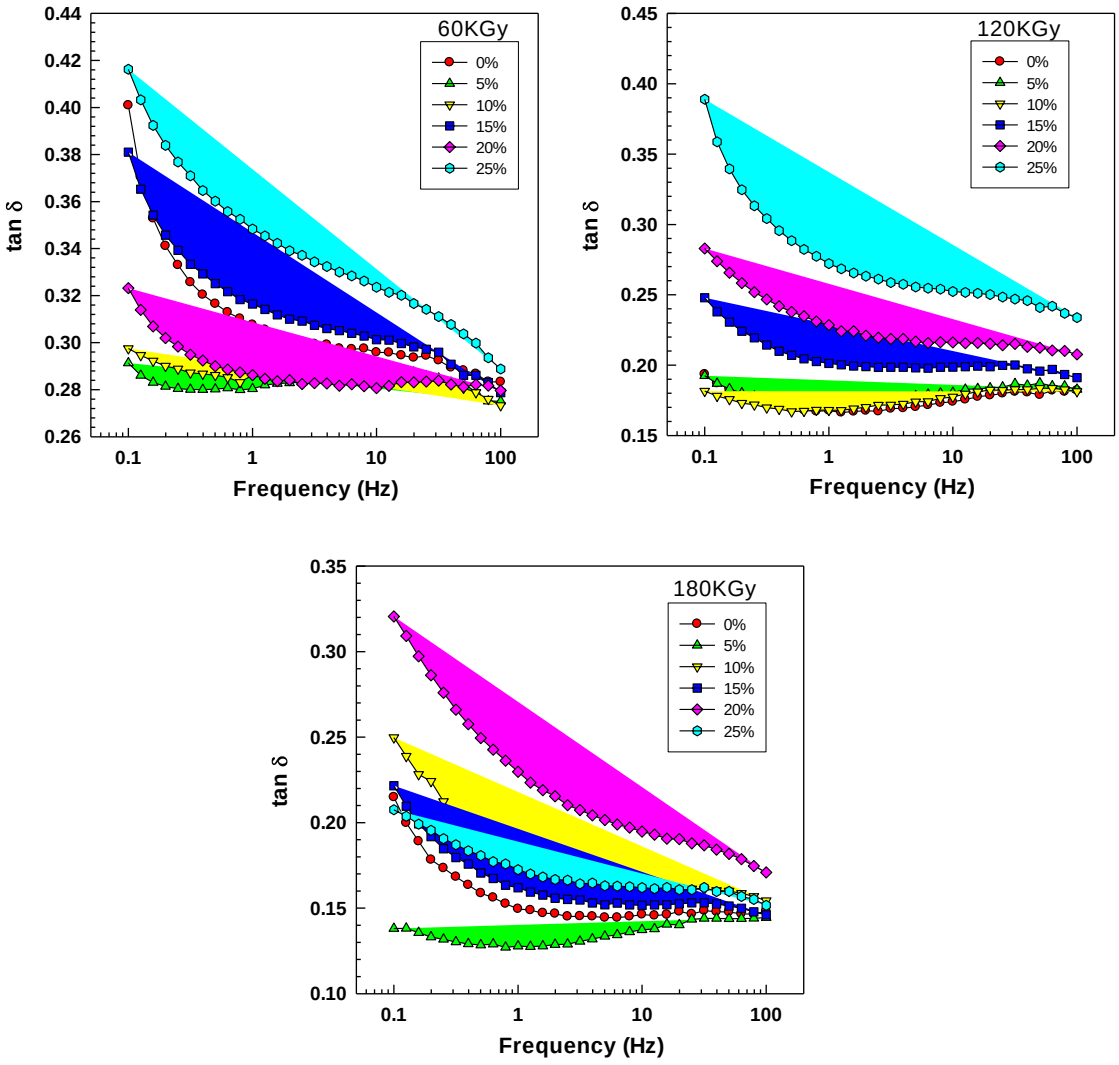

tan δ at 150 °C. as a function of frequency with different carbon fiber wt. %

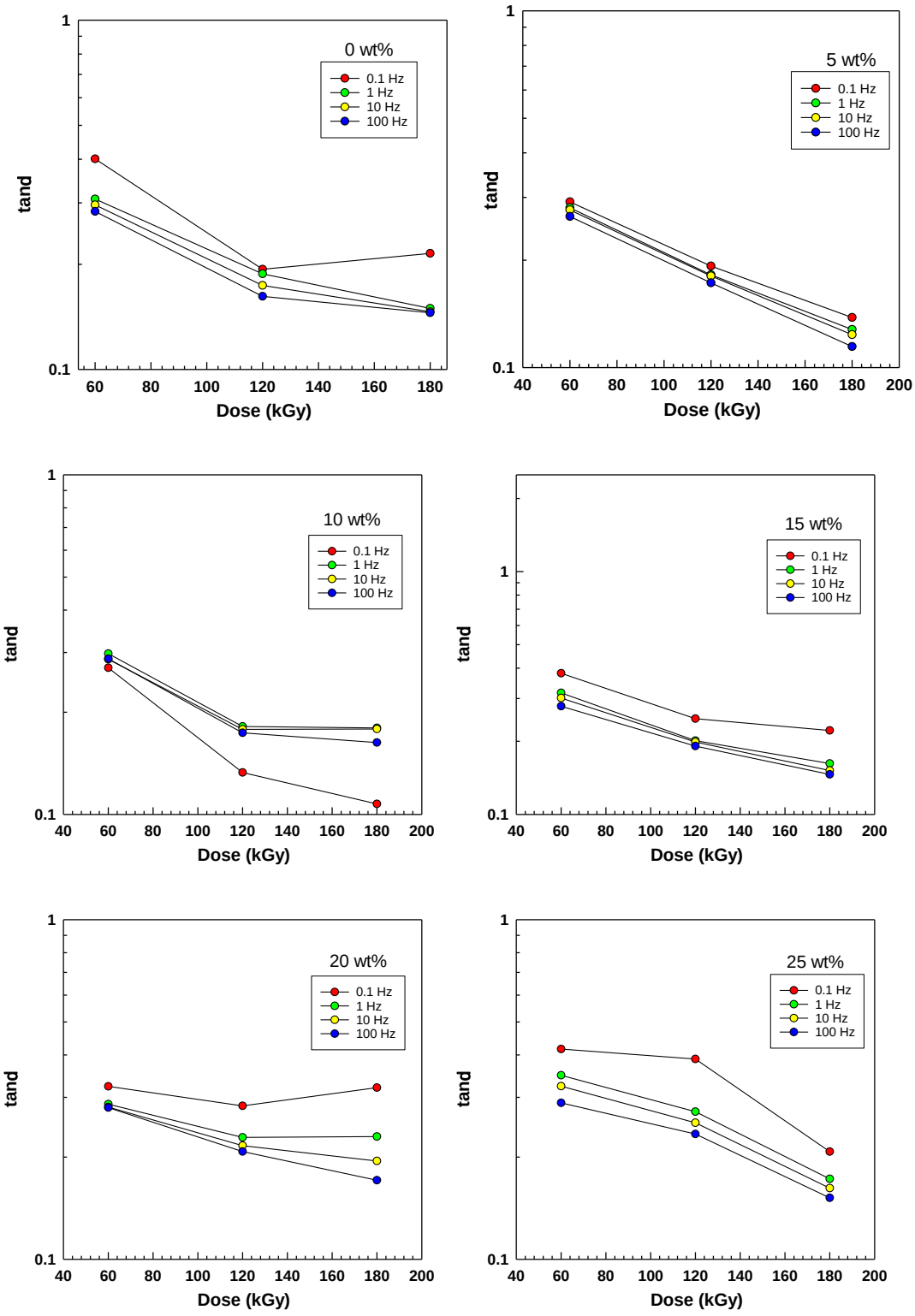

tan δ at 150 °C as a function of Dose (KGy) with different frequency Hz

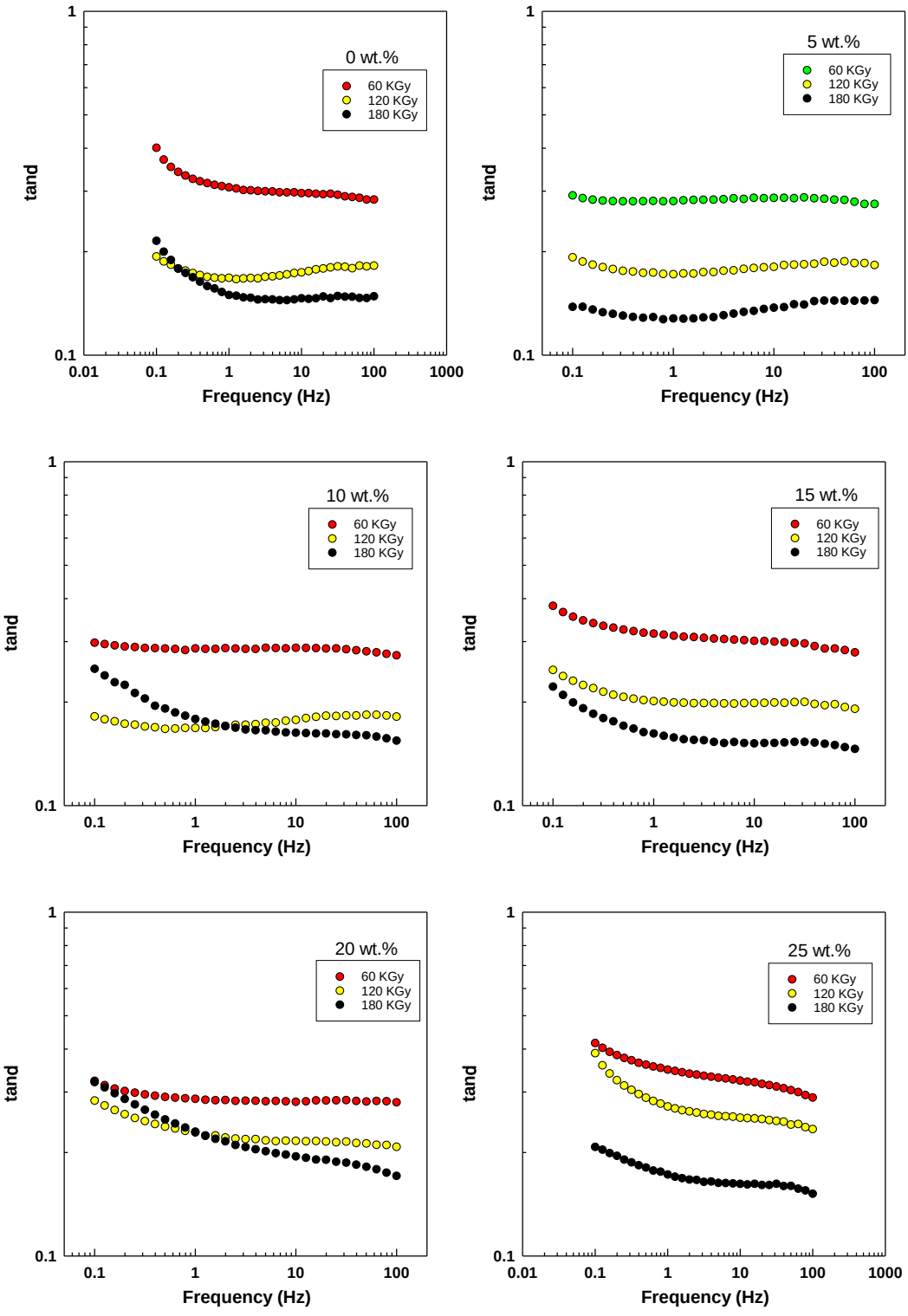

tan δ at 150 °C. as a function of frequency with different carbon fiber wt. %

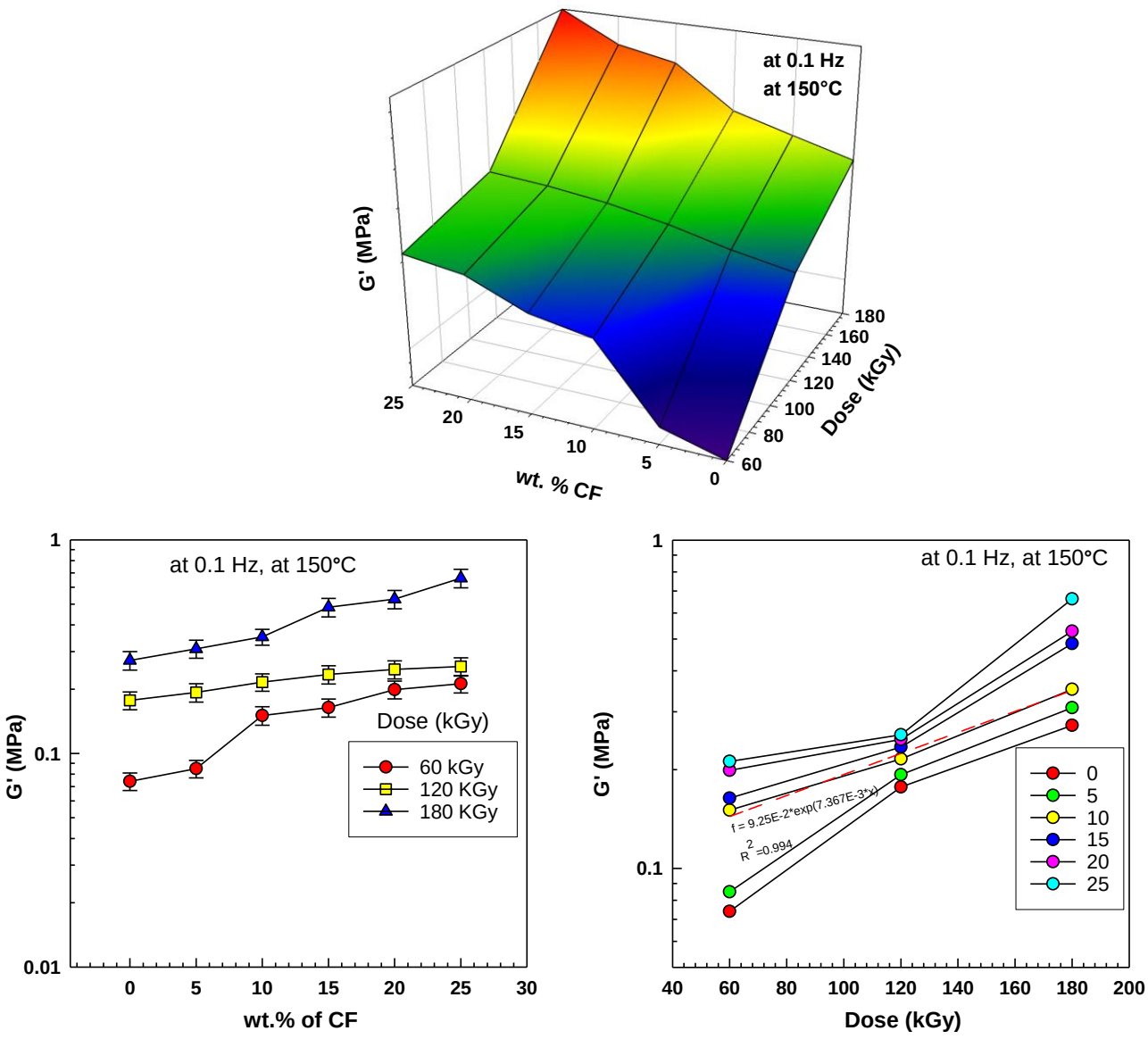

Shear modulus (real part) G' at 150 °C. as a function of Dose (KGy) and carbon fiber content

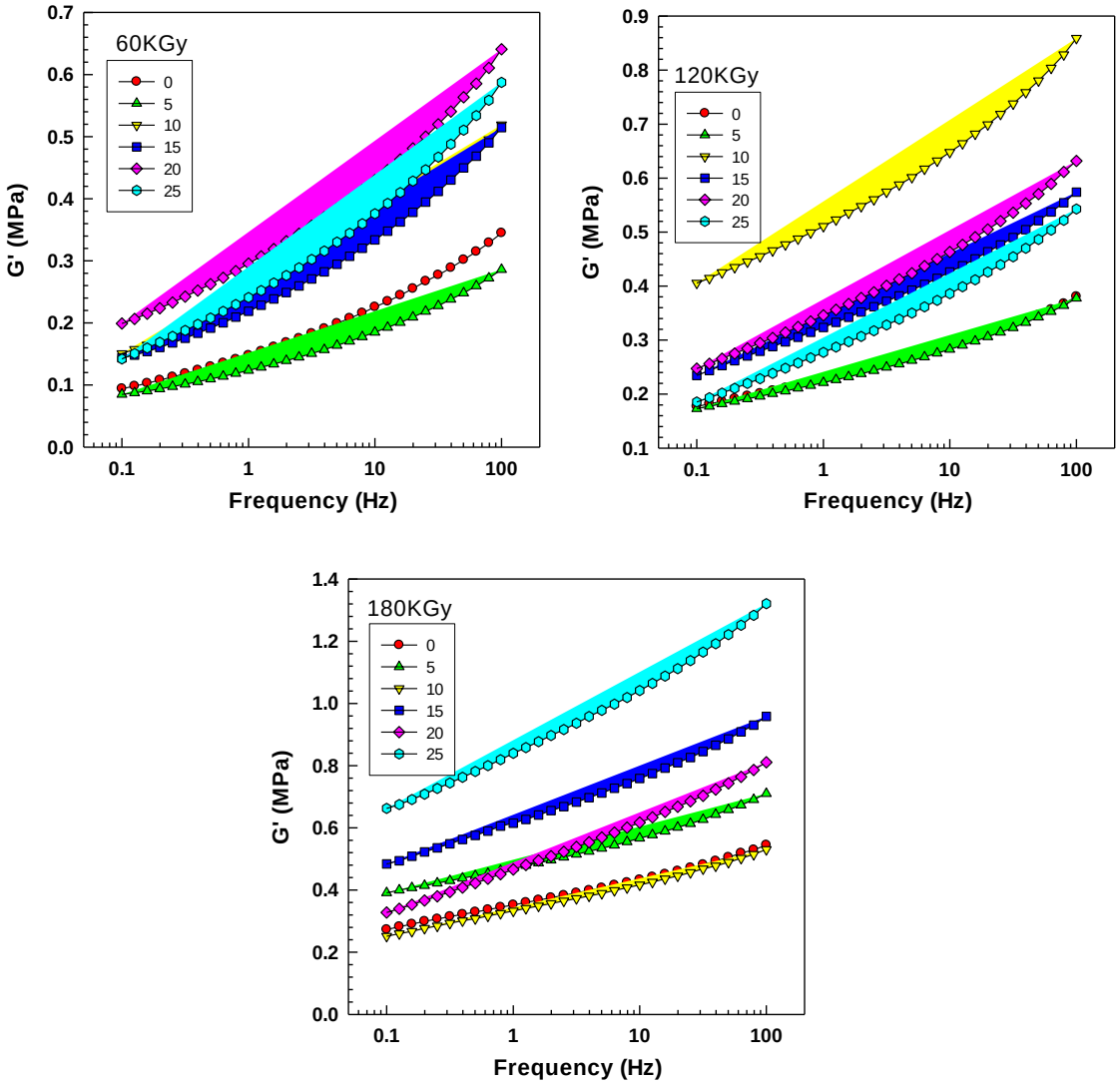

Shear modulus (real part) G'as a function of frequency for different Dose (KGy)

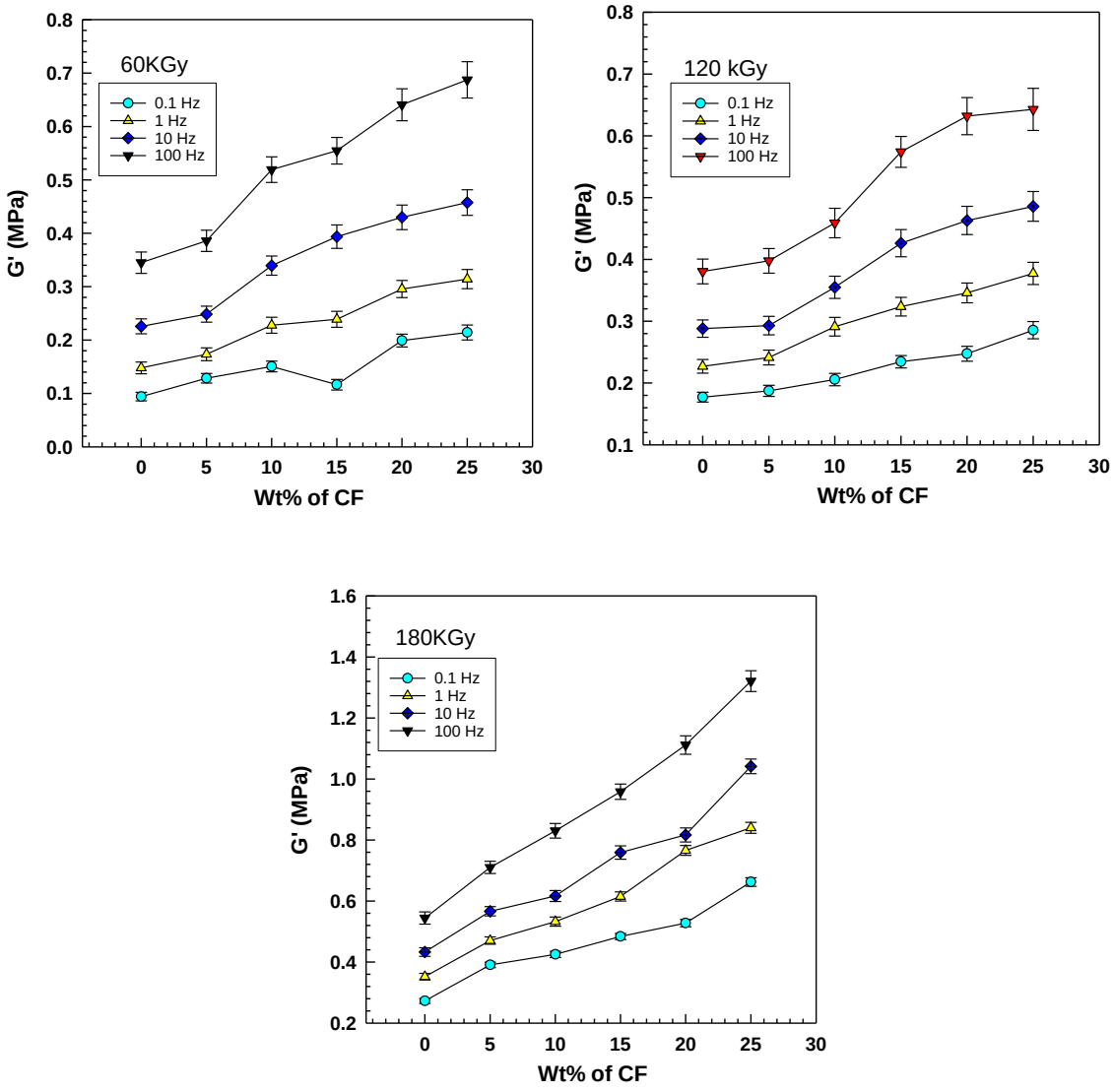

Shear modulus (real part) G'as a function of frequency for different Dose (KGy)

15.2. Influence of Carbon black on ethylene butene copolymer (EBC)

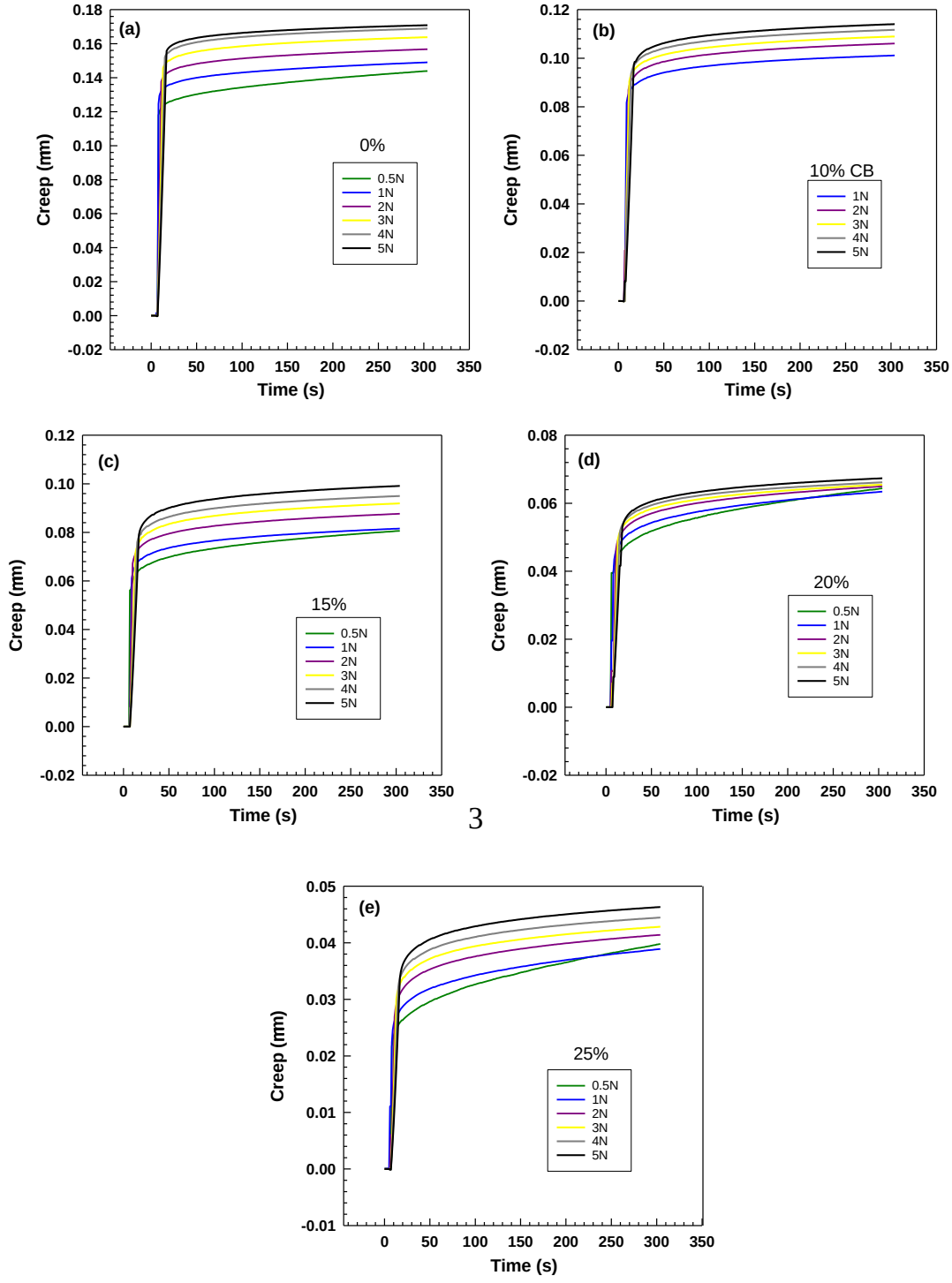

3

Creep–time for as a function of CB at 25 °C as a function of force (N)

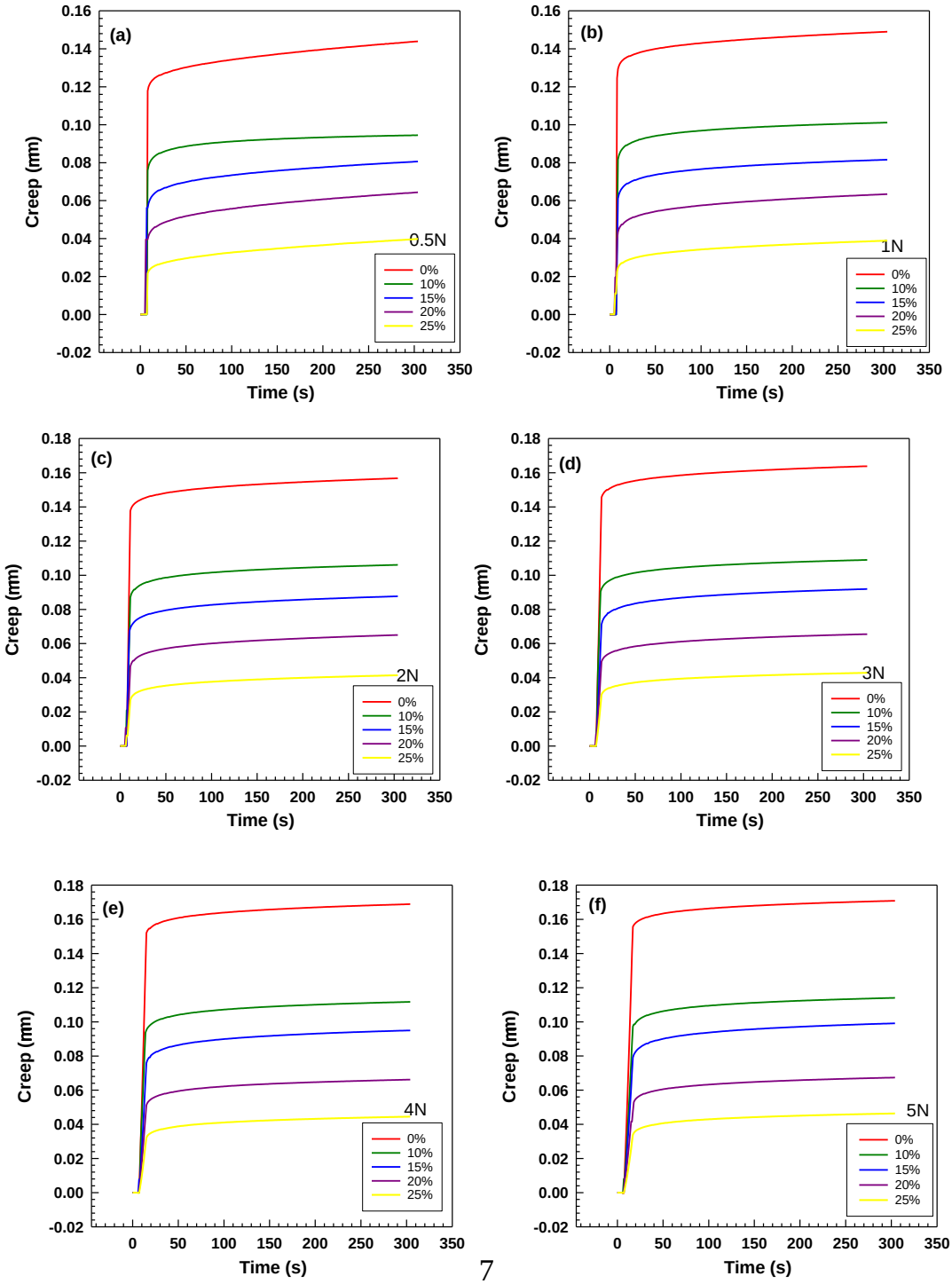

7

creep–time for as a function of CB at 25 °C for different CB wt%

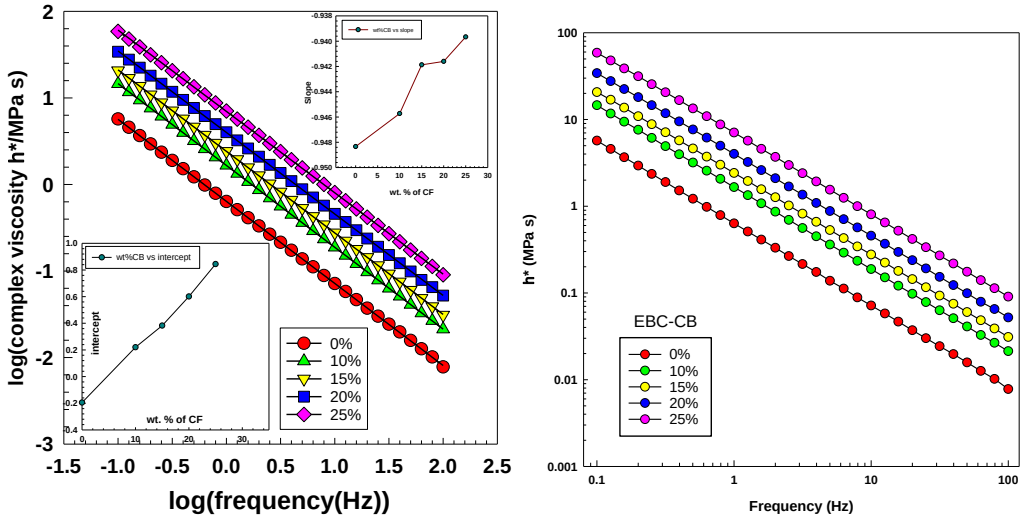

|η| as a function of frequency composites for different CB content for EBC/CB*

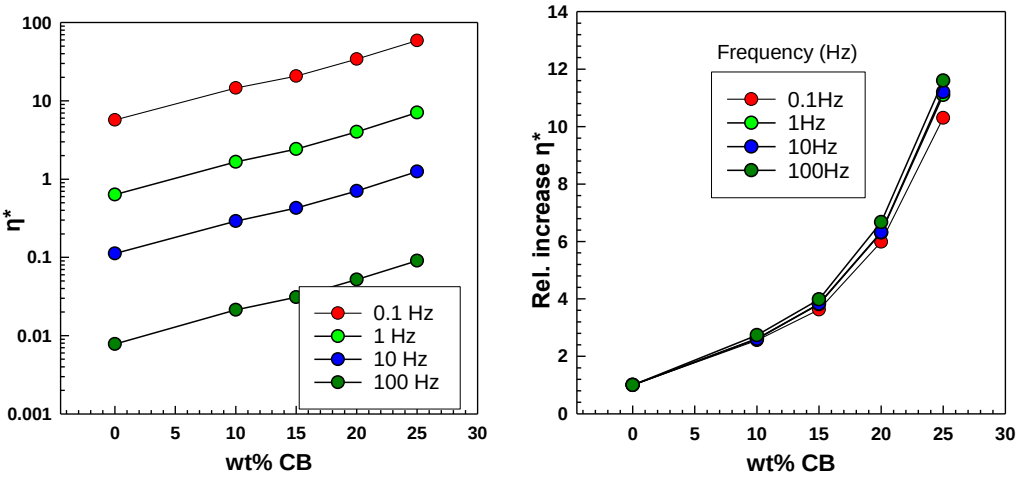

|η| as a function of CB wt. % composites for different frequency Hz'*

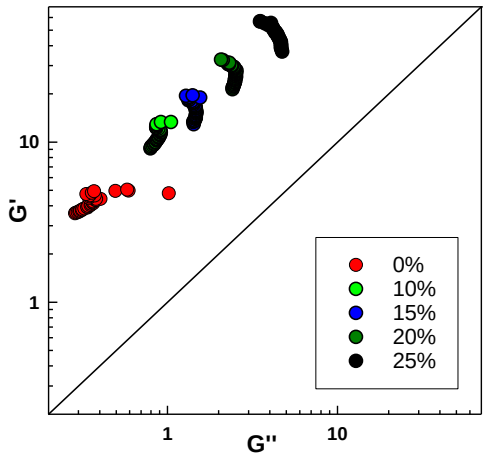

Vector diagram illustrating the relationship between complex shear modulus G*, storage modulus G' and loss modulus G''

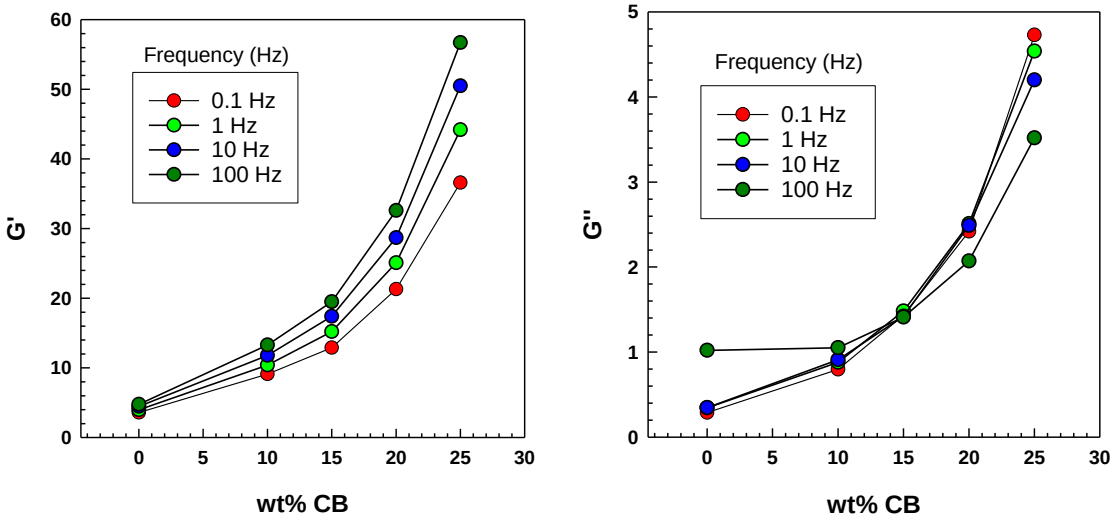

G', G'', as a function of wt. % CB for different frequency Hz

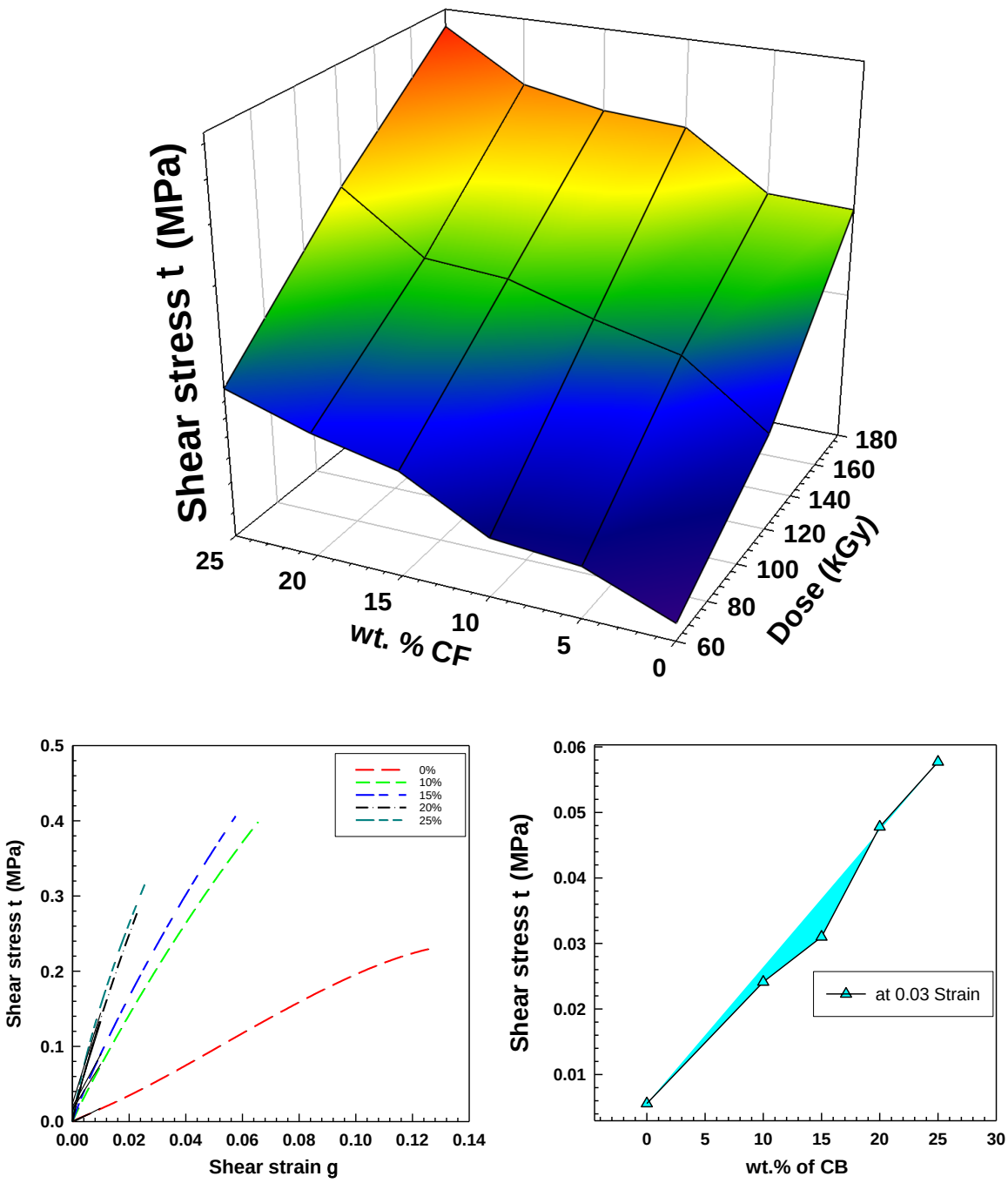

Representative tensile stress-strain curves for EBC/CB for different concentration and at 0.03 Strain

Materials Research Express

OPEN ACCESS

RECEIVED
18 October 2020

REVISED
26 November 2020

ACCEPTED FOR PUBLICATION
8 December 2020

PUBLISHED
22 December 2020

PAPER

Investigation of the influence of carbon black on the rheology and electromechanical properties of ethylene butene copolymer

Yasin Hamid and Petr Svoboda

Department of Polymer Engineering, Faculty of Technology, Tomas Bata University in Zlin, Vavreckova 275, 762 72 Zlin, Czech Republic

E-mail: svoboda@utb.cz

Keywords: conductive polymer, ethylene-butene copolymer, dynamic mechanical analysis, carbon black, mechanical properties

Abstract

In this scientific article, the potential of producing a highly capable sensor by the addition of electric conductive carbon black (CB) to polymer composite was studied, and the effects of various carbon black content on ethylene-butene copolymer (EBC) on rheological and electromechanical were investigated. Electric conductive composites have many attempts at producing original material in technology as a sensor. The amount of (0, 4.07, 6.31, 8.71, and 11.28) volume % of CB was introduced to EBC using Brabender, mixed, and homogenized for 5 min at 180 °C. The dynamic mechanical analysis (DMA) and electromechanical test show that the addition of CB to the EBC would increase the viscosity, modulus, while electric resistance significantly decreased and changed greatly with elongation. The modulus increased from 8.9 to 15 MPa by increase of from 15 to 25 wt% of CB while the gauge factor decreases for about five times by increasing the CB from 15 to 25 wt% under 5 N force. These works demonstrate the possibility of producing strain sensors using a cheap and versatile technique, with potential health and electromechanical sensors.

1. Introduction

The fast development of smart sensors has contributed to smart elastic strain sensors. However, to date, the low stretch-ability and sensitivity of conventional metals or inorganic semiconductor-based strain sensors have restricted their application in this field to some extent [1–4]. Ethylene-butene copolymer (EBC), which is metallocene-based, is widely used in polymer modifications since it has excellent physical properties and is easy to process. EBC has been used with other polymers to increase the physical properties like tensile strength, rebound resilience, and compression set [5–8].

Carbon black (CB) is used as a filler and conductive particle in polymer materials. Several studies [9–13] have been done on CB filler rheological and linear viscosity with the composite's electrical resistance. It is relatively cheap and easy to use with excellent performance in its high electrical conductivity to its automotive, pressure sensor, and gas sensor [14, 15]. Thus, CB is the filler to reinforce the polymer blends to form a polymer composite. Instead, electrically conductive composites have been adequately prepared by adding an electrically conductive filler to polymeric materials. Several researchers have investigated the effect of the addition of various inorganic fillers such as carbon black, carbon nanotubes (CNTs) [16, 17], SiO_2 [18] Nanoclay [19] on the mechanical and electromechanical study of composites with conductive fillers. Slobodian *et al* [20] reported that the Spherical particles like Carbon Black in polymer/carbon black composites exhibit percolation threshold, frequently up to 15–25 wt.%. However, lower values were also published. D'Aloia *et al* [21] investigated that graphene's addition leads to an increase in the graphene-thermosets polymer's electromechanical and mechanical properties graphene concentration increase, the graphene-polymer composite undergoes an insulator-to-metal transition due to the presence of conductive filler inside the matrix. It is also reported that the addition of carbon nanotube to SEBS elastomer could increase electrical resistance. At the same time, the sample is stressed and decreasing when the sample recovers to initial deformation. Additionally, it has been shown that the sample leads to stable after some aging cycles [22]. Yang *et al* [23] investigated the resistance response of

CNT/graphene RTV silicone rubber composites under static and dynamic cyclic loading. It is observed that CNT/graphene RTV silicone rubber composites exhibited a stable and reproducible resistance response under dynamic cyclic loading, indicating that they have potential applications in continuous monitoring. It is also observed that the addition of Carbon nanotube could increase electric conductivity and increase the strain, leading to increased electrical conductivity [24]. Mostly, strain sensors are based on piezoresistive materials, for example, those materials for which an applied strain, ε, results in a resistance change. Commonly, the gauge factor is measured at low strain, which is most metals is small in the range 2 for Nichrome V to 4.8 for Platinum [25]. However, composite strain sensors based on polymers filled with conductive fillers, like multiwalled carbon nanotubes [26] and carbon nanotube [27, 28], can gauge high gauge factors. Piezoresistive materials resistance increases with increasing tensile strain as they have positive gauge factors because interparticle intersections dominate the piezoresistance in composites, leading absolutely to the Gauge factor higher than 0. A small number of materials with negative gauge factors [29]; polymer fibers coated with conducting polymers have demonstrated small negative gauge factors due to chain alignment effects.

Creep study of isotactic polypropylene (iPP)-based graphene nanocomposites used to evaluate the load transfer efficiency by Gaska [30] *et al* they have investigated that significant increase of Young's modulus with increasing filler content which indicates reasonably good dispersion and adhesion between isotactic polypropylene (iPP)-based graphene nanocomposites the and the filler content indicates reasonably good dispersion and adhesion between the iPP and the filler. Wang [31] *et al* reported the same results for numerical analysis using the Finite Element Method used for unidirectional fibrous polymer matrix composites' computing material properties. Srivatsan and Sreekanth [32] investigated the experimental characterization of dynamic mechanical properties of carbon fiber-reinforced composite with sandwich configuration. The addition of carbon fiber up to 40% wt will increase the loss modulus and tan delta curve as the frequency increases. They also indicated that Carbon exhibiting high storage modulus due to its atomic structure directly indicates young's modulus. Sabet *et al* [33] studied the impacts of graphene inclusion on the mechanical, electrical, and low-density polyethylene. They reported that while the addition of 3 wt% of graphene had a significant impact on the performance and improvement of LDPE's electrical characteristics, which is because of the spreading of graphenes in LDPE, which makes to extend more conductive networks. The polymer composite's viscosity is rasing from 120.1 to 195.4 kPa because of the significant interaction between the filler and matrix that obstructed the movement of macromolecular polymeric links. Consequently, graphene has an excessive surface area and nanoscale fat surface that renders it generate resilient interfacial connections with LDPE and significantly affects an excellent consequence of LDPE's chain movement.

The scope of this paper is to investigate the mechanical and electromechanical properties of conductive carbon black (CB) on ethylene Butene copolymer prepared with Brabender contain a various ratio of CB have been investigated. Both mechanical and electromechanical properties characterized by the composites were investigated experimentally. The effect on the piezoresistive response of the mixture was analyzed with an experimental strain-dependent measured electromechanical data. It is shown that the composites realized using a higher amount of CB show a higher electrical conductivity and a substantial increase in Young's Modulus.

2. Methodology

2.1. Material

Ethylene-butene copolymer (ENR 7467) was purchased from DOW Engage® chemical company in the USA with specific properties like ultimate tensile strength 2 MPa, tensile elongation of 600%. The melt flow index (MFI) is 1.2 dg min^{-1} and 0.862 g cm^{-3}. The conductive Carbon Black (KETJENBLACK EC300J) with the composition of 10 wt% polycarbonate with 99.95% purity is used for this study were purchased from Akzo Nobel Polymer Chemicals Ltd. Shanghai, PR China, with a bulk density of 0.125–0.145 g cm^{-3} and apparent density of 2.26 g cm^{-3}, pore volume (DBP) 310–345 ml/100 g and 3.9Ω·cm. This CB is mainly used as an electro-conductive filler used in resin compounds, electro-conductive battery materials, paint, colorant, and toner.

2.2. Preparation of composite

EBC/CF was prepared using Brabender, mixed, and homogenized with different concentrations (0, 10, 15, 20, 25 wt%) for 5 min at 180 °C at 60 rpm according to ASTM D7723 [34]. Then, compression molding was used to prepare the sheets with a thickness of 0.5 mm at 10 MPa with 5 min preheating and 6 min pressing at 180 °C. Finally, the dumble was prepared with a compression cutter for the test. The porosity density was measured according to Archimedes method ASTM B962–15 and was found to be less than 1% which is acceptable.

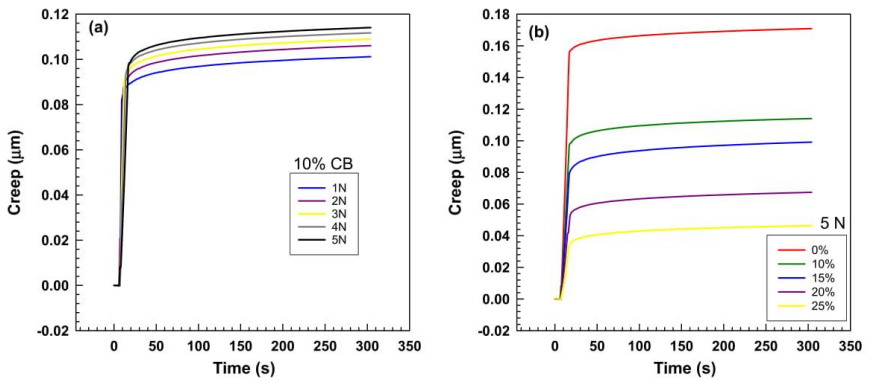

Figure 1. Creep–time for (a) 10% wt CB (b) 5 N curves of EBC/CB composite at 25 °C for different concentration and stress.

2.3. Electric resistance

The two-point probe method with a digital multimeter and four-point probe method using Hall Effect measurements is more common for electrical characterization. However, due to the limitation of four-probe measurement during the starching, the change in EBC/CB's electrical resistance change in strain-relaxation cycles was analyzed with precise weight using the two-point probe technique [35, 36]. Two single-terminal electrodes are attached to the surface of the conductive structure called the two-point probe technique. A DC or AC source current is then connected through the two electrodes, and the subsequent voltage over the same electrodes is estimated. The electrical resistance between these two electrodes is then determined, according to Ohm's law $I = V/R$ where I is the current through the conductor in units of amperes, V is the voltage measured across the conductor in units of volts, and R is the resistance of the conductor in units of ohms [37]. To increase the results' reliability, copper plates used as electrodes were attached to the sample, dissolved the backing adhesive, flooded into butanone solution, and then washed using tap water. After drying and cleaning copper plates, the pellets were sandwiched with upper and lower Ag's electrodes using silver paint around the surface of dumbbell specimens [38, 39]. The test was done using various forces (1, 2, 3, 4, 5 N) for 5 min to measure the strain and electric resistance change in time. When the samples are ready, an electrical circuit powered by a DC power source was applied to the DC source was used for the tests for its simplicity. Nonetheless, it is worth mentioning that, in reality, 1 kHz is commonly used to prevent polarization inaccuracy [37].

2.4. Dynamic mechanical analysis (DMA)

The dynamic mechanical analysis was calculated by the METTLER machine (Osaka, Japan). The samples with dimensions of $11 \times 11 \times 0.5$ mm were tested under Frequency sweep, stress-strain, and Creep relaxation. The stress-strain was analyzed by starting a force of 0 N to 5 N with a 0.5 N min^{-1} force rate at 25 °C. The creep relaxation was measured in three steps. At first, the sample was placed in the DMA machine for 1 min at 25 °C under 0.05 N. Then, the sample was under creep test for 5 min under 1 N force at 25 °C. This test was done for 1, 2, 3, 4, and 5 N respectfully, finally the force drops to 0.05 N for 5 min under 25 °C for relaxation. The frequency sweep test was done at 25 °C with a maximum force of 1 N between 0.1 to 100 Hz by ten steps per decade with 10 μm displacement. Higher frequency than 100 Hz is not recommended as all the specimen sizes except the one with 1 mm thickness are not useful due to their higher demand of displacement which the piezoelectric actuator is not capable of providing [40]

3. Results and discussion

The influence of Carbon black and force on shear stress, creep compliance, frequency sweep, and electromechanical study of the ethylene butene copolymer (EBC) was investigated by Dynamic Mechanical Analysis (DMA). Figure 1 indicates the effect of force and CB content on creep after 5 min of EBC/CB composite.

The creep of the composites with a content of 25 wt% of carbon fiber has the lowest value for almost four times compared to the pure EBC, which has the highest creep. Furthermore, increasing the force could increase

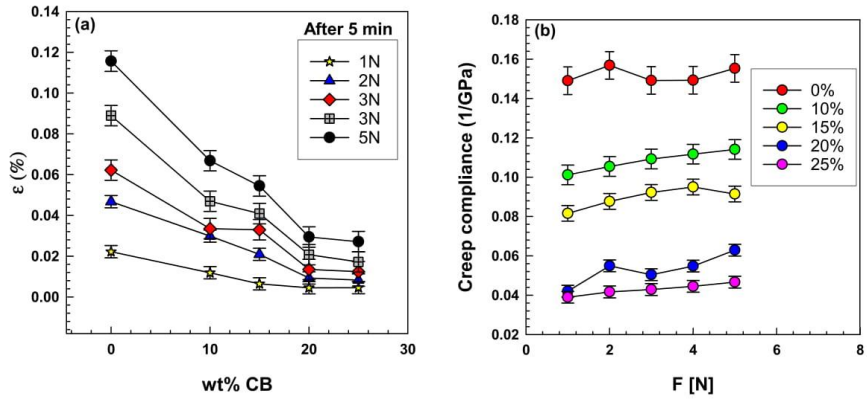

Figure 2. (a) Strain versus CB concentration for different force after 5 min (b) creep compliance versus force for different loading of CB content.

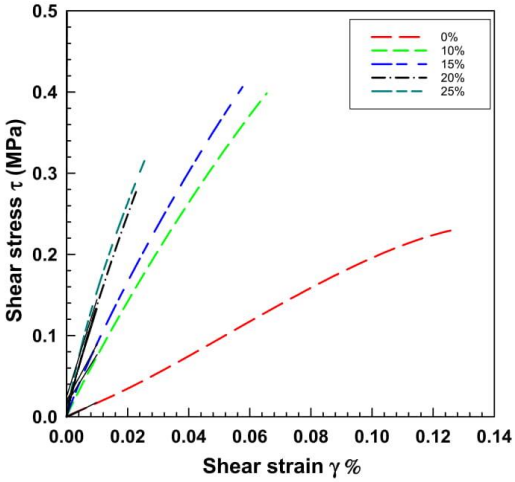

Figure 3. Representative tensile stress-strain curves for EBC/CB for different concentrations.

creep due to the improved interfacial action between the copolymer and the fiber [41]. Additionally, stiffness could be improved by fiber's addition by hindering the matrix material [42].

The stress and creep compliance was measured as a function of CB loading and forces in figure 2. It shows that elongation (ε) significantly decreased by increasing the CB content up to 20% wt. On the other hand, there is not much difference from 20% wt to 25% wt as the fiber looks well dispersed, and the filler covers the matrix. It also indicates that increasing the force up to 5 N could increase elongation six times due to the butene polymer composite's rubber behavior. The creep compliance graph shows that the addition of carbon black to the matrix decreases the creep compliance due to the significant interaction between the fiber and matrix, which leads to the increased modulus.

The Stress-strain tensile curves from DMA tests are shown in figure 3. It shows that the addition of CB to EBC would increase the modules Pa. Table 1 shows the modulus change by the addition of CB fiber at 0.01 shear strain [43] as mathematical representations rely on the linearity of response of both elastic and viscous components. It shows that by increasing the CB content to the matrix, the Young modulus would increase from 7.414 for 10 wt% Pa to 15.305 for 25 wt%. Savetlana *et al* reported that the addition of 20 wt%carbon black to the natural rubber could increase the modulus for 18 times from 2.5 to 47 MPa because of the reinforcing potential

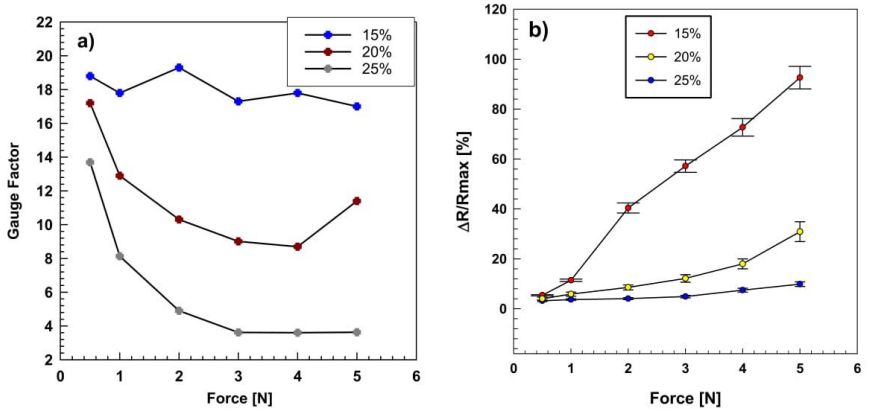

Figure 4. (A) Gauge factor (b) change of electrical resistance versus force for different concentrations of CB.

Table 1. Shear modulus G of EBC/CB composite at 0.01% shear strain.

CB content (wt.%)	Shear modulus G (MPa)
0	1.720 ± 0.08
10	7.414 ± 0.35
15	8.902 ± 0.38
20	13.670 ± 0.52
25	15.305 ± 0.71

from flexible filler formation network and strong polymer-filler coupling. The principal factors determined the capability of reinforcement were (i) Van der walls force between CB and polymer, (ii) the chemical cross-link of polymer into the filler surface due to the free radical reaction between carbon atoms in filler and polymer, and (ii) the mechanical interlocking of the polymer on to the filler surface [44]. Moreover, it looks like increasing fiber content. The copolymer composite tend to acts more brittle, which might be because of the quality of the fibers dispersion and good interaction between carbon black and ethylene butene copolymer. This is the global result of an efficient load transfer from the matrix to the first, strong chemical interactions and second, geometric interactions, such as the high specific surface area between the carbon black surface and the ethylene butane copolymer segments [45–47]. It has been established by numerous studies that addition of carbon base fibers exhibit a significant increase in modulus as compared to the matrix resin. As mentioned earlier, this is mainly due to the fact that functionalization improves both dispersion and stress transfer.

The electric resistance versus force is shown in figure 4(b). In this test, the electrical resistance was measured with a variety of loads for 5 min. However, the addition of CB up to 10% would not affect resistance. It might be related to the low concentration of carbon black in the matrix caused by disassociation between CB particles. That could decrease the resistance to almost zero. There are two types of electrical conduction in the EBC/CB: 'Contact' or 'tunneling' mechanism. Conductive fillers are physically in contact with each other and form a conducting network in the contact mechanism. Nevertheless, the electron's mobility has tunneled between the neighboring conductive fillers separated by the tunneling mechanism's polymeric layers [48, 49].

The gauge factor can be defined as [29, 50]

$$G = \frac{1}{\varepsilon}\left(\frac{\Delta R}{R_0}\right) \tag{1}$$

Where R_0 is initial resistance, ΔR is the change of resistance and ε is a strain. For a composite with strain-independent conductivity behavior, the following relationship is generally followed [51]:

$$\frac{\Delta R}{R_0} = \varepsilon(2 + \varepsilon) \tag{2}$$

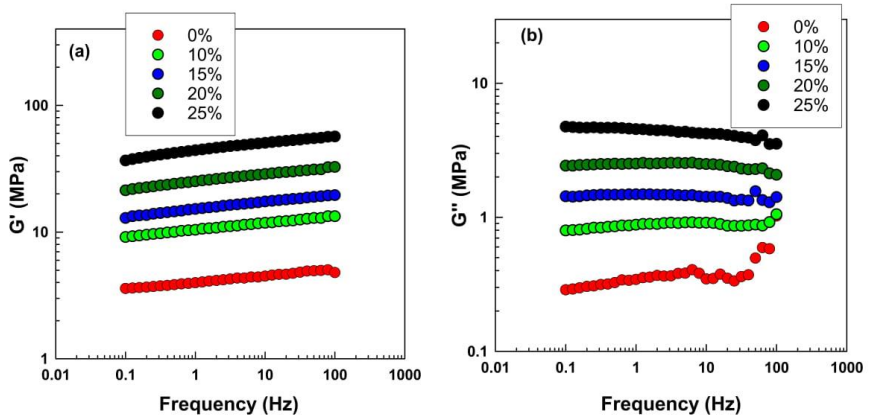

Figure 5. G′ (a), G'' (b), as a function of frequency composites for different CB content for EBC/CB.

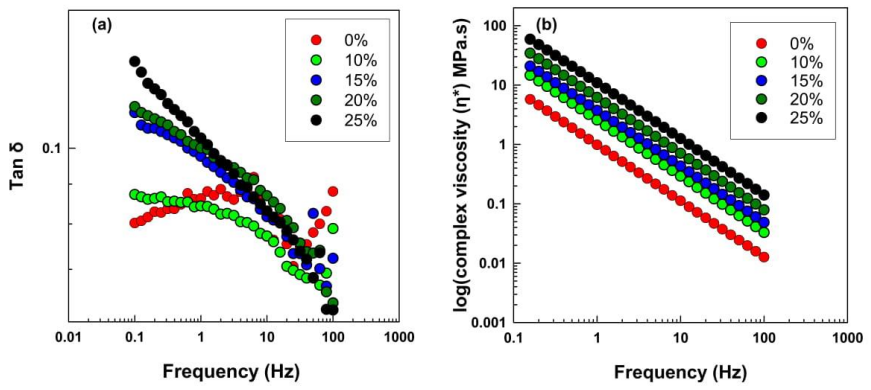

Figure 6. (a) tan δ (b) $|\eta^*|$ as a function of frequency composites for different CB content for EBC/CB.

Figure 4(a) indicates the gauge factor for different CB concentrations under force between 4 and 20, which is around five times higher than conventional metal gauge. It shows that the addition of CB to EBC could decrease the gauge factor with force. The gauge factor is around two at low strain, but it may be as high as 1300 for carbon nanotube/epoxy composite [52]. However, the most reported value is below 100 [50, 53, 54]. The addition of CB from 15 Wt% to 25 wt% leads to an increase in the resistance dramatically, increasing interaction and contacting the CB particles. Moreover, increasing the force leads to a decrease in the thickness of the sample. It caused an increase in the interaction of CB particles. Storage modulus (G') and loss modulus (G'') was tested as a function of shear strain (γ%). In the frequency sweep test, a small amplitude oscillatory shear, $\gamma^{\circ} = \gamma_o \sin(\omega t)$ was applied to the samples. Resulting shear stress was recorded as:

$$\sigma(t) = \gamma_o[G'(\omega)\sin(\omega t) + [G''(\omega)\cos(\omega t)] \quad (3)$$

G', G'' and dynamic viscosity (η^*) were measured as a function of angular frequency (ω) in the range of 0.1–100 rad s^{-1} at a strain value in the linear viscoelastic region [55, 56]. Figure 5 indicates the storage modulus (G′) and loss modulus (G′), Tan δ, and complex viscosity $|\eta^*|$ of the samples as a frequency function.

It is observed that the loose modulus (G′) is more sensitive than G′. It is well known that the storage modulus with the changes of CB content. There is no significant change in storage modulus observed for EBC/CB up to 20 percent because there is no interfacial interaction between CB fiber and EBC. However, EBC with 25% wt content will decrease the storage modulus up to 30% from 5 to 3.5 MPa for the entire frequency rate. On the other hand, it can be observed that G′ is increased significantly by increasing the frequency. It also can be

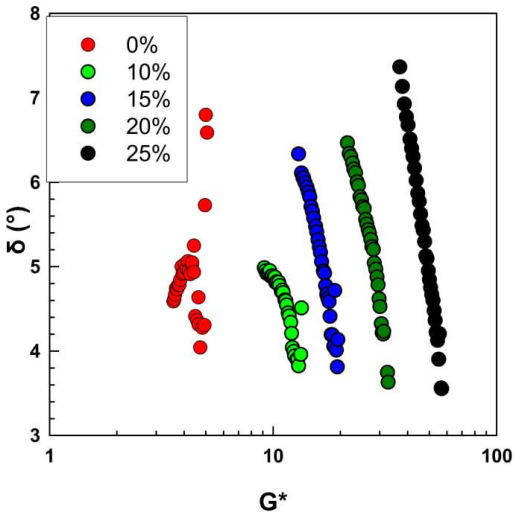

Figure 7. vGP of EBC for different CB content.

Table 2. Power-law factors determined from the $|\eta^*|$ versus log ω from figure 6(b).

ϕ% CB	Composite density g cm^{-3}	k	ω
0	0.862	−0.19512 ± 0.087	−0.94834
4.07	0.92	0.21998 ± 0.0103	−0.94573
6.31	0.95	0.382447 ± 0.0183	−0.94187
8.71	0.98	0.600717 ± 0.0284	−0.9416
11.28	1.02	0.84419 ± 0.0325	−0.93966

observed that the addition of CB up to 25% wt could increase G′ up to 3 times. Dependence of loss factor (tan δ) and complex viscosity $|\eta^*|$ of the samples on frequency is given in figure 6.

Tan δ curves of the polymer copolymer with CB decreased with increasing frequency. The negative slope in the Tan δ curve is a normal behavior of viscoelastic. In contrast, the positive slope refers to the elastic response of the viscoelastic samples dominating this elastic behavior.

$$\tan\ \delta = \frac{G''}{G'} \tag{4}$$

Figure 6(b). $|\eta^*|$ curves with frequency region were fitted by the power-law model to determine the shear-thinning phenomena. The dynamic viscosity is defined by [57]

$$\eta'' = \frac{G'}{\omega} \tag{5}$$

moreover, the elastic part of the complex viscosity:

$$\eta' = \frac{G''}{\omega} \tag{6}$$

$$|\eta^*| = (\eta'^2 + \eta''^2)^{\frac{1}{2}} \tag{7}$$

The power-law equation is written as:

$$|\eta^*| = \mathrm{k}\omega^n \tag{8}$$

Where $|\eta^*|$ is complex viscosity, k is a sample-specific pre-exponential factor, ω is the oscillation frequency in the frequency sweep test, and n is the shear-thinning exponent, which can be directly calculated from the logarithmic plot of complex viscosity $|\eta^*|$ versus frequency (ω) as

$$\log|\eta^*| = \log k + n\log(\omega) \tag{9}$$

The shear-thinning exponent, n, is the straight-line slope obtained by plotting $\log|\eta^*|$ versus $\log\omega$ [58–60].

Calculation of volume fraction (ϕ)

$$w_A = \frac{m_A}{m_A + m_B} \tag{10}$$

Furthermore, since:

$$V = \frac{m_A}{\varrho_A} \tag{11}$$

So

$$\phi = \frac{V_A}{V_A + V_B} \tag{12}$$

While the density of CB and EBC is 2.26 g cm^{-3} and 0.862 g cm^{-3}, respectively. The volume fraction is shown in table 2.

The van Gurp-Palmen (vGP) plot, which plots phase angle $\delta°$ versus complex modulus $|G^*|$, is sensitive to polydispersity and long-chain branching [61, 62].

The complex modulus $|G^*|$ is reported:

$$|G^*| = (G'^2 + G''^2)^{\frac{1}{2}} \tag{13}$$

As shown in figure 7, van Gurp-Palmen curves of EBC/CB show that the addition of CB to the EBC would increase. The blend shows the vGP plot predicted for linear polymers, i.e., a plateau at b = 7° in the low |G*| region.

The graphs show that additional CB content could increase $\delta°$ from 3.5° to 7°. Several studies have been reported about vGP, which have been similar tend peak followed by a downward tendency [62–65].

4. Conclusion

The linear viscosity and electromechanical properties of ethylene butene copolymers filled with electric conductive carbon black are investigated. The dynamic mechanical viscosity and modulus were found to be increased with the addition of carbon black into ethylene butene copolymer. Moreover, the electrical resistance is growing with carbon black content due to the interaction and contact between the particles. The elongation (ε) significantly decreases by increasing the CB content regarding the well disperses and hardening effect of CB. These work results establish manufacturing elastic strain sensors' potential using an economical and multipurpose method, with potential applications in flexible electronics products.

ORCID iDs

Yasin Hamid https://orcid.org/0000-0001-9786-6879
Petr Svoboda https://orcid.org/0000-0002-7320-5467

References

[1] Liu H, Li Q, Zhang S, Yin R, Liu X, He Y, Dai K, Shan C, Guo J and Liu C 2018 *Journal of Materials Chemistry C* **6** 12121
[2] Kim K-H, Hong S K, Ha S-H, Li L, Lee H W and Kim J-M 2020 *Materials Horizons* **7** 2662
[3] Akhtar I and Chang S-H 2020 *Nanoscale* **12** 21447–58
[4] Ke K, Sang Z and Manas-Zloczower I 2019 *Nanoscale Advances* **1** 2337
[5] Liu Z Y, Chen S J and Zhang J 2011 *J. Polym. Res.* **18** 2403
[6] Park K W, Chowdhury S R, Park C C and Kim G H 2007 *J. Appl. Polym. Sci.* **104** 3879
[7] Deng K Q, Felorzabihi N, Winnik M A, Jiang Z H, Yin Z H, Yaneff P V and Ryntz R A 2009 *Polym. Advan Technol.* **20** 235
[8] Escher F F N, Galland G B and Ferreira M R 2003 *J. Polym. Sci. Pol. Chem.* **41** 2531
[9] Wang Y K, Zhu G M, Cui X P, Liu T T, Liu Z and Wang K 2014 *Colloid Polym. Sci.* **292** 2311
[10] Oliveira F A, Alves N, Giacometti J A, Constantino C J L, Mattoso L H C, Man A M O A and Job A E 2007 *J. Appl. Polym. Sci.* **106** 1001
[11] Harea E, Datta S, Stenicka M and Stocek R 2019 *Express Polym. Lett.* **13** 1116
[12] Elhaouzi F, Mdarhri A, Brosseau C, El Aboudi I and Almaggoussi A 2019 *Polym. Bull.* **76** 2765
[13] Duan L, Spoerk M, Wieme T, Cornillie P, Xia H, Zhang J, Cardon L and D'Hooge D R 2019 *Compos. Sci. Technol.* **171** 78
[14] Gouma P I, Prasad A K and Iyer K K 2006 *Nanotechnology* **17** S48
[15] Biccai S, Boland C, O'Driscoll D *et al* 2019 *Acs Nano* **13** 6845–55
[16] Kumar Patel K, Purohit R, Hashmi S, Kumar Gupta R and Kumar Dwivedi S 2019 *Applied Innovative Research (AIR)* **1** 21–4 (http://nopr.niscair.res.in/handle/123456789/45842)
[17] Abidin M S Z, Herceg T, Greenhalgh E S, Shaffer M and Bismarck A 2019 *Compos. Sci. Technol.* **170** 85

[18] Qin J Q, Zhao H, Zhu R Q, Zhang X Y and Gu Y 2007 *J. Appl. Polym. Sci.* **104** 3530
[19] Islam M E, Mahdi T H, Hosur M V and Jeelani S 2015 *Procedia. Engineer* **105** 821
[20] Slobodian P, Lengálová A, Sáha P and Šlouf M 2007 *J. Reinf. Plast Comp.* **26** 1705
[21] D'Aloia A G, Proietti A, Bidsorkhi H C, Tamburrano A, De Bellis G, Marra F, Bregnocchi A and Sarto M S 2018 *Polymers* **10** 82
[22] Dios J R, García-Astrain C, Costa P, Viana J C and Lanceros-Méndez S 2019 *Materials* **12** 1405
[23] Yang H, Yao X F, Yuan L, Gong L H and Liu Y H 2019 *Nanoscale* **11** 578
[24] Slobodian P, Riha P and Olejnik R 2011 *New Developments and Applications in Sensing Technology* ed S. C. Mukhopadhyay, A Lay-Ekuakille and A Fuchs (Berlin: Springer) (https://doi.org/10.1007/978-3-642-17943-3_12)
[25] Fiorillo A, Critello C and Pullano S 2018 *Sens. Actuators, A* **281** 156
[26] Sanli A, Muller C, Kanoun O, Elibol C and Wagner M F X 2016 *Compos. Sci. Technol.* **122** 18
[27] Zhu Z H 2015 *IEEE Nanotechnol Mag.* **9** 11
[28] Ferreira A and Lanceros-Mendez S 2016 *Compos Part B-Eng.* **96** 242
[29] Biccai S, Boland C S, O'Driscoll D P, Harvey A, Gabbett C, O'Suilleabhain D R, Griffin A J, Li Z, Young R J and Coleman J N 2019 *ACS Nano* **13** 6845–55
[30] Gaska K, Manika G C, Gkourmpis T, Tranchida D, Gitsas A and Kádár R 2020 *Polymers* **12** 1309
[31] Wang Z and Smith D E 2019 *Compos. Struct.* **229** 111394
[32] Srivatsava M and Sreekanth P S R 2020 *Materials Today: Proceedings* **27** 931
[33] Sabet M, Soleimani H and Hosseini S 2020 *Polym. Bull.* **77** 459
[34] Thongnuanchan B, Nantayos W, Lopattananon N, Rattanapan S, Thitithammawong A and Nakason C 2019 *J. Polym. Environ.* **27** 1807
[35] Yee M J, Mubarak N M, Khalid M, Abdullah E C and Jagadish P 2018 *Scientific Reports* **8** 17295
[36] Tadesse M G, Mengistie D A, Loghin C, Chen Y, Wang L, Catalin D, Muller C and Nierstrasz V 2017 *17th World Textile Conf. Autex - Shaping the Future of Textiles*
[37] Ngabonziza Y and Li J 2011 *IMETI 2010-3rd International Multi-Conference on Engineering and Technological Innovation, Proceedings* 1, 241
[38] Huang Y, Li H and Qian S 2018 *Constr. Build. Mater.* **174** 253
[39] Sudakar C and Kutty T R N 2004 *J. Electron. Mater.* **33** 1280
[40] Esmaeeli R, Aliniagerdroudbari H, Hashemi S R, Jbr C and Farhad S 2019 *Modelling and Simulation in Engineering* **2019** 7026267
[41] Yu K J, Wang M L, Wu J Q, Qian K, Sun J and Lu X F 2016 *Nanomaterials* **6** 1–11
[42] Hamid Y, Abu Bakar A and Deirram N 2013 *J. Appl. Polym. Sci.* **128** 1170–5
[43] Capela C, Oliveira S and Ferreira J 2017 *Fibers Polym.* **18** 1200
[44] Savetlana S, Zulhendri, Sukmana I and Saputra F A 2017 *IOP Conf. Ser.: Mater. Sci. Eng.* **223** 1–9
[45] Hamid Y, Bakar A A and Deirram N 2013 *J. Appl. Polym. Sci.* **128** 1170
[46] Hamid Y, Svoboda P and Svobodova D 2020 *J. Vinyl Add. Tech.* **26** 325
[47] Le T-T 2020 *J. Compos. Mater.* **9** 1–25
[48] Varghese A M, Rangaraj V M, Mun S C, Macosko C W and Mittal V 2018 *Ind. Eng. Chem. Res.* **57** 7834
[49] Yousefi N, Sun X, Lin X, Shen X, Jia J, Zhang B, Tang B, Chan M and Kim J K 2014 *Adv. Mater.* **26** 5480
[50] Bhandari S 2019 *Carbon-Containing Polymer Composites* ed M Rahaman, D Khastgir and A K Aldalbahi (Singapore: Springer) (https://doi.org/10.1007/978-981-13-2688-2_14)
[51] Chen S, Lou Z, Chen D, Jiang K and Shen G 2016 *Adv Mater Technol-Us* **1** 1600136
[52] Anand S V and Mahapatra D R 2009 *Smart Mater. Struct.* **18** 045013
[53] Costa P, Oliveira J, Horta-Romarís L, Abad M-J, Moreira J A, Zapiráin I, Aguado M, Galván S and Lanceros-Mendez S 2018 *Compos. Sci. Technol.* **168** 353
[54] Zhou J and Hsieh Y-L 2018 *Acs Appl. Mater Inter* **10** 27902
[55] Adefisan O O and McDonald A G 2019 *Maderas. Ciencia y Tecnología* **21** 3–14
[56] Arulmurugan M, Prabu K, Rajamurugan G and Selvakumar A 2019 *Mater. Res. Express* **6** 1–13
[57] Macosko C W 1994 *Rheology - Principles, Measurements and Applications* (New York: John Wiley & Sons.)
[58] Durmuş A, Woo M, Kaşgöz A, Macosko C W and Tsapatsis M 2007 *Eur. Polym. J.* **43** 3737
[59] Durmus A, Kasgoz A and Macosko C W 2007 *Polymer* **48** 4492
[60] Mussatti F G and Macosko C W 1973 *Polymer Engineering & Science* **13** 236
[61] Gu L, Xu Y, Fahnhorst G W and Macosko C W 2017 *J. Rheol.* **61** 785
[62] Trinkle S, Walter P and Friedrich C 2002 *Rheol. Acta* **41** 103
[63] López-Barrón C and Macosko C 2014 *Journal of Rheology* **58** 1935–53
[64] Rulduà M L M, Raquez J, Re G, Santana O, Dubois P and Cailloux J 2019 *Materiales Compuestos* **3** 107–11
[65] Delgado D E, Sturdy L F, Burkhart C W and Shull K R 2019 *J. Polym. Sci., Part B: Polym. Phys* **57** 1246–54

Influence of Electron Beam Irradiation on High-Temperature Mechanical Properties of Ethylene Vinyl Acetate/Carbon Fibers Composites

Yasin Hamid[1], **Petr Svoboda**[1], **Dagmar Svobodova**[2]

[1]*Department of Polymer Engineering, Faculty of Technology, Tomas Bata University in Zlin, Vavreckova 275, 762 72, Zlin, Czech Republic*

[2]*Language Centre, Faculty of Humanities, Tomas Bata University in Zlin, Stefanikova 5670, 760 01, Zlin, Czech Republic*

The purpose of this study was to investigate the effect of carbon fiber (*CF*) and electron-beam (EB) radiation on high-temperature mechanical properties of ethylene-vinyl acetate (EVA). Polymer composites were prepared by mixing on a two-roll mill. After compression molding, the samples were irradiated between 60 and 180 kGy, and dynamic mechanical analysis (DMA) was used to characterize physical properties. The effects of filler content and radiation level on the mechanical properties of EVA/*CF* were evaluated. The shear stress and modulus were observed to increase with increasing of the filler level. However, there was a dramatic decrease in creep compliance. It was also shown that introduction of irradiation on EVA composite increases the shear stress and the real part of the dynamic shear modulus G' due to the increase in molecular weight and cross-linking of the polymer after irradiation. J. VINYL ADDIT. TECHNOL., 2019.

INTRODUCTION

Carbon-filled polymer composites have been popular due to their extensive utilization in various electronic equipment like temperature, pressure, dielectric, strain, gas, and biosensor materials [1].

Carbon fibers (*CF*) have become an important reinforcing material in advanced composites because of their extremely high strength, stiffness, and heat-resistance, and low weight. Fiber-reinforced polymer composites are of great interest due to their very high strength-to-weight and stiffness-to-weight ratios. These properties are sought after in materials used in aerospace, engineering, marine industries, and automobile industries [2].

The adhesion at the interface between matrix and fiber is an important issue in controlling the composite properties. An excellent interface between fiber and matrix can increase the stability and transfer the stress from matrix to fiber. However, chemical inertness and smooth surface of the fiber causes poor adhesion and lower enhancement in the properties of the composite [3,4].

E-beam radiation leads to cross-linking, to free radical formation and to chain scission, which cause a modification to the polymer structure. It was reported that e-beam radiation cross-linking could increase the electrical, mechanical, and optical properties in the polymer [5].

It has also been observed that introducing carbon fiber or nanotube to EVA can improve the modulus and the tensile strength of the composite. Following, the mechanical properties and dynamic properties can be enhanced by entering the e-beam irradiation due to improving the filler to matrix interaction, which was shown in swelling resistance studies [6].

Polymer material radiation processing involves ionizing radiation of polymer treatment to enhance their chemical and mechanical properties. During the ionizing irradiation, polymers can cross-link, be grafted, or degrade. [7,8] Mateev *et al*. investigated the effect of e-beam irradiation on gel formation process of EVA/PE films in range 40-250 kGy when the major change in gel content occurred in range 40-170 kGy [9]. This fact and our experience from our previous experiments [10] influenced our range of e-beam radiation, being this time 60, 120, and 180 kGy.

Electron beam (EB) irradiation on EVA/*CF* composite has been used in this study, and a variety of fiber concentration has been investigated. In this article, the mechanical properties of EVA/*CF* composite under EB irradiation have been studied in detail. Testing of mechanical properties was done at room temperature (25 °C) and also at 150 °C. We are presenting only high-temperature results since they better reflect the influence of e-beam cross-linking.

At room temperature, the amorphous polymer chains are held together by crystal lamellae and by covenant bonds

Correspondence to: Y. Hamid; e-mail: hamid@utb.cz
Univerzita Tomáše Bati ve Zlíně; contract grant number: IGA/FT/2017/007.
DOI 10.1002/vnl.21747
Published online in Wiley Online Library (wileyonlinelibrary.com).

(from cross-linking). However, at 150 °C, only the chemical cross-linking holds the amorphous chain together.

EXPERIMENT

Material

Ethylene vinyl acetate with a trade name Supreme Ultra FL 00328 has been used. It was supplied by ExxonMobil Chemical Belgium (Antwerp Belgium), and the melt flow index (MFI) is 3.0 g/10 min and density is 0.951 g/cm^3; with 28 wt% of vinyl acetate. Carbon fiber was T700SC 12000-50C; it was provided by Torayca (Toray Carbon Fibers America) from Japan. It is a high strength, standard modulus fiber. This never twisted fiber is used in the high-tensile application. The specification of fiber is given in Table 1.

Preparation of the Composite

EVA copolymer with carbon fiber was mixed and homogenized with various concentrations (5, 10, 15, 20, 25 wt%) using two-roll mill at 150 °C for 5 min. Following, a sheet with a thickness of 0.5 mm was prepared by compression molding at 10 MPa with 5 min preheating at 150 °C and 5 min pressing; it was then placed into another cold press under pressure.

Electron-Beam Irradiation

Electron-beam irradiation was applied at room temperature in BGS Beta-Gama-Service Gmbh, Germany. The process was controlled not to surpass 50 °C. The source of radiation was toroid electron accelerator Rhodotron (10 MeV, 200 kW). The irradiation was applied in a tunnel on a moderately moving conveyor with the irradiation dosage ranging from 60 to 180 kGy (30 kGy per pass) with 3 m/min belt speed and 10 mA with 78 cm sample distance from the scanner for 2 s irradiation.

Dynamic Mechanical Analysis (DMA)

The dynamic mechanical analysis was performed by METTLER Toledo Switzerland. Samples with dimensions of $11 \times 11 \times 0.5$ mm were tested for creep-relaxation, stress–strain, and frequency sweep. The stress–strain was performed in a force range 0 to 2 N with 0.4 N/min force rate at 150 °C.

The creep relaxation was measured in three steps. At first, the sample was placed in DMA machine for 1 min at 150 °C under 0.05 N. Then, the sample was under creep test for 5 min at 150 °C under 1 N force. Finally, the force dropped to 0.05 N for 5 min at 150 °C for relaxation.

The frequency sweep test was done at 150 °C with a preload force of 0.1 N in the frequency range 0.1 to 100 Hz by 10 steps per decade with 10 μm displacement.

TABLE 1. Carbon fiber properties.

Tensile strength	2,450 MPa
Tensile modulus	125 GP
Strain	2.1%
Density	1.8 g/cm^3
Filament diameter	7 μm

Gel Content

The gel contents of electron beam cross-linked EVA samples were obtained by a calculation of the insoluble cross-linked material after extracting the solvent according to ASTM D2765-01. A small amount of cross-linked material (about 0.15 g) was wrapped in a stainless steel cage and placed in boiling xylene solvent for 6 h with 1 wt% of an antioxidant. The sample was weighted after evaporation of the solvent. Finally, the gel content was calculated as the percent ratio of the final weight to the initial weight of the sample multiplied by one hundred.

Optical Microscopy

Dimensions of carbon fibers were evaluated by optical microscopy using an Olympus RX41 microscope (Tokyo, Japan) to calculate the aspect ratio (L/D length over diameter) of carbon fibers in the composite.

Size-Exclusion Chromatography

The molecular weight measurement was performed at 160 °C on a Polymer Laboratories PL 220 high-temperature chromatograph (Polymer Laboratories, Varian Inc., Church Stretton, Shropshire, England) equipped with three 300 mm x 7.5 mm PLgel Olexis columns and a differential refractive index detector. 1,2,4-trichlorobenzene (TCB) was used as an eluent, stabilized with butylhydroxytoluene (BHT) (Ciba, Basel, Switzerland) as an antioxidant. A mobile phase flow rate of 1 mL min^{-1} was used, and the volume 200 μL was injected. Sample was prepared to a concentration of 0.5 mg mL^{-1} in TCB. Narrowly distributed polyethylene standards (Polymer Standards Service GmbH, Mainz, Germany) were used for calibration purposes.

RESULTS AND DISCUSSION

The influence of carbon fibers and radiation on shear stress, on creep compliance and on frequency sweep of ethylene vinyl acetate (EVA) was investigated by dynamic mechanical analysis. The addition of carbon fiber into EVA leads to a significant increase in shear stress (see Fig. 1). This behavior is similar to the one reported by Das *et al.* [11].

The shear stress of the EVA composites with a content of 20 wt% of carbon fiber has the highest value, while the pure EVA has the lowest shear stress at the same shear strain (such as at 0.10 strain the values are about 0.004 and 0.007 MPa for 0 and 20 wt% of *CF*, respectively), due to

DOI 10.1002/vnl

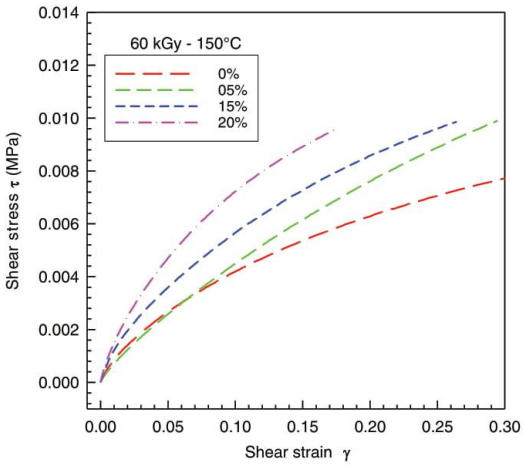

FIG. 1. Shear stress–strain curves of EVA/*CF* composites. [Color figure can be viewed at wileyonlinelibrary.com]

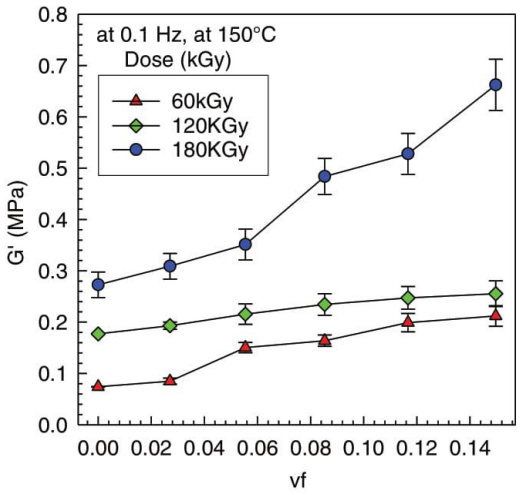

FIG. 2. Experimental dynamic shear modulus (real part) G' at 150 °C at frequency 0.1 rad/s [Color figure can be viewed at wileyonlinelibrary.com]

the improved interfacial action [12]. Hamid *et al*. reported that fiber could impart an extreme improvement in stiffness by hindering the movement within the matrix [13].

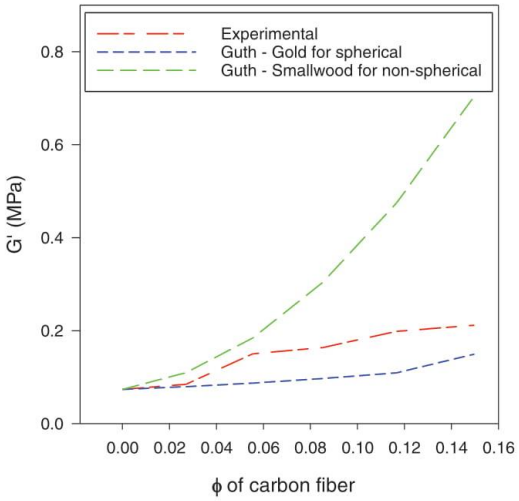

FIG. 3. Prediction of modulus with Guth‑Gold for spherical and Guth‑Smallwood for non-spherical filler versus experimental data. [Color figure can be viewed at wileyonlinelibrary.com]

Increase of shear modulus as a function of increasing CF content is illustrated in Fig. 2. The highest values of G' were found for the sample irradiated by 180 kGy. These results are in agreement with other scientists. Increase in G' due to increasing volume fraction of carbon nanotubes was reported by Potschke *et al*. [14]. Increase in G' values at 0.1 rad/s due to increasing e-beam radiation for ethylene-octene copolymer was reported by Poongavalappil *et al*. [15].

To calculate the relative G' increase, it is necessary to calculate the volume fraction of the fiber in the composite.

Calculation of volume fraction (Φ_A) from weight fraction w_A

$$w_A = \frac{m_A}{m_A + m_B} \tag{1}$$

Furthermore, since:

$$V_A = \frac{m_A}{\varrho_A} \tag{2}$$

So

TABLE 2. Shear modulus for experimental data, Guth-Gold model for spherical particles, and Guth-Smallwood model for non-spherical particles.

Wa	Φa	Density (g/cm^3)	Experimental at 0.1 Hz	G = Gm (1+ 2.5Φ + 14.1Φ^2)	Gc = Gm (1 + 0.67 f Φ + 1.62f ^{2}Φ^2)
0	0	0.951	0.0740	0.0740	0.0740
0.05	0.0270	0.974	0.0849	0.0797	0.1100
0.10	0.0554	0.998	0.1505	0.0874	0.1847
0.15	0.0852	1.023	0.1638	0.0973	0.3040
0.20	0.1166	1.050	0.1990	0.1097	0.4748
0.25	0.1497	1.078	0.2119	0.1497	0.7044

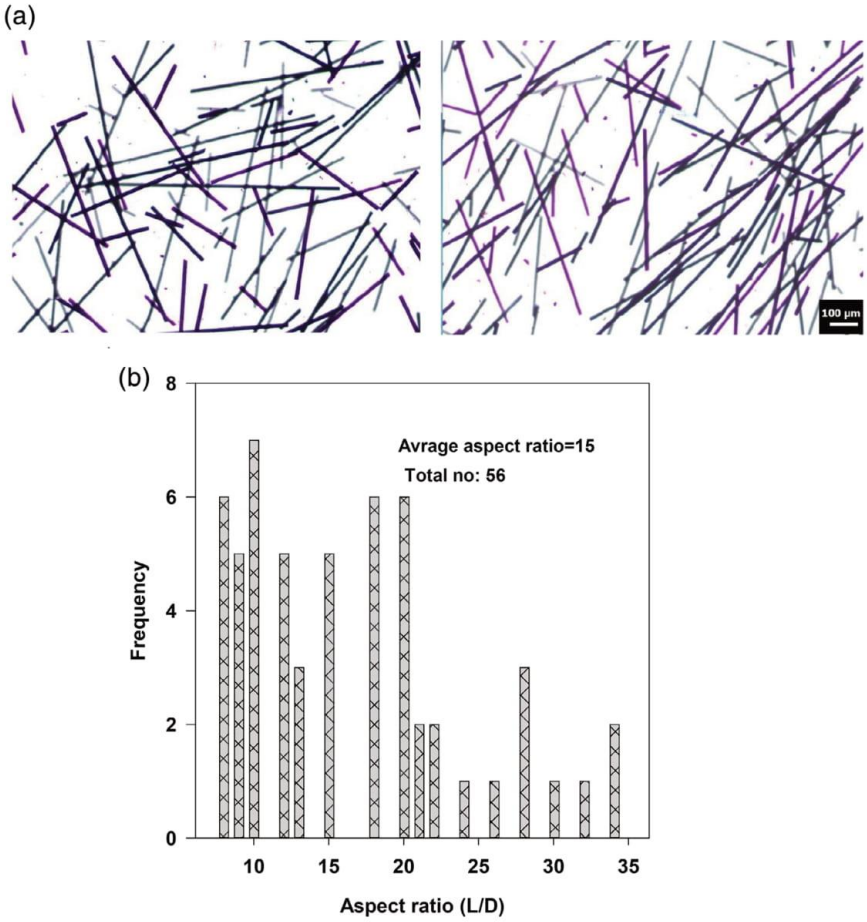

$$\phi_A = \frac{V_A}{V_A + V_B} = \frac{\frac{m_A}{\varrho_A}}{\frac{m_A}{\varrho_A} + \frac{m_B}{\varrho_B}} \quad \left[\cdot \frac{\frac{1}{m_A + m_B}}{\frac{1}{m_A + m_B}} \right] \tag{3}$$

$$= \frac{\frac{m_A}{\varrho_A \cdot (m_A + m_B)}}{\frac{m_A}{\varrho_A \cdot (m_A + m_B)} + \frac{m_A}{\varrho_A \cdot (m_A + m_B)}} = \frac{\frac{w_A}{\varrho_A}}{\frac{w_A}{\varrho_A} + \frac{w_B}{\varrho_B}}$$

While the densities of *CF* and EVA 328 are 1.80 and 0.951 g/cm^3, respectively. The volume fraction is shown in Table 2.

There are several theoretical models to describe the molecular behavior of filled composites. The earliest theory was Einstein's hydrodynamic theory for viscosity of colloidal suspensions. Einstein model describes increase of viscosity due to the addition of spherical rigid particles. This model was modified for nonspherical particles, such as fibers. In case of fibers, the length to diameter (L/D) aspect ratio *f* plays an important role [16,17]. Guth and Gold generalized the Einstein's by replacing the viscosity with elastic modulus. However, different shape and size of fibers can lead to an unexplained and unpredictable modulus and formation of aggregates in the matrix. The modified equation of Guth and Smallwood [18] and Guth and Gold model is shown in Equation 4. The equation is designed for spherical particles [19].

Gm = unfilled modulus

$$\frac{Gc}{Gm} = \left(1 + 2.5\Phi + 14.1\Phi^2\right) \tag{4}$$

where *Gc* = shear modulus of the composite. *Gm* = shear modulus of the gum. Φ = volume fraction of the filler.

Thus reinforcement factor $\frac{Gc}{Gm}$ is dependent only on the volume fraction of spherical filler in lower concentration. At higher concentration of the filler, it is observed that the reinforcement factor increases rapidly more than predicted by the equation. This is attributed to network formation or organization of filler particles into chain-like structures. To account for the "accelerated stiffening" caused by these

DOI 10.1002/vnl

chain-like or nonspherical fillers, Guth-Smallwood use shape factor (f) for nonspherical particles and since the f>1, therefore the reinforcement factor will increase rapidly by increasing the fiber content.

$$\frac{Gc}{Gm} = \left(1 + 0.67\, f\, \Phi + 1.62\, f^2 \Phi^2\right) \tag{5}$$

where: f = shape factor.

The volume fraction, density of each composite, experimental (see Fig. 3), Guth–Gold for spherical and Guth-Smallwood for nonspherical particle are shown in Table 2.

In order to illustrate the modulus of EVA-*CF* composite, the aspect ratio of carbon fiber should be determined.

Figure 3 shows the comparison between the experimental modulus with Guth-Gold for spherical and Guth-Smallwood for nonspherical particles. It indicates that the nonspherical Guth-Smallwood is closer to the experimental data at lower concentrations, however, at higher concentrations, the Guth-Gold model is closer.

Correlation of experimental increase in modulus with theoretical predictive models was well illustrated by Mandal *et al*. [20].

The statistical data of the aspect ratio for EVA/*CF* composite are shown in Fig. 4b. This data were obtained from a variety of electronic microscope photographs of EVA in Fig. 4a having different *CF* contents, that is, 5-20 wt%.

The effect of irradiation dose on shear stress at 0.03 shear strain is visible in Fig. 5b. It is also common throughout the rubber industry to observe M100 modulus and M300 of the modulus (at 100 and 300% elongation), and our choice was the stress at 0.03 shear strain. The graph indicates that EVA with a higher dose exhibited higher shear stress due to the fact that EVA with a higher dose contains more radiation cross-links compared to lower dose. It was observed that the shear stress of EVA with 5 wt% of carbon fiber was following an exponential rise with R^2 = 0.999 regression. As demonstrated in Fig. 5a, an addition of *CF* fiber with a higher radiation dose can enhance the shear stress, since *CF* as a filler and cross-linking can improve the stiffness by restricting the movement of the matrix [21,22]. Improvements of physical and mechanical properties of electron beam irradiation cross-linked EVA foams were also reported by Rezaeian *et al*. [23]. Mechanical changes of electron-beam irradiated EVA film were reported by Matsui *et al*. [24].

The development of creep in time is shown in Fig. 6a. The addition of carbon fiber to EVA causes reduction of the creep. It indicates that the addition of 20 wt% of *CF* caused almost three times lower creep compared to pure EVA. The graph also shows that not only the creep is decreasing with the addition of carbon fiber but also the rate of the creep (slope) decreases from 26 to 11 for pure EVA and 20 wt% of carbon fibers, respectively. Figure 6b suggests that there is a systematic decrease in creep with increasing content of the *CF* fibers after 5 min and also after recovery observed after 10 min. Our results follow the trend of other researchers. Creep reduction due to the addition of nanofillers was reported by Shokrieh *et al*. [25].

Figure 6c,d shows the sensitivity of creep to *CF* content and radiation dose. The graph (Fig. 6d) indicates that there is a significant decrease in creep with a radiation dose (kGy). It shows that EVA composite with a dose of 180 kGy has nearly seven times lower creep in comparison with a dose of 60 kGy, which is caused by cross-linking. We have found an exponential decrease in creep compliance with increasing level of radiation in our previous

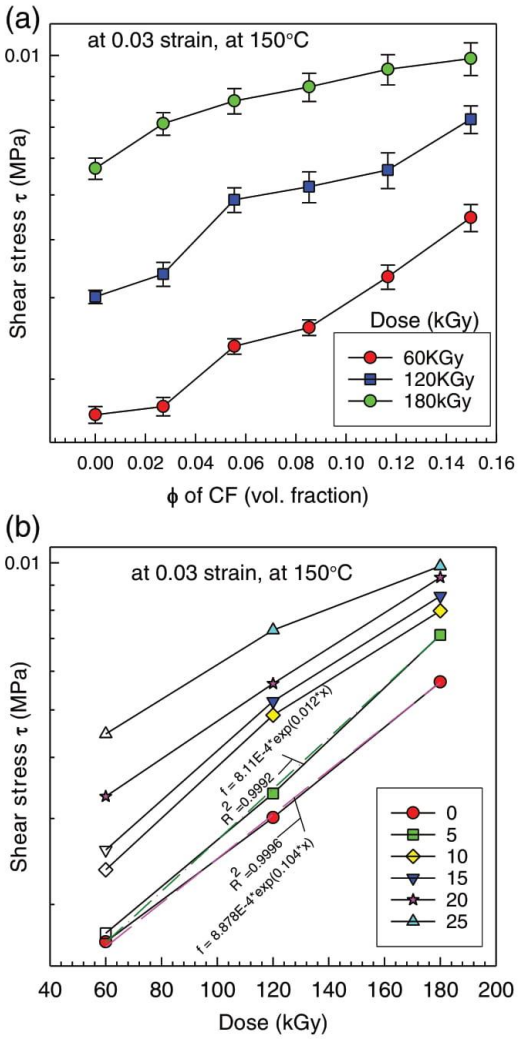

FIG. 5. (a) Shear stress versus volume fraction of *CF*; (b) shear stress versus dose for EVA/*CF* composites. [Color figure can be viewed at wileyonlinelibrary.com]

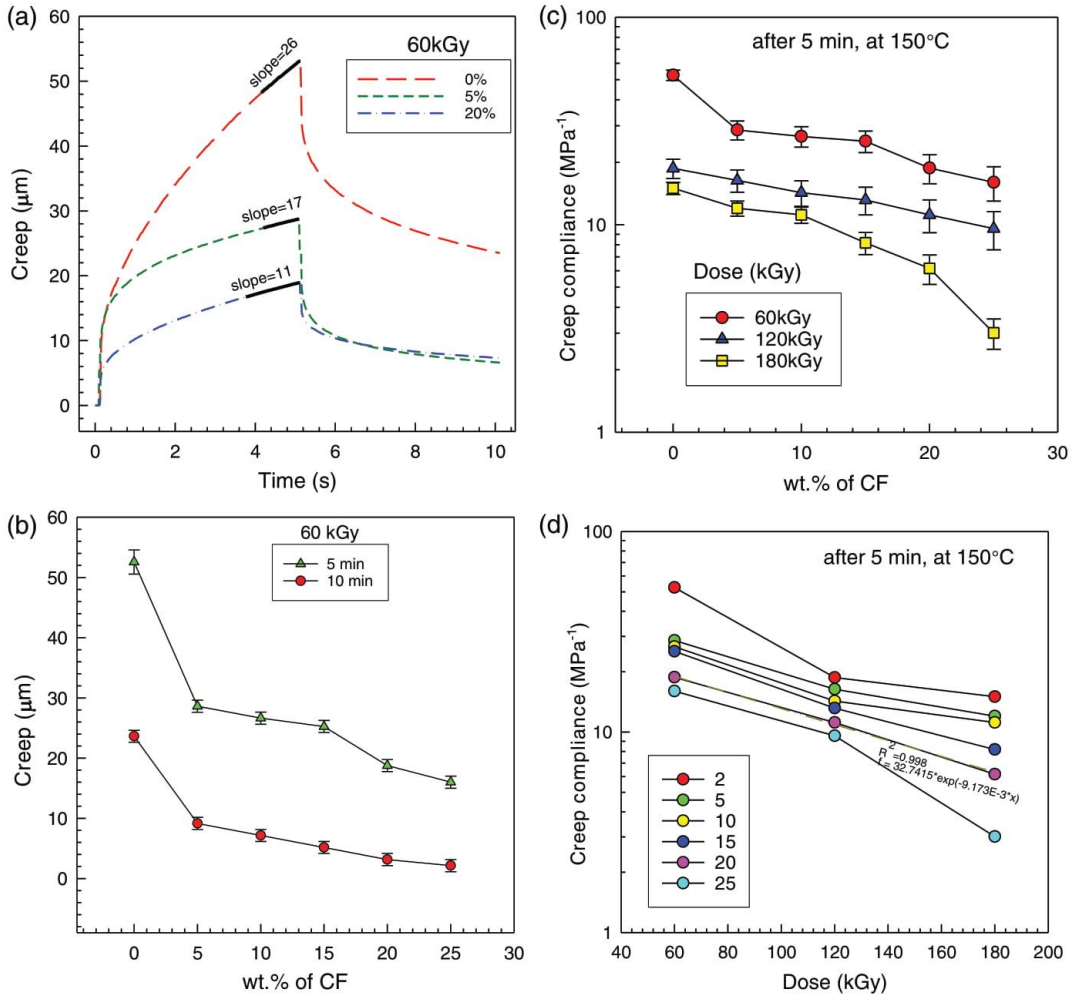

FIG. 6. (a) creep versus time; (b) creep (recovery) versus *CF* content at 150 °C, (c) creep compliance versus *CF* content for various doses, (d) creep compliance versus dose for various *CF* contents. [Color figure can be viewed at wileyonlinelibrary.com]

study of ethylene-octene copolymer [26]. Creep reduction with increasing level of cross-linking (by the addition of peroxide) was also reported by Theravalappil *et al*. [27].

Figure 7 shows the tan δ versus frequency, dose or *CF* content. The graph indicates that addition of fiber to EVA will increase the tan δ. The tan δ for EVA composite (120 kGy) with 25% content of *CF* is nearly 0.4, while the pure EVA is around 0.2 followed by 0.25 and 0.3 for 15% and 20%, respectively. Decrease of tan δ value with increasing cross-linking level due to the addition of peroxide was reported by Poongavalappil *et al*. [28].

Tan δ values have dropped by raising the radiation level from 60 to 180 kGy. That is caused by an increase in molecular weight, which hinders the free flow of the material.

It is also evident that the tan δ of the composites decreases significantly with increasing of the frequency, as shown in Figure 7a,b. The influence of frequency on the tan δ is complex. The chain motion can be restricted with the change of the external force, and the internal friction is low at low frequency; so, the tan δ is low [29]. While in our cross-linked EVA system, the *CF* has caused increase in tan δ McNally *et al.* [30] reported a decrease in tan δ values due to the addition of carbon nanotubes in an uncross-linked PE. Figure 7c indicates the tan δ change with the dose at all frequencies. It shows that with increase of the dose, tan δ is decreasing for all frequencies.

Figure 8 shows the G' increases after irradiation. The increase of G' was observed in the irradiation dose ranging 60–180 kGy. For the EVA 25 wt% of carbon fiber, the increase of G' was higher. The highest increase of G' was

DOI 10.1002/vnl

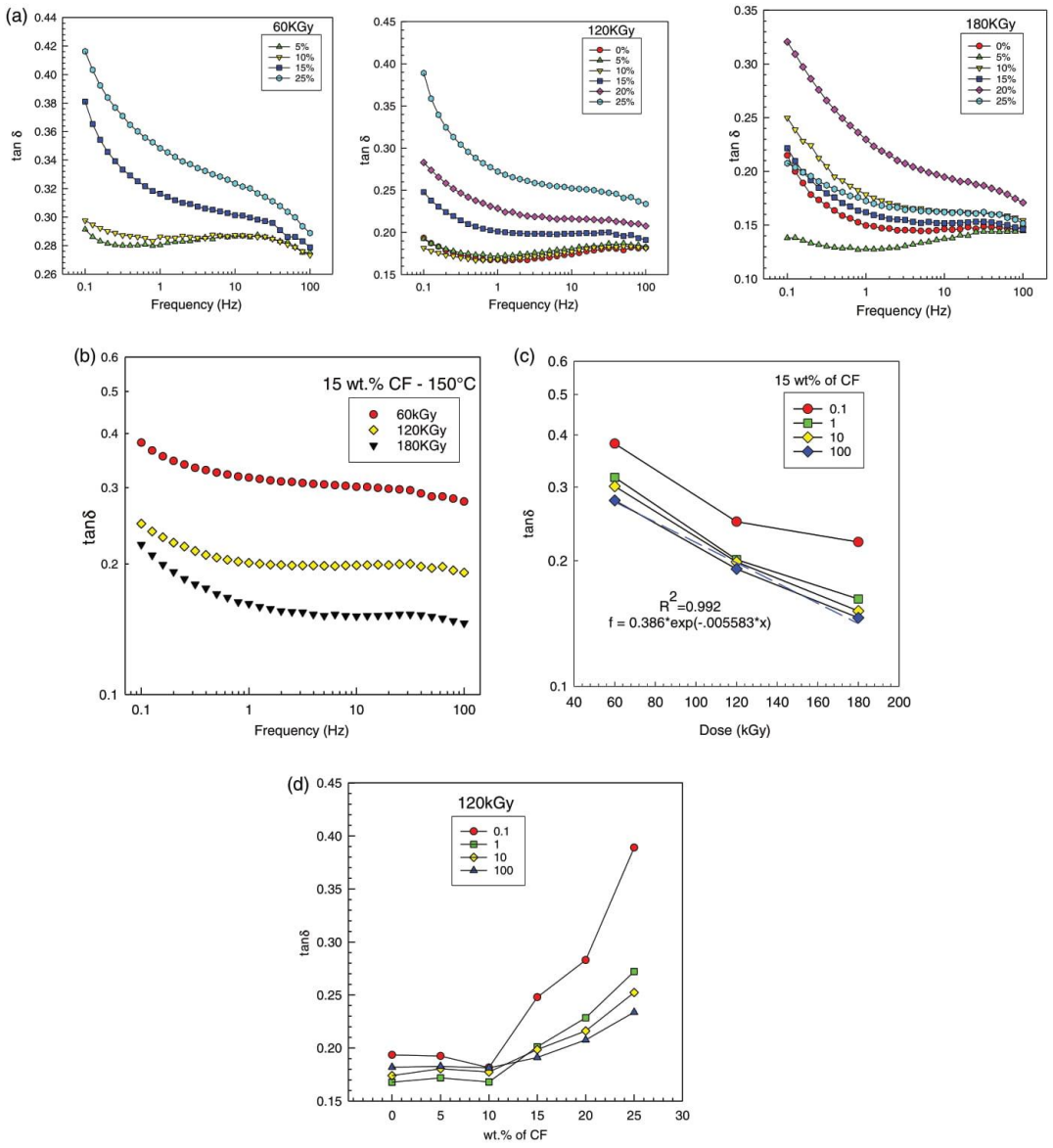

FIG. 7. Tan δ at 150 °C (a), (b) as a function of frequency, (c) as a function of dose at 0.1 rad/s, and (d) as a function of *CF* content. [Color figure can be viewed at wileyonlinelibrary.com]

found for EVA 25 wt% of carbon fiber (in the range 20–67 kPa). For the range of 60, 120, and 180 kGy, the G' values for pure EVA were 8, 17, and 28 kPa, respectively, and for EVA 15 wt% of carbon fiber they were 16, 23, and 43 kPa. Increase in G' due to the cross-linking was reported by Mussatti and Macosko [31].

It has been also observed that fiber has an increased influence at a higher frequency. Increase in G' value due to the increasing level of carbon nanotubes was reported by Potschke *et al*. [14,32], and also due to the increasing level of graphene, by Kim and Macosko [33] or by Varghese *et al*. [34].

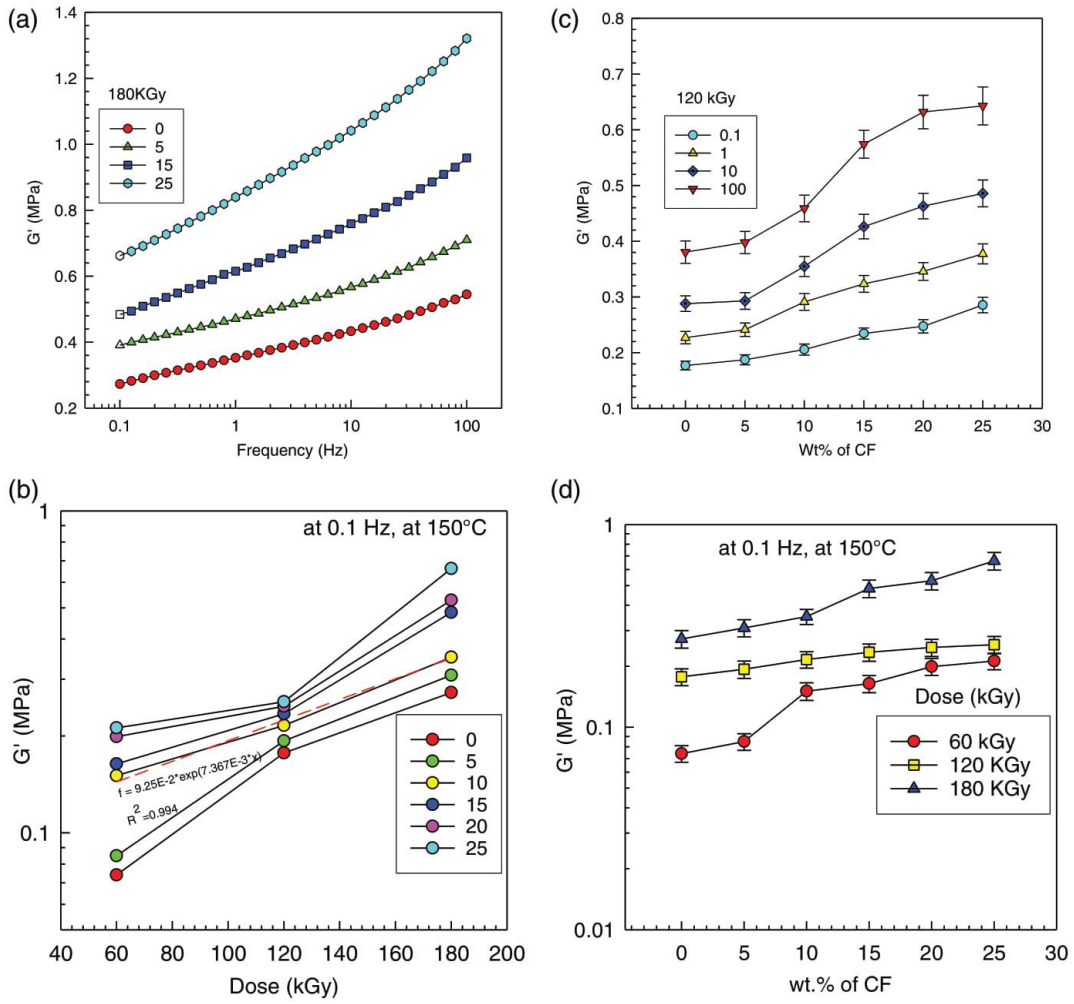

FIG. 8. Shear modulus (real part) G' at 150 °C (a), (b) as a function of frequency, (c) as a function of *CF* content for various frequencies, and (d) as a function of *CF* content for various irradiation doses. [Color figure can be viewed at wileyonlinelibrary.com]

CALCULATION OF G PARAMETERS ACCORDING TO CHARLESBY-PINNER EQUATION

In order to be able to calculate Charlesby-Pinner parameters, it is necessary to have data of molecular weight and data of gel content for various levels of irradiation [10,35].

Figure 9 depicts the EVA molecular weight distribution using gel permeation chromatography (GPC). The graph shows that the molecular weight of EVA used in this study is between 300 and 5,000,000 g/mol. The peak position is around 100,000 g/mol. The results from GPC test are listed in Table 3.

Figure 10 shows that increasing the radiation dose to 60 kGy caused the generation of an insoluble 3D network with gel content being 72 wt%. In the radiation range 60–180 kGy, the gel content is increasing only moderately as shown in Fig. 10 for 72%, 81%, and 89%, respectively, which could be ascribed to the increase in molecular weight and cross-linking. These results are in good agreement with Sharif *et al*. [36] who studied radiation effects on LDPE, EVA, and their blends.

Figure 10b was used in Charlesby-Pinner calculation as shown below.

Calculation of the Degree of Polymerization

EVA 328 MFI = 3, Vinyl acetate = 28%

DOI 10.1002/vnl

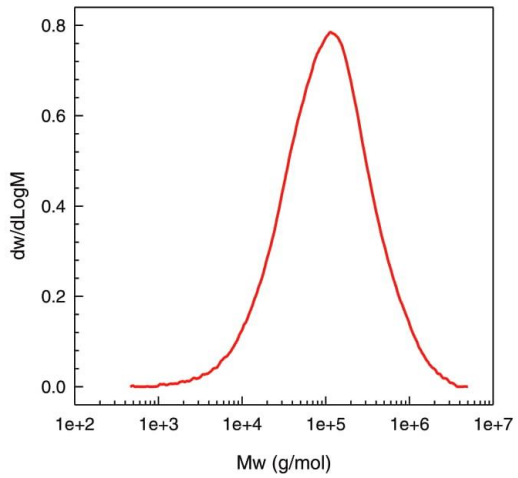

FIG. 9. The molecular weight distribution of EVA. [Color figure can be viewed at wileyonlinelibrary.com]

$$\text{etylen} = -CH_2-CH_2-, \quad M_{ET} = 2\cdot C + 4\cdot H = 2\cdot 12.011 + 4\cdot 1.008 = 28.054\ g/mol$$

$$\text{vinyl acetate} = -CH_2-CH(O-CO-CH_3)-, \quad M_{VA} = 4\cdot C + 2\cdot O + 6\cdot H = 4\cdot 12.011 + 2\cdot 15.9994 + 6\cdot 1.008 = 86.09\ \text{g/mol}$$

$$\text{wt. fraction of vinyl acetate } w_{VA} = \frac{28}{100} = 0.28$$

$$\text{wt. fraction of ethylene } w_{ET} = 1 - w_{VA} = 1 - 0.28 = 0.72$$

$$\text{molar fraction of vinyl acetate} = x_{VA}$$

$$x_{VA} = \frac{\frac{w_{VA}}{M_{VA}}}{\frac{w_{VA}}{M_{VA}} + \frac{w_{ET}}{M_{ET}}} = \frac{\frac{0.28}{86.09}}{\frac{0.28}{86.09} + \frac{0.72}{28.054}} = 0.1124717$$

$$\text{molar fraction of ethylene} = x_{ET} = 1 - x_{VA} = 1 - 0.1124717 = 0.8875283$$

average molecular weight of repeating unit

$$M_{ET-OCT} = x_{ET}M_{ET} + x_{VA}M_{VA} = 0.8875\cdot 28.054 + 0.1125\cdot 86.09 = 34.58\ g/mol$$

$$\textit{Polymerization degree} = P_n = \frac{M_{nEVA}}{M_{ET-VA}} = \frac{43400}{34.58} = 1255$$

Charlesby-Pinner equation [10,35]

$$s + \sqrt{s} = \frac{p_0}{q_0} + \frac{1}{q_0 P_n D} \quad Eq.6$$

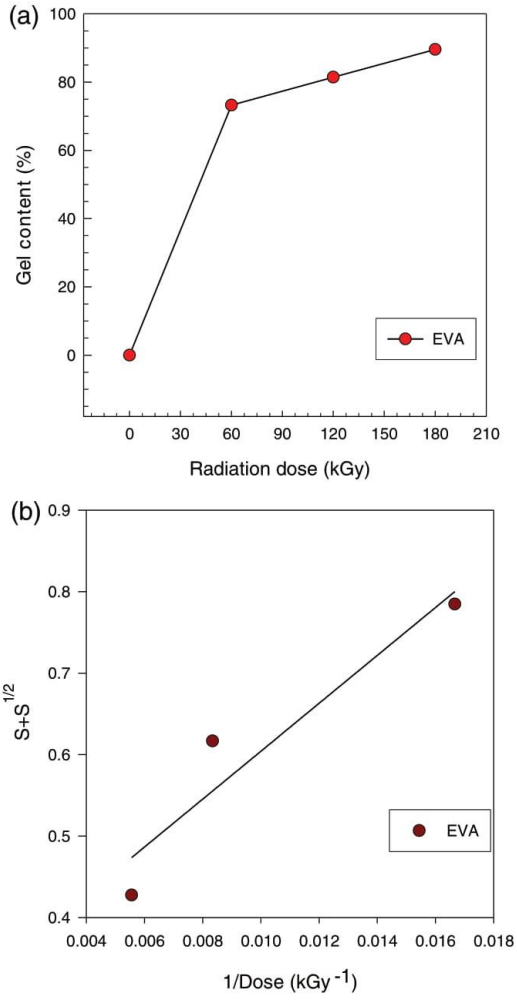

FIG. 10. (a) Gel content versus dose, and (b) Charlesby-Pinner analysis. [Color figure can be viewed at wileyonlinelibrary.com]

$$\textit{In plot } s + \sqrt{s} \textit{ vs. } \frac{1}{D}: \quad \textit{intercept} = \frac{p_0}{q_0}, \ \textit{slope} = \frac{1}{q_0 P_n}$$

$$\textit{In case of EVA-28}: \quad \textit{intercept} = 0.3103, \ \textit{slope} = 39.38$$

$$\textit{then } \frac{p_0}{q_0} = 0.3103 \textit{ and } \frac{1}{q_0 P_n} = 39.38$$

TABLE 3. GPC results of EVA 328

Sample name	M_p g/mol	M_n	M_w	M_z	$M_z + 1$	PDI
EVA 328	113,000	43,400	196,000	625,000	1,286,000	4.5

TABLE 4. Results of the calculated Charlesby-Pinner parameters

wt.% of vinyl acetate	wt. fraction of vinyl acetate	wt. fraction of ethylene	Molar fraction of vinyl acetate	Molar fraction of ethylene	$M_{ET\text{-}VA}$	M_n	P_n
28	0.28	0.72	0. 8,875	0.1125	34.58	43,400	1,255
Slope	p_0/q_0	q_0	p_0	G(X)/G(S)	G(X)		G(S)
29.38	0.3103	2.7121×10^{-05}	8.4156×10^{-06}	1.6113	3.7797		2.3456

$$q_0 = \frac{1}{slope \cdot P_n} = \frac{1}{29.38 \cdot 1255} = 0.000027121$$

$$then \quad p_0 = q_0 \cdot intercept = q_0 \cdot \frac{p_0}{q_0} = 0.000027121 \cdot 0.3103 = 0.0000084156$$

$$s + \sqrt{s} = \frac{G(S)}{2G(X)} + \frac{4.82 \times 10^6}{G(X) M_n D}$$

$$then \quad \frac{G(S)}{2G(X)} = \frac{p_0}{q_0}$$

$$\frac{G(X)}{G(S)} = \frac{1}{2\frac{p_0}{q_0}} = \frac{1}{2 \cdot 0.3103} = 1.6113$$

$$slope = \frac{4.82 \times 10^6}{G(X) M_n}$$

$$G(X) = \frac{4.82 \times 10^6}{slope \cdot M_n} = \frac{4.82 \times 10^6}{29.3832 \cdot 43400} = 3.7797$$

$$intercept = \frac{G(S)}{2G(X)}$$

$$G(S) = 2 \cdot G(X) \cdot intercept = 2 \cdot 3.7797 \cdot 0.3103 = 2.3456$$

All the important parameters are listed in Table 4. Parameters G(X) = 3.78 and G(S) = 2.35 mean that both cross-linking and chain scission occur during e-beam irradiation. The ratio of the parameters G(X)/G(S) = 1.61 indicates that cross-linking prevails over the scission for this copolymer. The ratio G(X)/G(S) = 1.61 is comparable to our previous results on ethylene-octene copolymer with 30 wt% of octene [37] when the ratio was 1.77.

CONCLUSIONS

Ethylene vinyl acetate combined with carbon fiber was prepared, and the mechanical properties and irradiation effect at 150 °C were studied. The EVA-*CF* composites were found to have higher shear modulus for given shear strain by adding of filler and with increasing irradiation, which was due to the interaction between the matrix and fiber and by increasing of the molecular weight with irradiation due to cross-linking. It was also observed that tan δ decreased with increasing of the dose from 60 to 180 kGy for 0.1 to 100 Hz frequencies. There was a dramatic decrease in creep with increasing *CF* content and increasing irradiation, which confirmed the high interaction and raised cross-linking level. The analysis of unsolvable gel content confirmed the effect of irradiation on cross-linking since application of the radiation dose up to 180 kGy increased the amount of insoluble gel.

APPENDIX

The densities of the composites were calculated according to these equations:

$$V_A + V_B = V_{comp}$$

$$\rho = \frac{m}{V}, \quad V = \frac{m}{\rho}$$

$$\frac{m_A}{\rho_A} + \frac{m_B}{\rho_B} = \frac{m_{comp}}{\rho_{comp}}$$

$$w_A = \frac{m_A}{m_{comp}}, \quad w_B = \frac{m_B}{m_{comp}}, \quad w_A + w_B = 1$$

$$\frac{m_A}{\rho_A} + \frac{m_B}{\rho_B} = \frac{m_{comp}}{\rho_{comp}} \quad \cdot \left[\frac{1}{m_{comp}}\right.$$

$$\frac{w_A}{\rho_A} + \frac{w_B}{\rho_B} = \frac{1}{\rho_{comp}}$$

$$\rho_{comp} = \frac{1}{\frac{w_A}{\rho_A} + \frac{w_B}{\rho_B}}$$

Densities of the composites are listed in Table 2. These values are in a good agreement (within ±3%) to the experimentally obtained values (by pycnometer).

ACKNOWLEDGMENT

This work has been supported by the Internal Grant Agency (IGA/FT/2017/007) of the Tomas Bata University in Zlin.

REFERENCES

1. N.A. Mohd Radzuan, M. Yusuf Zakaria, A.B. Sulong, and J. Sahari, *Compos. Part B Eng.*, **110**, 153 (2017).
2. F.L. Jin, S.Y. Lee, and S.J. Park, *Carbon Lett.*, **14**(2), 76 (2013).
3. S. Tiwari, J. Bijwe, and S. Panier, *Wear*, **271**(9–10), 2184 (2011).

4. J. Li and F. Sun, *Polym.-Plast. Technol. Eng.*, **48**(7), 711 (2009).
5. J.M. Raj and C. Ranganathaiah, *J. Polym. Sci. Pol. Phys.*, **47** (6), 619 (2009).
6. J.J. George and A.K. Bhowmick, *Nanoscale Res. Lett.*, **3**(12), 508 (2008).
7. Makuuchi K, Cheng S. *Radiation Processing of Polymer Materials and its Industrial Applications*: Hoboken-New Jersy, John Wiley & Sons; 2012.
8. S. Ramarad, C.T. Ratnam, M. Khalid, A.L. Chuah, and S. Hanson, *Radiat. Phys. Chem.*, **130**, 362 (2017).
9. M. Mateev and S. Karageorgiev, *Radiat. Phys. Chem.*, **51**(2), 205 (1998).
10. P. Svoboda, *Polymers-Basel.*, **7**(12), 2522 (2015).
11. A. Das, K.W. Stockelhuber, R. Jurk, M. Saphiannikova, J. Fritzsche, H. Lorenz, et al., *Polymer*, **49**(24), 5276 (2008).
12. K.J. Yu, M.L. Wang, J.Q. Wu, K. Qian, J. Sun, and X.F. Lu, *Nanomaterials-Basel*, **6**(5), 89 (2016).
13. Y. Hamid, A. Abu Bakar, and N. Deirram, *J. Appl. Polym. Sci.*, **128**(2), 1170 (2013).
14. P. Potschke, T.D. Fornes, and D.R. Paul, *Polymer*, **43**(11), 3247 (2002).
15. S. Poongavalappil, P. Svoboda, R. Theravalappil, D. Svobodova, M. Danek, and M. Zatloukal, *J. Appl. Polym. Sci.*, **128**(5), 3026 (2013).
16. J.W. Qian, M. Wang, D.L. Han, and R.S. Cheng, *Eur. Polym. J.*, **37**(7), 1403 (2001).
17. K. Jayanarayanan, S. Thomas, and K. Joseph, *Iran Polym. J.*, **25**(4), 373 (2016).
18. V. Jha, A.A. Hon, A.G. Thomas, and J.J.C. Busfield, *J. Appl. Polym. Sci.*, **107**(4), 2572 (2008).
19. C.A. Rezende, F.C. Braganca, T.R. Doi, L.T. Lee, F. Galembeck, and F. Boue, *Polymer*, **51**(16), 3644 (2010).
20. S. Mandal and S. Alam, *J. Appl. Polym. Sci.*, **126**(2), 724 (2012).
21. W.L. Oliani, L.F.C.P. Lima, D.F. Parra, D.B. Dias, and A. B. Lugao, *Radiat. Phys. Chem.*, **79**(3), 325 (2010).
22. K.H. Matthews, H.N.E. Stevens, A.D. Auffret, M. J. Humphrey, and G.M. Eccleston, *Int. J. Pharm.*, **313**(1–2), 78 (2006).
23. I. Rezaeian, S.H. Jafari, P. Zahedi, M. Ghaffari, and S. Afradian, *Polym. Advan. Technol.*, **20**(5), 487 (2009).
24. T. Matsui, M. Shimoda, and Y. Osajima, *Polym. Int.*, **29**(2), 85 (1992).
25. Z. Shokrieh, M.M. Shokrieh, and Z. Zhao, *Polym. Test.*, **65**, 414 (2018).
26. P. Svoboda, D. Svobodova, P. Mokrejs, V. Vasek, K. Jantanasakulwong, T. Ougizawa, et al., *Polymer*, **81**, 119 (2015).
27. R. Theravalappil, P. Svoboda, S. Poongavalappil, and D. Svobodova, *Macromol. Mater. Eng.*, **297**(8), 761 (2012).
28. S. Poongavalappil, P. Svoboda, R. Theravalappil, D. Svobodova, V. Vasek, K. Jantanasakulwong, et al., *Eur. Polym. J.*, **47**(10), 1949 (2011).
29. M.H. Liu, R. Li, G. Wang, Z.Y. Hou, and B. Huang, *J. Therm. Anal. Calorim.*, **126**(3), 1281 (2016).
30. T. McNally, P. Potschke, P. Halley, M. Murphy, D. Martin, S.E.J. Bell, et al., *Polymer*, **46**(19), 8222 (2005).
31. F.G. Mussatti and C.W. Macosko, *Polym. Eng. Sci.*, **13**(3), 236 (1973).
32. P. Potschke, M. Abdel-Goad, I. Alig, S. Dudkin, and D. Lellinger, *Polymer*, **45**(26), 8863 (2004).
33. H. Kim and C.W. Macosko, *Polymer*, **50**(15), 3797 (2009).
34. A.M. Varghese, V.M. Rangaraj, S.C. Mun, C.W. Macosko, and V. Mittal, *Ind. Eng. Chem. Res.*, **57**(23), 7834 (2018).
35. J.D. Turgis and X. Coqueret, *Macromol. Chem. Physic.*, **200** (3), 652 (1999).
36. J. Sharif, S.H.S.A. Aziz, and K. Hashim, *Radiat. Phys. Chem.*, **58**(2), 191 (2000).
37. P. Svoboda, *Polym. Bull.*, **74**(1), 121 (2017).